Characterizing Chemical Tools for the Discovery of Novel Antiviral Therapeutics

Tyler Shaw

Thesis submitted to the University of Ottawa in partial fulfillment of the requirements for the Doctorate in Philosophy degree in Chemistry and Biomolecular Science

Department of Chemistry and Biomolecular Science

Faculty of Science

University of Ottawa

Abstract

Despite our growing knowledge of virus biology they continue to present a problem to global public health. This problem arises from their high mutation rates that allow them to evade antiviral therapies that we have developed to date. An alternative solution for developing antiviral therapies could be to target host cell factors that are hijacked by the virus. The basis of this hypothesis is that if we can stop the virus from using host cell machinery or from evading host immune mechanisms we could treat the infection more efficiently. With the major research focus being on viral proteins and how we can prevent their functions, there is a lot of work to be done in finding host factors that could be the key to treating an infection. The three themes presented in this thesis broadly focus on this goal. The first theme looks at miRNAs, their interacting partners, and their dysregulation during HCV infection. A microRNA is identified from a small molecule screen of miRNAs that are dysregulated during HCV infection and its role in liver immunometabolism is examined to determine its antiviral potential and identify host factors that could be of interest to target with antiviral therapeutics. The second theme examines the potential of activity-based protein profiling techniques for complementing existing antiviral therapies. An azauracil probe is characterized to examine its ability to interact with viral polymerases and its suitability as a building block for antiviral research or therapies. The final theme uses activity-based protein profiling techniques to study a novel carbamate-hydrazone chemotype and establish its suitability as a chemical probe. The hydrazone probe's reactivity with the mammalian proteome was determined and its interacting partners were identified using chemoproteomic techniques with an overall goal of examining its suitability for antiviral research. Overall, this thesis uses chemical and molecular biology techniques to present three differing perspectives on how to approach the discovery of host factors and develop novel antiviral therapies

Acknowledgements

I'd like to thank Dr. John Pezacki for taking a chance on me when no one else would. I started off strong with lots of collaborative works but lost steam during COVID lockdown and he continued to encourage me and help me find ways to be productive and finish my graduate studies despite working full-time at the end of my studies to support my family.

Secondly, I would like to thank Megan Powdrill for training me to be her prodigy and Dennis Özcelik for his many insightful consultations and comic relief. I'd like to thank the members of the Pezacki lab who started their graduate journey with me and put up with my bad jokes over the years while lending a helping hand when I needed it, namely, Roxana Filip, Geneviève Desrochers, Didier Bilodeau, Rhea Alonzi, Nadine Ahmed, and Noreen Ahmed.

I'd also like to thank former members of the Pezacki lab from over the years who shared their knowledge and experiences with me and made the lab feel like home. Namely, Ragunath Singaravelu, Mirka Strmiskova, Matthew Lafreniere, Chris Ablenas, Kaitlyn Margison, David Lefebvre, Mariam Serhan, and Dave Prescott among others.

I'd like to thank my parents for giving me the opportunity to attend university and pursue my love of science and knowledge. And lastly, I'd like to thank my loving wife and kids for always supporting me and being there for me at the end of the day. Most of all I would like to thank (and apologize to) Kierra Shaw for being my life partner and embarking on this wonderful rollercoaster of a life we've made together.

.

Table of Contents

List of Tables

List of Figures

List of Abbreviations

^{1}H-NMR	Proton nuclear magnetic resonance
^{13}C-NMR	Carbon-13 nuclear magnetic resonance
18S rRNA	Ribosomal small subunit 18S RNA
25-HC	25-hydroxycholesterol
^{31}P-NMR	Phosphorus-31 nuclear magnetic resonance
A3A	Apolipoprotein B mRNA editing enzyme, catalytic polypeptide-like 3A
A3G	Apolipoprotein B mRNA editing enzyme, catalytic polypeptide-like 3G
A3H	Apolipoprotein B mRNA editing enzyme, catalytic polypeptide-like 3H
AADAC	Arylacetamide deacetylase
AADACL1	Arylacetamide deacetylase-like 1
ABPP	Activity-based protein profiling
ABP	Activity-based probe
ACAA2	Acetyl-CoA acyltransferase 2
ACADSB	Acyl-CoA dehydrogenase short/branched chain
ACADVL	Acyl-Coa dehydrogenase very long chain
ACN	Acetonitrile
Ago2	Argonaute RISC catalytic subunit 2
AIDS	Acquired immunodeficiency syndrome
ALDH9A1	Aldehyde dehydrogenase 9 family member A1
APOBEC	Apolipoprotein B mRNA editing enzyme, catalytic polypeptide

ATCC	American Type Culture Collection
ATGL	Adipose triglyceride lipase
ATP	Adenosine triphosphate
AzT	Azidothymidine
AzTTP	Azidothymidine triphosphate
BSA	Bovine serum albumin
CES1	Carboxylesterase 1
CoA	Coenzyme A
Con-miR	Control microRNA mimic
CPT1A	Carnitine palmitoyl transferase 1A
CuAAC	Copper-catalyzed azide-alkyne cycloaddition
DAPI	4', 6-diamidino-2-phenylindole
DENV	Dengue virus
DMEM	Dulbecco's modified Eagle medium
DMSO	Dimethylsulfoxide
DNA	Deoxyribonucleic acid
dNTP	Deoxynucleotide triphosphate
DTT	Dithiothreitol
ECI2	Enoyl-CoA delta isomerase 2
EDTA	Ethylenediaminetetraacetic acid
ESI	Electrospray ionization
FADH2	Flavin adenine dinucleotide

FASN	Fatty acid synthase
FBS	Fetal bovine serum
FDA	Food and Drug Administration
FDR	False discovery rate
FFU	Focus-forming unit
FP	fluorophosphonate
FT-IR	Fourier transform infrared
FXR	Farnesoid X receptor
G SEM	Generalized standard error of the mean
GTP	Guanosine triphosphate
HADH	Hydroxyacyl-CoA dehydrogenase
HADHA	Hydroxyacyl-CoA dehydrogenase trifunctional multienzyme complex subunit alpha
HADHB	Hydroxyacyl-CoA dehydrogenase trifunctional multienzyme complex subunit β
HCD	Higher-energy C-trap dissociation
HCV	Hepatitis C virus
HIV-1	Human immunodeficiency virus type 1
HMBC	Heteronuclear multiple bond correlation
HSQC	Heteronuclear single quantum coherence
HRMS	High-resolution mass spectrometry
IC_{50}	Half maximal inhibitory concentration
IF	Immunofluorescence

IFN	Interferon
IgG	Immunoglobulin G
IRF1	Interferon regulatory factor 1
IRF3	Interferon regulatory factor 3
IRF9	Interferon regulatory factor 9
ISG	Interferon stimulated gene
ISGF3	Interferon stimulated gene factor 3
JAK1	Janus kinase 1
JFH-1	Japanese fulminant hepatitis 1 strain of HCV
JFH-AM1	Japanese fulminant hepatitis AM1 strain of HCV
KEGG	Kyoto encyclopedia of genes and genomes
LC-MS/MS	Liquid chromatography tandem mass spectrometry
MAPK	Mitogen-activated protein kinase
MFI	Mean fluorescence intensity
miRNA	MicroRNA
MOI	Multiplicity of infection
mRNA	Messenger RNA
NADH	Nicotinamide adenine dinucleotide
NCBI	National center for biotechnology information
NIH	National Institutes of Health
NMR	nucleur magnetic resonance
NP-40	Nonyl phenoxypolyethoxylethanol

NR1H4	Nuclear receptor subfamily 1 group H member 4
NRTI	Nucleoside reverse transcriptase inhibitor
Opti-MEM	Optimized minimum essential medium
ORF	Open reading frame
PAMP	Pathogen associated molecular pattern
PANTHER	Protein analysis through evolutionary relationships
PBS	Phosphate buffered saline
PECR	Peroxisimal trans-2-enoyl-CoA reductase
PES	Polyethersulfone
PFA	Paraformaldehyde
PNPLA2	Patatin-like phospholipase domain-containing protein 2
PPAR-α	Peroxisome proliferator-activated receptor alpha
PPARGC1A	Peroxisome proliferator-activated regulator gamma coactivator 1 alpha
PROTAC	Proteolysis targeting chimera
PRR	Pattern recognition receptor
PSM	Peptide spectra match
PVDF	Polyvinylidene fluoride
qRT-PCR	quantitative real-time polymerase chain reaction
RIG-I	Retinoic acid inducible gene I
RISC	RNA-induced silencine complex
RNA	Ribonucleic acid
RT	Reverse transcriptase

RNU6B	RNA, U6 small nuclear 6, pseudogene
SARS-CoV-2	Severe acute respiratory syndrome coronavirus-2
SDS	Sodium dodecyl sulphate
SDS-PAGE	Sodium dodecyl sulphate polyacrylamide gel electrophoresis
SLC22A5	Solute carrier family 22 member 5
SLC25A20	Solute carrier family 25 member 20
SMPDB	Small molecule pathway database
SREBP	Sterol regulatory element binding protein
STAT1	Signal transducer and activator of transcription
STAT2	Signal transducer and activator of transcription 2
TBS-T	Tris-buffered saline with Tween-20
TCEP	Tris(2-carboxyethyl)phosphine
TEAB	Tetraethylammonium bicarbonate
TFA	Trifluoroacetic acid
TG	Triglyceride
TGH	Triglycerol hydrolase
TLR3	Toll-like receptor 3
TRIB3	Tribbles pseudokinase 3
TYK2	Tyrosine kinase 2
UTP	Uridine triphosphate
UTR	Untranslated region
Xcorr	Cross correlation

X-gal	5-bromo-4-chloro-3-indoyl-β-D-galacto-pyranoside
ZIKV	Zika virus

Chapter 1: Introduction

1.1 Preface

The development of treatments for viral infections is often met with the challenge of making the treatment specific enough to treat the infection while also broad enough that it will work on different strains of a virus or even families of viruses. This is a huge undertaking as viral genomes are constantly mutating and result in ever-evolving viral proteins. As a result, therapeutics that directly target viral proteins are not always feasible. An alternative is to develop therapeutics that target the interface where viruses interact with host cell machinery. This interface is where viruses will hijack host biology to make their microenvironment more amenable to the viral life cycle. This process relies on host-virus interactions. This is to say that viruses directly interact with host proteins, lipids, and other macromolecules, and these may be candidates for antiviral therapeutics. The goal of these therapeutics being to disrupt the interaction of the virus with host machinery or to disrupt the microenvironment that the virus requires in order to progress through its life cycle.

1.2 Viruses and Antiviral Strategies

1.2.1 General Considerations

Viruses are obligate intracellular parasites that have a reputation for causing disease in the cells in which they replicate. They are the causative agents of epidemics and global pandemics due to their ability to infect and replicate within a wide range of host organisms, and most notably for global public health, some families of viruses cause disease in humans. In general, a virus particle contains a DNA or RNA genome surrounded by a capsid, with some families of viruses also possessing a protein core and/or a lipid envelope surrounding the capsid. As obligate intracellular

parasites, viruses lack translational and metabolic machinery and cannot reproduce on their own. Instead, viruses rely on the biology of a host cell to replicate their genetic code, translate viral proteins, and package new viral particles. Host cells are cells within an organism that harbor factors that viral proteins can recognize and use to facilitate the formation of new virus particles. The interactions of a virus with a host cell are referred to as host-virus interactions, the goal of which being to progress the viral life cycle or evade the immune response. For example the hepatitis C virus is known to modulate lipid metabolism in host cells in order to make a lipid rich environment that it can use for its replication and for packaging new viral particles.[1,2] Current research interests in antiviral therapeutics lay in determining how host biology is altered during viral infections and finding ways to circumvent these changes in order to treat the infections.

Prior to the interest in host-virus interactions, the strategy for treating viral infections was driven by the biology of the viral proteins. Early treatments for viral infections were tailored to the structure and function of viral proteins with treatment strategies being developed for most classes of viral enzymes. The most effective method in treating viral infections has been in preventing their replication by targeting viral polymerases.

1.2.2 Some Strategies for Targeting Viral Replication

Following the release of the genetic material into the cytoplasm of the host cell, the viral genome is copied by a viral polymerase and prepared to be packaged into new viral particles. The method through which it is copied depends on the composition of the genome.[3] For example, many pathogenic viruses have positive sense single-stranded RNA genomes. This type of genome would be present in DENV, HCV, SARS-CoV-2, HIV-1, ZIKV, and many other viruses that are of global interest. The positive sense single stranded RNA is an important design factor for these viruses

because it can be immediately bound by viral RNA polymerases or host ribosomes that can use it directly to reproduce the viral RNA or to translate viral proteins. This process differs slightly in the case of retroviruses like HIV-1, where the single stranded RNA is reverse transcribed by a viral reverse transcriptase, producing a double stranded DNA that is then integrated into the host genome by a viral integrase.[4] The result is the viral genome being replicated by the host replication machinery each time it replicates its own genome. The development of therapeutics targeting viral replication would therefore rely on inhibiting the viral polymerase, and in the case of retroviruses would extend to the reverse transcriptase.[5,6]

Disruption of a viral polymerase is commonly achieved through a process called chain termination. The chain in this case would be the RNA or DNA genome of the virus that is being replicated and termination would involve stopping the polymerase from copying the viral genome, in essence terminating the replication. The most commonly used strategy to achieve this is to use a synthetic molecule that mimics the nucleotide substrate of the polymerase but lacks the functional groups required to continue the elongation of the strand. At a mechanistic level this would mean introducing a nucleoside analog that lacks a 3' hydroxyl group or that would possess a different functional group that sterically blocks the site of nucleotide incorporation in the polymerase.[7,8]

In 1987, efforts to treat HIV infection used a thymidine analog called azidothymidine.[9] This nucleoside analog lacked a 3' hydroxyl group and caused chain termination in the reverse transcriptase. The caveat of this treatment was that it also targeted other polymerases and caused side effects. Despite these undesirable side effects the drug is still FDA-approved and used in modern HIV-1 treatments that pair it with a non-thymidine nucleoside analog and a non-nucleoside

inhibitor of HIV-1 RT.[10] Treatment regimens that target multiple host-virus interactions have proven to be the most effective and least likely to fail. Issues arise when only using a nucleoside inhibitor due to the frequency of mutations in the viral genome and adherence problems with the treatment regimen. Adherence problems are an issue because while the infection might be caused by a wildtype virus, there can be mutations in the genome introduced by the lack of proofreading by the reverse transcriptase, giving rise to a chimeric population of viruses in the infection.[11] While some of these chimeric variants are less infectious or have less reproductive capacity than the wildtype virus, they could persist following a treatment of the wildtype virus due to mutations in the wildtype genome giving rise to conformational changes in the viral proteins that make them resistant to the therapy. Some mutants will persist following the end of the antiretroviral treatment and due to the error rate of their polymerases, they will eventually give rise to the more infectious or better replicating wildtype-like genomes.

The chain termination strategy has also been employed in HCV treatments with Sofosbuvir being approved in 2014 as an HCV polymerase inhibitor. Sofosbuvir is a uridine analog that possesses a 3' hydroxyl group and sterically blocks the incorporation of nucleotides into the replicating strand in the HCV polymerase.[12,13] Treatment regimens employing Sofosbuvir combine it with Ribavirin and a protease inhibitor and are approaching a 100% cure rate for all HCV genotypes. Ribavirin was first approved as an HCV treatment in 1999 in combination with PEG-Interferon. Ribavirin's mechanism is more primitive than modern nucleoside analogs in that it is a guanosine analog that pairs with cytidine or uridine nucleotides and induces mutations in viral RNA.[14] Treatment with Ribavirin can cause anemia and other undesirable side effects that are exasperated when used in combination with PEG-interferon. Polymerase inhibitors were proposed to complement Ribavirin and led to the discontinuation of PEG-interferon. Nucleoside analogs

remain an area of interest for HCV and other viruses as they have encountered the same problems seen in HIV RT inhibitors with their genotypic limitations.[15,16] Given the difficulties of developing effective direct acting antivirals, the next line of research to treat viral infections lies in understanding the host-virus interface. This interface is where viral proteins interact with host proteins and hijack them in order to manipulate the cellular environment to promote the viral life cycle while also circumventing the immune system.

1.3 Considerations for the Host Response to Infection

The innate immune system is the first line of defense during viral infection. The response to an infection begins with PRRs recognizing PAMPs primarily consisting of viral nucleic acids. PAMP recognition induces production of IFNs and ISGs to inhibit the viral infection. In the case of HCV infection, RIG-I and TLR3 detect the viral RNA and initiate a signalling cascade that culminates in the dimerization of IRF3 which can then translocate into the nucleus to induce the expression of type I and type III IFNs, cytokines, and ISGs.[17,18] In the canonical defense against HCV infection the type I and type III interferons will bind to their receptors, initiating conformational changes in the receptors that will activate the JAK/STAT pathway. The phosphorylation of JAK1 and TYK2 will stimulate the heterodimerization of STAT1 and STAT2 which can then bind to IRF9 to form the ISGF3 complex that translocates into the nucleus where it binds ISREs and acts as a transcription factor to stimulate the expression of ISGs.[19] For example, IFN-α will activate IRF1-mediated chemokine production, recruiting lymphocytes and natural killer cells. Although this mechanism should be sufficient to clear the virus, it has evolved ways to circumvent the innate immune system by using its viral proteins to cleave PRRs and to bind

intermediates in the signalling cascade to prevent the signal from reaching the nucleus and expressing antiviral factors.

During the immune response the liver cells will also secrete IFNs extracellularly, leading to the stimulation of circulating and resident immune cells. Liver resident macrophages become activated by these IFNs and will secrete chemokines to help fight the infection. These chemokines can lead to the recruitment of additional immune cells or can act directly on liver cells to fight infection. Such actions would include modifying the microenvironment within the cells to subvert the intracellular changes that the virus has induced. One of the molecules secreted following IFN stimulation of liver macrophages is 25-HC.[20,21] This oxysterol was recently shown to have a potent antiviral effect against HCV infection, largely due to its role in modifying cholesterol and lipid metabolic pathways in liver cells.[22] The immunometabolic changes induced by 25-HC were additionally linked to changes in miRNA expression profiles.[23–25]

1.3.1 The Role of MicroRNAs in Viral Infections

MicroRNAs are small non-coding RNAs that are transcribed in the nucleus and act as regulators of gene expression. The primary transcript is processed by the Drosha enzyme complex and exported from the nucleus where it is then cleaved by the Dicer enzyme complex to generate a 20-26 nucleotide miRNA duplex. The miRNA is then loaded into the RISC complex as a single stranded guide RNA and will bind mRNA that are complementary. Once bound by the RISC complex, the mRNA is translationally repressed or sent to be degraded, preventing the expression of the associated gene. miRNAs have been shown to play a role in many biological processes, notably metabolism and immunity.[26,27]

The canonical method of action for miRNAs is to have the RISC complex bind a complementary sequence on an mRNA and prevent it from being used by a cell. In the case of a viral infection there is an added complication in that the viral genome is constantly mutating and more replicative genomes are selected for. When a miRNA directly binds a viral RNA transcript there could be a shift in viral populations to increase the representation of genomes that are not affected by the repressive effects of the miRNA.[28] Despite this limitation there remains miRNAs who's expression and suppressive effects greatly affect viral infection.[29–31] Alternatively, miRNAs can affect viral infections through the modulation of host mRNAs. This can be via a single transcript and its downstream effectors or through concerted control of an entire host pathway.[32–34] Therein lies the link for miRNA-modulated host-virus interactions to contribute to antiviral therapeutics.

The role of miRNAs in liver infections is highlighted by the dependence of HCV on miR-122. This miRNA is the most highly expressed miRNA in the liver and is sequestered by HCV RNA during infection. The sequestered miR-122 binds two locations on the 5' UTR of the HCV RNA, stabilizing the viral RNA and protecting it from degradation.[35] Additionally, the sponging of miR-122 enables the virus to subvert detection by some PRRs. Given the tropism of HCV for liver cells and the requirement of miR-122 for viral replication, it has been proposed as a target for antiviral therapeutics with several antagomir-based therapies in various stages of development and clinical trials.[36,37] In other cases miRNAs have been demonstrated as important antiviral factors by either binding the HCV RNA or through regulated control of lipid metabolic pathways.[38,39] While these miRNAs have proven to be of interest for novel viral therapeutics, there are many miRNAs whose expression profiles are modified during viral infection and should be examined for their potential as future treatment options.[40,41] For example, miR-185 has been examined in the context

of HCV infection and biochemical assays have linked its antiviral effect to the regulation of lipid metabolic processes. Using activity-based protein profiling this regulation was examined further and established a role for serine hydrolases in the immunometabolic response to HCV infection.[24]

1.4 ABPP as a Tool to Study Host-virus Interactions

Activity-based protein profiling is a technique that is used to study the active proteome. This is to say that it doesn't rely on the abundance of a protein, but rather its activity. This activity can be affected by post-translational modifications and can be misleading if you are only measuring abundance.[42] To achieve this, ABPP employs small molecule probes that form irreversible bonds with target enzymes in a proteome. The stereotypical ABP has a warhead group who's functional group allows it to bind to the active site of an enzyme class of interest. Following this warhead is a targeting group that can be used to tune the selectivity of the ABP.[43] The last component of an ABP is the reporter group. This is typically a biotin or a fluorophore that allow the ABP to be pulled from a lysate or to visualize the labelled proteome on a gel. The reporter group can also be a biorthogonal handle such as an alkyne that would allow the ABP to later be tagged using a click reaction to add an azide-linked fluorophore or biotin.

Activity-based protein profiling has given light to new avenues of research for antiviral therapies. A fluorophosphonate probe in particular has been used to identify host factors that play roles in the viral life cycle.[44] FP selectively targets serine hydrolases, a class of enzymes with many important roles in metabolic pathways. In particular CES1 was identified as a proviral factor. CES1 is involved in the processing of cholesterol and triglycerides, important intermediates in lipid metabolism.[45] Given the reliance of HCV on lipid metabolic pathways, it speaks to reason that more serine hydrolases should be examined in the context of viral infections.

1.5 Rationale and Chapter Objectives

The works presented in this thesis all contribute to the field of antiviral research by examining proteins and other macromolecules involved in host-virus interactions and the viral life cycle. In the second chapter the role of miR-124 in lipid metabolism is examined for its potential as an antiviral therapy. This chapter has the largest focus on host-virus interactions and establishes miR-124 as an antiviral miRNA through its modulation of enzymes involved in fatty acid oxidation. In the third chapter the reactivity of an azauracil probe is studied in the context of viral polymerases and a bifunctional approach is used to improve its antiviral potential. In chapter four the reactivity of a novel hydrazone probe is characterized in the context of the mammalian proteome and a protein involved in the antiviral response is used to model the reactivity of the probe. Lastly, Chapter 5 serves to contextualize the findings of each chapter and discuss future research directions.

1.6 References

(1) Popescu, C.-I.; Riva, L.; Vlaicu, O.; Farhat, R.; Rouillé, Y.; Dubuisson, J. Hepatitis C Virus Life Cycle and Lipid Metabolism. *Biology (Basel).* **2014**, *3*, 892–921. https://doi.org/10.3390/biology3040892.

(2) Alvisi, G.; Madan, V.; Bartenschlager, R. Hepatitis C Virus and Host Cell Lipids: An Intimate Connection. *RNA Biol.* **2011**, *8* (2), 258–269. https://doi.org/10.4161/RNA.8.2.15011.

(3) Louten, J. Virus Replication. In *Essential Human Virology*; Elsevier, 2016; pp 49–67. https://doi.org/10.1016/B978-0-12-800947-5.00004-1.

(4) Hu, W.-S.; Hughes, S. H. HIV-1 Reverse Transcription. *Cold Spring Harb. Perspect. Med.* **2012**, *2* (10), 1–22. https://doi.org/10.1101/cshperspect.a006882.

(5) Rice, C. M. New Insights into HCV Replication: Potential Antiviral Targets. *Top. Antivir. Med.* **2011**, *19* (3), 117–120.

(6) Frick, D. N. HCV Helicase: Structure, Function, and Inhibition. In *Hepatitis C Viruses: Genomes and Molecular Biology*; Tan, S.-L., Ed.; Horizon Bioscience: Norfolk, 2006; pp 207–244.

(7) Menéndez-Arias, L. Mechanisms of Resistance to Nucleoside Analogue Inhibitors of HIV-1 Reverse Transcriptase. *Virus Res.* **2008**, *134* (1–2), 124–146. https://doi.org/10.1016/J.VIRUSRES.2007.12.015.

(8) Eltahla, A. A.; Luciani, F.; White, P. A.; Lloyd, A. R.; Bull, R. A. Inhibitors of the Hepatitis C Virus Polymerase; Mode of Action and Resistance. *Viruses* **2015**, *7* (10), 5206–5224. https://doi.org/10.3390/v7102868.

(9) Quan, Y.; Rong, L.; Liang, C.; Wainberg, M. A. Reverse Transcriptase Inhibitors Can Selectively Block the Synthesis of Differently Sized Viral DNA Transcripts in Cells Acutely Infected with Human Immunodeficiency Virus Type 1. *J. Virol.* **1999**, *73* (8), 6700–6707. https://doi.org/10.1128/JVI.73.8.6700-6707.1999.

(10) Gardner, K.; Hall, P. A.; Chinnery, P. F.; Payne, B. A. I. HIV Treatment and Associated Mitochondrial Pathology: Review of 25 Years of in Vitro, Animal, and Human Studies. *Toxicol. Pathol.* **2014**, *42*, 811–822. https://doi.org/10.1177/0192623313503519.

(11) Ibe, S.; Suguira, W. Clinical Significance of HIV Reverse-Transcriptase Inhibitor-Resistance Mutations. *Futur. Microbiol* **2011**, *6* (3), 295–315. https://doi.org/10.2217.

(12) Fung, A.; Jin, Z.; Dyatkina, N.; Wang, G.; Beigelman, L.; Deval, J. Efficiency of Incorporation and Chain Termination Determines the Inhibition Potency of 2=-Modified Nucleotide Analogs against Hepatitis C Virus Polymerase. *Antimicrob. Agents Chemother.* **2014**, *58* (7), 3636–3645. https://doi.org/10.1128/AAC.02666-14.

(13) Ma, H.; Jiang, W.-R.; Robledo, N.; Leveque, V.; Ali, S.; Lara-Jaime, T.; Masjedizadeh, M.; Smith, D. B.; Cammack, N.; Klumpp, K.; et al. Characterization of the Metabolic Activation of Hepatitis C Virus Nucleoside Inhibitor-D-2-Deoxy-2-Fluoro-2-C-Methylcytidine (PSI-6130) and Identification of a Novel Active 5-Triphosphate Species *. *J. Biol. Chem.* **2007**, *282* (41), 29812–29820. https://doi.org/10.1074/jbc.M705274200.

(14) Ortega-Prieto, A. M.; Sheldon, J.; Grande-Pérez, A.; Tejero, H.; Gregori, J. Extinction of Hepatitis C Virus by Ribavirin in Hepatoma Cells Involves Lethal Mutagenesis. *PLoS One* **2013**, *8* (8), 1–18. https://doi.org/10.1371/journal.pone.0071039.

(15) Cihlar, T.; Ray, A. S. Nucleoside and Nucleotide HIV Reverse Transcriptase Inhibitors: 25 Years after Zidovudine. *Antiviral Res.* **2010**, *85* (1), 39–58. https://doi.org/10.1016/J.ANTIVIRAL.2009.09.014.

(16) Esposito, F.; Corona, A.; Tramontano, E. HIV-1 Reverse Transcriptase Still Remains a New Drug Target: Structure, Function, Classical Inhibitors, and New Inhibitors with Innovative Mechanisms of Actions. *Mol. Biol. Int.* **2012**, *2012*, 1–23.

https://doi.org/10.1155/2012/586401.

(17) Ferreira, A. R.; Ramos, B.; Nunes, A.; Ribeiro, D. Hepatitis C Virus: Evading the Intracellular Innate Immunity. *J. Clin. Med.* **2020**, *9* (3), 790. https://doi.org/10.3390/jcm9030790.

(18) Sularea, V. M.; Sugrue, J. A.; O'Farrelly, C. Innate Antiviral Immunity and Immunometabolism in Hepatocytes. *Curr. Opin. Immunol.* **2023**, *80*, 102267. https://doi.org/10.1016/j.coi.2022.102267.

(19) Sung, P. S.; Shin, E. C. Interferon Response in Hepatitis C Virus-Infected Hepatocytes: Issues to Consider in the Era of Direct-Acting Antivirals. *Int. J. Mol. Sci.* **2020**, *21* (7), 9–11. https://doi.org/10.3390/ijms21072583.

(20) Odnoshivkina, U. G.; Kuznetsova, E. A.; Petrov, A. M. 25-Hydroxycholesterol as a Signaling Molecule of the Nervous System. *Biochem.* **2022**, *87* (6), 524–537. https://doi.org/10.1134/S0006297922060049.

(21) Cao, Q.; Liu, Z.; Xiong, Y.; Zhong, Z.; Ye, Q. Multiple Roles of 25-Hydroxycholesterol in Lipid Metabolism, Antivirus Process, Inflammatory Response, and Cell Survival. *Oxid. Med. Cell. Longev.* **2020**, *2020*. https://doi.org/10.1155/2020/8893305.

(22) Singaravelu, R.; O'Hara, S.; Jones, D. M.; Chen, R.; Taylor, N. G.; Srinivasan, P.; Quan, C.; Roy, D. G.; Steenbergen, R. H.; Kumar, A.; et al. MicroRNAs Regulate the Immunometabolic Response to Viral Infection in the Liver. *Nat Chem Biol* **2015**, *11* (12), 988–993.

(23) Singaravelu, R.; Quan, C.; Powdrill, M. H.; Shaw, T. A.; Srinivasan, P.; Lyn, R. K.; Alonzi, R. C.; Jones, D. M.; Filip, R.; Russell, R. S.; et al. MicroRNA-7 Mediates Cross-Talk between Metabolic Signaling Pathways in the Liver. *Sci. Rep.* **2018**, *8* (1), 361. https://doi.org/10.1038/s41598-017-18529-x.

(24) Filip, R.; Desrochers, G. F.; Lefebvre, D. M.; Reed, A.; Cravatt, B. F.; Pezacki, J. P. Profiling : Linking Enzyme Activity to MicroRNA-185 Function. *Cell Chem. Biol.* **2022**, *28* (2), 202–212. https://doi.org/10.1016/j.chembiol.2020.12.009.Profiling.

(25) Desrochers, G. F.; Filip, R.; Bastianelli, M.; Stern, T.; Pezacki, J. P. MicroRNA-27b Regulates Hepatic Lipase Enzyme LIPC and Reduces Triglyceride Degradation during Hepatitis C Virus Infection. *J. Biol. Chem.* **2022**, *298* (6), 101983. https://doi.org/10.1016/j.jbc.2022.101983.

(26) Rottiers, V.; Näär, A. M. MicroRNAs in Metabolism and Metabolic Disorders. *Nat Rev Mol Cell Biol* **2014**, *13* (4), 239–250. https://doi.org/10.1038/nrm3313.

(27) Zhu, S.; Pan, W.; Qian, Y. MicroRNA in Immunity and Autoimmunity. *J. Mol. Med.* **2013**, *91* (9), 1039–1050. https://doi.org/10.1007/S00109-013-1043-Z/FIGURES/4.

(28) Seitz, H.; Sullivan, C.; Jurak, I.; Pfeffer, S.; Girardi, E.; López, P. On the Importance of Host MicroRNAs During Viral Infection. **2018**. https://doi.org/10.3389/fgene.2018.00439.

(29) Scheel, T. K. H.; Luna, J. M.; Liniger, M.; Nishiuchi, E.; Rozen-Gagnon, K.; Shlomai, A.; Auray, G.; Gerber, M.; Fak, J.; Keller, I.; et al. A Broad RNA Virus Survey Reveals Both MiRNA Dependence and Functional Sequestration. *Cell Host Microbe* **2016**, *19* (3), 409.

https://doi.org/10.1016/J.CHOM.2016.02.007.

(30) Trobaugh, D. W.; Gardner, C. L.; Sun, C.; Haddow, A. D.; Wang, E.; Chapnik, E.; Mildner, A.; Weaver, S. C.; Ryman, K. D.; Klimstra, W. B. RNA Viruses Can Hijack Vertebrate MicroRNAs to Suppress Innate Immunity. *Nature* **2014**, *506* (7487), 245. https://doi.org/10.1038/NATURE12869.

(31) Guo, X.-K.; Zhang, Q.; Gao, L.; Li, N.; Chen, X.-X.; Feng, W.-H. Increasing Expression of MicroRNA 181 Inhibits Porcine Reproductive and Respiratory Syndrome Virus Replication and Has Implications for Controlling Virus Infection. *J. Virol.* **2013**, *87* (2), 1159–1171. https://doi.org/10.1128/JVI.02386-12.

(32) Gao, L.; Guo, X.-K.; Wang, L.; Zhang, Q.; Li, N.; Chen, X.-X.; Wang, Y.; Feng, W.-H. MicroRNA 181 Suppresses Porcine Reproductive and Respiratory Syndrome Virus (PRRSV) Infection by Targeting PRRSV Receptor CD163. **2013**, *87*, 8808–8812. https://doi.org/10.1128/JVI.00718-13.

(33) Lodge, R.; Ferreira Barbosa, J. A.; Lombard-Vadnais, F.; Gilmore, J. C.; Deshiere, A.; Gosselin, A.; Wiche Salinas, T. R.; Bego, M. G.; Power, C.; Routy, J. P.; et al. Host MicroRNAs-221 and -222 Inhibit HIV-1 Entry in Macrophages by Targeting the CD4 Viral Receptor. *Cell Rep.* **2017**, *21* (1), 141–153. https://doi.org/10.1016/J.CELREP.2017.09.030.

(34) Shim, B.-S.; Wu, W.; Kyriakis, C. S.; Bakre, A.; Jorquera, P. A.; Perwitasari, O.; Correspondence, R. A. T.; Tripp, R. A. MicroRNA-555 Has Potent Antiviral Properties

against Poliovirus. *J. Gen. Virol.* **2016**, *97*, 659–668. https://doi.org/10.1099/jgv.0.000372.

(35) Luna, J. M.; Scheel, T. K. H.; Danino, T.; Shaw, K. S.; Mele, A.; Fak, J. J.; Nishiuchi, E.; Takacs, C. N.; Catanese, M. T.; De Jong, Y. P.; et al. Hepatitis C Virus RNA Functionally Sequesters MiR-122. *Cell* **2015**, *160* (6), 1099–1110. https://doi.org/10.1016/j.cell.2015.02.025.

(36) Machlin, E.; Sarnow, P.; Sagan, S. Combating Hepatitis C Virus by Targeting MicroRNA-122 Using Locked Nucleic Acids. *Curr. Gene Ther.* **2012**, *12* (4), 301–306. https://doi.org/10.2174/156652312802083558.

(37) Sarnow, P.; Sagan, S. M. Unraveling the Mysterious Interactions Between Hepatitis C Virus RNA and Liver-Specific MicroRNA-122. *Annu. Rev. Virol.* **2016**, *3*, 309–332. https://doi.org/10.1146/annurev-virology-110615-042409.

(38) Pedersen, I. M.; Cheng, G.; Wieland, S.; Volinia, S.; Croce, C. M.; Chisari, F. V; David, M. Interferon Modulation of Cellular MicroRNAs as an Antiviral Mechanism. *Nature* **2007**, *449* (7164), 919–922. https://doi.org/10.1038/nature06205.

(39) Shirasaki, T.; Honda, M.; Shimakami, T.; Horii, R.; Yamashita, T.; Sakai, Y.; Sakai, A.; Okada, H.; Watanabe, R.; Murakami, S.; et al. MicroRNA-27a Regulates Lipid Metabolism and Inhibits Hepatitis C Virus Replication in Human Hepatoma Cells. *J. Virol.* **2013**, *87* (9), 5270–5286. https://doi.org/10.1128/JVI.03022-12.

(40) Li, Q.; Lowey, B.; Sodroski, C.; Krishnamurthy, S.; Alao, H.; Cha, H.; Chiu, S.; El-Diwany, R.; Ghany, M. G.; Liang, T. J. Cellular MicroRNA Networks Regulate Host

Dependency of Hepatitis C Virus Infection. *Nat. Commun.* **2017**, *8* (1). https://doi.org/10.1038/s41467-017-01954-x.

(41) El-Diwany, R.; Wasilewski, L. N.; Witwer, K. W.; Bailey, J. R.; Page, K.; Ray, S. C.; Cox, A. L.; Thomas, D. L.; Balagopal, A. Acute Hepatitis C Virus Infection Induces Consistent Changes in Circulating MicroRNAs That Are Associated with Nonlytic Hepatocyte Release. *J. Virol.* **2015**, *89* (18), 9454–9464. https://doi.org/10.1128/JVI.00955-15.

(42) Kobe, B.; Kemp, B. E. Active Site-Directed Protein Regulation. *Nature* **1999**, *402* (6760), 373–376. https://doi.org/10.1038/46478.

(43) Niphakis, M. J.; Cravatt, B. F. Enzyme Inhibitor Discovery by Activity-Based Protein Profiling. *Annu. Rev. Biochem.* **2014**, *83*, 341–377. https://doi.org/10.1146/ANNUREV-BIOCHEM-060713-035708.

(44) Blais, D. R.; Nasheri, N.; McKay, C. S.; Legault, M. C. B.; Pezacki, J. P. Activity-Based Protein Profiling of Host–Virus Interactions. *Trends Biotechnol.* **2012**, *30* (2), 89. https://doi.org/10.1016/J.TIBTECH.2011.08.001.

(45) Blais, D. R.; Lyn, R. K.; Joyce, M. A.; Rouleau, Y.; Steenbergen, R.; Barsby, N.; Zhu, L. F.; Pegoraro, A. F.; Stolow, A.; Tyrrell, D. L.; et al. Activity-Based Protein Profiling Identifies a Host Enzyme, Carboxylesterase 1, Which Is Differentially Active during Hepatitis C Virus Replication. *J. Biol. Chem.* 2010, *285* (33), 25602–25612. https://doi.org/10.1074/jbc.M110.135483.

Chapter 2: MicroRNA-124 Regulates Fatty Acid and Triglyceride Homeostasis

Initially published as Tyler A. Shaw, Raguath Singaravelu, Megan H. Powdrill, Jordan Nhan, Nadine Ahmed, Dennis Özcelik, and John Paul Pezacki. (2018) MicroRNA-124 Regulates Fatty Acid and Triglyceride Homeostasis. *iScience* 10:149-157

2.1 Statement of Contribution

Conceptualization, J.P.P., R.S., and M.H.P.; Methodology, R.S., M.H.P, and T.A.S.; Formal Analysis, R.S., M.H.P., T.A.S., D.Ö ., and J.P.P.; Investigation, M.H.P., T.A.S., J.N., N.A., and D.Ö .; Writing – Original Draft, R.S., T.A.S., M.H.P., N.A., and J.P.P.; Review & Editing, all authors; Funding Acquisition, R.S. and J.P.P.; Supervision, R.S., M.H.P., and J.P.P.

2.1.1 Acknowledgements

J.P.P. is supported by grant funding from the Canadian Institutes of Health Research (CIHR), Canada (220886) and Natural Sciences and Engineering Research Council of Canada (NSERC), Canada (210719). R.S. received graduate student funding from the Canadian Network on hepatitis C and is the recipient of post-doctoral funding from the Life Science Research Foundation. M.H.P. received postdoctoral funding from the Canadian Network on Hepatitis C. D.O¨ . is the recipient of post-doctoral funding from the CIHR. N.A. is the recipient of doctoral postgraduate scholarship from the Natural Sciences and Engineering Research Council of Canada. mRNA microarray profiling was performed by The Center for Applied Genomics (TCAG), The Hospital for Sick Children, Toronto, ON, Canada. Gene expression profiling data from miR-124 and control mimic-transfected Huh7.5 cells have been deposited to NCBI Gene Expression Omnibus under the following accession number: GSE122134.

2.2 Summary

MicroRNAs (miRNAs) are part of a complex regulatory network that modulates cellular lipid metabolism. Here, we identify miR-124 as a regulator of triglyceride (TG) metabolism. This study advances our knowledge of the role of miR-124 in human hepatoma cells. Transcriptional profiling of Huh7.5 cells overexpressing miR-124 reveals enrichment for host factors involved in fatty acid oxidation among repressed miRNA targets. In addition, miR-124 down-regulates arylacetamide deacetylase (AADAC) and adipose triglyceride lipase, lipases proposed to mediate breakdown of hepatic TG stores for lipoprotein assembly and mitochondrial β-oxidation. Consistent with the inhibition of TG and fatty acid catabolism, miR-124 expression promotes cellular TG accumulation. Interestingly, miR-124 inhibits the production of hepatitis C virus, a virus that hijacks lipid pathways during its life cycle. Antiviral activity of miR-124 is consistent with repression of AADAC, a pro-viral host factor. Overall, our data highlight miR-124 as a novel regulator of TG metabolism in human hepatoma cells.

2.3 Introduction

Fatty acids serve as an important energy source for mammals in the fasted state.[1] The liver is the central organ in fatty acid metabolism, responsible for fatty acid uptake from serum, de novo lipid synthesis, and fatty acid oxidation or secretion in the form of lipoproteins.[2] Fatty acid oxidation serves to produce acetyl CoA, nicotinamide adenine dinucleotide (NADH), and flavin adenine dinucleotide (FADH2). NADH and FADH2 serve as electron carriers to feed into the electron transport chain to generate ATP. Both saturated and unsaturated fatty acids are broken down through reactions catalyzed in both mitochondria and peroxisomes. Although the key

enzymes catalyzing fatty acid breakdown have been elucidated, the regulatory mechanisms governing fatty acid oxidation are not fully understood.

Under pathological conditions, hepatic fatty acid trafficking can be disrupted, resulting in increased fatty acid storage in the form of triglycerides (TGs). This manifests clinically as hepatic steatosis, as observed in hepatitis C virus (HCV) infection and fatty liver disease.[3] In the case of viral infection, the pathogen may manipulate fatty acid flux to create specific lipid-rich microenvironments to facilitate its life cycle.[4] Proper regulatory controls on metabolic gene networks are integral to maintaining proper energy homeostasis and preventing hepatic metabolic disorders.

Recent work has demonstrated that microRNAs (miRNAs) are crucial to proper regulation of hepatic TG homeostasis.[5] These small RNAs, ranging in size from 21 to 24 nucleotides, modulate gene expression through partial pairing with mRNAs, generally in the 3' untranslated region (3'-UTR).[6] Canonical miRNA targeting of mRNAs results in a combination of transcript destabilization and translation repression.[6] These small RNAs simultaneously regulate multiple targets within the same pathway.[7] The critical role of miRNAs in the maintenance of hepatic lipid homeostasis has been established, with several miRNAs regulating aspects of fatty acid oxidation, lipid biosynthesis, and lipid excretion.[5,8–11] For example, miR-122 has been shown to extensively modulate hepatic lipid microenvironments.[12] Given the abundance of the miRNA in the liver, it has been found to be directly involved in modulating cholesterol and hepatic fatty acid metabolism.[12–14] In addition, modulation of HCV replication by miR-122 has been well established.[15] A thorough understanding of the functional role of miRNAs in hepatic fatty acid metabolism is critical to properly define the etiology of metabolic disorders.

Recent studies have demonstrated the involvement of miR-124-3p (miR-124) in hepatobiliary pathologies.[16,17] Expression of miR-124 has been shown to be directly regulated by the liver-enriched transcription factor, hepatocyte nuclear factor 4a.[17] Recent work demonstrated that hepatic delivery of the miRNA suppresses tumorigenesis in mice.[17] To date, miR-124 has mainly been examined in the context of processes in the central nervous system, where it is highly expressed, whereas its physiological function in the liver remains poorly studied.[18]

Herein, we examine the role of miR-124 in hepatic lipid homeostasis. Our data suggest a novel role for this miRNA in the metabolic stress response. Genome-wide expression profiling reveals that miR-124 concertedly represses multiple genes involved in fatty acid oxidation and TG hydrolysis. Through repression of these catabolic pathways, miR-124 promotes hepatocellular TG storage. Interestingly, we also demonstrate that miR-124 impairs the infectivity of HCV, a hepatotropic virus with a strong dependence on hepatic lipid pathways for its propagation. Overall, our work demonstrates that miR-124 is a novel regulator of fatty acid homeostasis and HCV infection.

2.4 Methods

2.4.1Materials

The human hepatocellular carcinoma cell line Huh7.5 was a kind gift from Dr. Charles M. Rice (Rockefeller University, New York, NY). All mirVana mimics and inhibitors, along with controls, were purchased from Ambion (Austin, TX).

2.4.2 Cell Culture, Transfections, and Viral Infection

Huh7.5 cells were maintained in Dulbecco's Modified Eagle Medium (DMEM) supplemented with 10 % fetal bovine serum (FBS) and 100 nM non-essential amino acids. For transfections of uninfected cells, cells were seeded in 6-well plates. The following day, the transfection mixture containing RNAiMax (Thermo Fisher Scientific) and the miRNA control mimic/inhibitor or miR-124 mimic/inhibitor at a final concentration of 100 nM in Opti-MEM was added to the cells. For RNA analysis, after 48 h, cells were harvested in RLT Plus lysis buffer (RNeasy Plus kit, Qiagen, Mississauga, ON). For western blot analysis, cells were lysed 48 h post-transfection in 1X SDS lysis buffer (50 mM Tris-HCl [pH 6.8], 2 % SDS, and 10 % glycerol).

Serum starvation experiments were performed by seeding Huh7.5 cells in 6-well plates and growing cells in serum free media for 48 h. Cells were then lysed using ML Buffer (NucleoSpin miRNA Isolation Kit lysis buffer; Macherey-Nagel, Düren, Germany).

HCV infections of Huh7.5 cells were performed with the HCV JFH1T strain. This strain is derived from the cell culture-adapted JFH-AM1 strain and contains three amino acid substitutions.[1] Briefly, cells were infected at an MOI of 0.1 then virus was removed following a 5 h infection. Forty-eight hours post infection, supernatant was collected for virus titration and cells were lysed in ML Buffer (Macherey-Nagel) for RNA extraction. For examining miRNA's antiviral effects, Huh7.5 cells were transfected with 100 nM of miRNA mimic (control or miR-124). Twenty-four hours post-transfection, cells were infected with HCV JFH1T. At 48 h post-infection, cell supernatants were removed and used for infectious titer determination, and cells were lysed with RLT Plus lysis buffer (Qiagen) for RNA isolation.

2.4.3 Quantitative Real-Time PCR

RNA was quantified using a NanoDrop (Thermo Fisher Scientific). Reverse transcription of 250 ng of RNA was performed with random hexamers using a SuperScript II Reverse Transcriptase kit (Life Technologies, Carlsbad, CA) according to the manufacturer's protocol. qPCR was subsequently performed on a CFX Connect Real-Time PCR Detection System (Bio-Rad, Hercules, CA) using SsoAdvanced Universal SYBR Green Supermix (Bio-Rad) according to the manufacturer's instructions. Primers were added to a final concentration of 500 nM in a total reaction volume of 10 µL. Primers used for qPCR are listed in Table S3. All primers were validated prior to use with melt curves and standard curves. For determination of miRNA expression levels, 5 ng total RNA was reverse transcribed using the TaqMan MicroRNA Reverse Transcription Kit (Life Technologies), and qPCR reactions were performed using TaqMan Universal PCR Mastermix (No AmpErase UNG; Life Technologies) with primers specific for miR-124 or RNU6B. For both mRNA and miRNA quantification, the $2^{-\Delta\Delta Ct}$ method was used to calculate fold changes in expression relative to control samples, with 18S rRNA or RNU6B levels being used for normalization.[2]

2.4.4 Immunoblotting

Lysates were thawed and passed through a 21G needle (BD Biosciences) before determining their protein concentration by DC assay (Bio-Rad). SDS-PAGE was performed using 10 to 20 ug of protein lysate loaded on a 12 % TGX gel (Bio-Rad) and the migrated proteins were visualized on a ChemiDoc MP (Bio-Rad) using the Stain Free activation protocol for 5 min. The migrated proteins were then transferred onto a PVDF membrane using a Trans-Blot Turbo (Bio-Rad). Membranes were then blocked with 5 % BSA or 5 % milk in TBS-T prior to incubation with

primary antibodies. The membrane was then probed with either mouse anti-AADAC (1:1000 dilution; Santa Cruz Biotechnology, sc-390591), mouse anti-HADHA (1:1000 dilution, Santa Cruz Biotech., sc-374497), or mouse anti-PECI (1:1000 dilution, Santa Cruz Biotech., sc-136374) followed by goat anti-mouse antibody conjugated to horseradish peroxidase (1:20000; Jackson ImmunoResearch Laboratories, Inc., 115-035-062). Blots were visualized with Clarity ECL Western blotting reagents (Bio-Rad) on a ChemiDoc MP (Bio-Rad). Stain-free detection of total protein loading was used for the control. Blot images were cropped and adjusted for contrast using Image Lab (Bio-Rad).

2.4.5 Triglyceride Assays

Triglyceride levels were quantified by spectrophotometric analyses, using the TG quantification kit (BioVision) as per manufacturer's protocols, with a few minor modifications. Cells were lysed from a 6-well plate in 5 % NP-40 substitute (BioShop, Canada) in water. Samples were diluted 1 in 10 in TG assay buffer; then 50 uL was added to a 96-well plate in duplicate, with and without lipase. The remainder of the protocol mirrored the manufacturer's protocol.

2.4.6 Oil Red O Lipid Staining and Microscopy

Huh7.5 were seeded in 4-well chamber slides. The next day cells were transfected with 100 nM of miRNA mimic (control or miR-124). 48h post-transfection, cells were washed with 1X with PBS and then fixed with 10% formaldehyde for 10 mins at RT. Following the incubation, 10% formaldehyde was replaced with fresh 10% formaldehyde and incubated at RT for an hour. Fixed cells were then washed 2X with water and incubated for 5 minutes with 60% isopropanol. Cells were completely dried before incubation with 60% isopropanol containing oil red O for 10 minutes. Oil Red O (sigma) stock solution was prepared at 0.35% final concentration in

isopropanol and filtered through 0.2μm filter. Cells were immediately washed 5X with water and chamber slide was then mounted with ProLong™ Gold Antifade Mountant with DAPI (Thermofisher). Images were then acquired with Axiophot fluorescence microscope (Zeiss) attached to a DP-70 Colour CCD camera (Olympus) with a 50W mercury fluorescence excitation light source. Images were taken using ImagePro 6 software suite (mediaCybernetics) and analyzed using ImageJ (NIH).

2.4.7 Infectivity Assay

Supernatants of HCV infected cells were filtered through a 45 μm PES filter (Ultident , Saint- Laurent, Canada) before being serially diluted 10-fold in medium. For HCV infectivity assays, 100 μL of each dilution was then used to infect Huh7.5 cells seeded (at 5×10 4 per well) onto 8-well Lab-Tek II chamber slides (NUNC) for 4 h. Following incubation, the infectious medium was removed and replaced with fresh medium. Forty-eight hours post infection, cells were fixed and stained with HCV core monoclonal antibody (1:100; ThermoFisher Scientific; MA1080), followed by a secondary antibody, Alexa Fluor 488–conjugated goat anti-mouse (1:250; ThermoFisher Scientific; A-11029). Viral titers are expressed as the number of focus-forming units (FFU) per mL of supernatant.

2.4.8 mRNA Microarray

RNA isolation from Huh7.5 cells was performed with the RNeasy kit (Qiagen). Gene expression profiling was performed using Affymetrix Human Gene ST.2.0 arrays. Data was normalized and analyzed using the Applied Biosystems Transcriptome Analysis Console (v4.0), according to the manufacturer's protocols. Pathway enrichment analysis was performed on genes repressed by miR-124 more than 1.5-fold and predicted by TargetScan, irrespective of

conservation, to be a miR-124 target.[3] This analysis was performed using the ToppGene Suite.[4] For ToppGene pathway enrichment analysis, P-values were adjusted with Bonferroni correction.

2.5 Results

2.5.1 miR-124 Expression Is Modulated during HCV Infection and Serum Depletion

The antiviral oxysterol 25-hydroxycholesterol (25-HC) plays an important role in regulating the immune response to viral infection. The oxysterol has multifaceted effects through modulation of lipid metabolism and inflammatory and stress response pathways.[19] Recent work by our group identified numerous miRNAs that are differentially expressed following treatment with 25-HC.[10] One of these 25-HC-regulated miRNAs, hsa-miR-124-3p (miR-124), has been shown to play a role in liver disease.[16,17]

We sought to examine whether miR-124 plays a functional role in the liver. Based on its regulation by 25-HC, we hypothesized that miR-124 is dysregulated during metabolic stresses in hepatocytes. We first measured the expression of the miRNA during serum depletion. We found that cultivation of Huh7.5 hepatoma cells for 48 hr in serum-free media increased miR-124 expression approximately 2-fold compared with normal culturing conditions (Figure 2-1A). We also considered viral infection as another source of metabolic stress, which could influence miR-124 expression. HCV is a hepatotropic virus that alters liver metabolism to facilitate its viral life cycle. Our previous work, along with others', demonstrated that HCV infection decreases miR-124 expression.[10,20] We reproduced this finding using a cell-culture-adapted high-titer strain of HCV.[21] Forty-eight hours post-infection, we observed a 2-fold decrease in miR-124 expression levels (Figure 2-1B). Taken together, these results demonstrate that miR-124 levels are modulated

during metabolic stresses (i.e., serum depletion and HCV infection) and point toward a metabolic regulatory role for the miRNA in liver cells.

2.5.2 miR-124 Targets Genes with Functional Roles in Fatty Acid Catabolism

To investigate the hepatic pathways regulated by miR-124, we performed gene expression profiling in Huh7.5 cells transfected with control or miR-124 mimic. A summary of the top 10 up- and down-regulated genes is given in Table 6-1. To identify the direct targets of miR-124 in the hepatic cells, we examined the overlap between predicted targets of miR-124 (4,450 genes as per TargetScan) and genes repressed by miR-124 mimic transfection by over 1.5-fold (1,693 genes).[22] For our analysis, a cutoff of 1.5-fold was utilized given that direct targeting of a specific gene by a single miRNA may induce modest overall changes in the gene's expression. However, cooperative targeting of multiple genes, involved in the same pathway, by a single miRNA may induce more pronounced phenotypic changes.[23,24] The overlap produced a list of 425 genes. Bioinformatics analysis via the ToppGene Suite was performed to identify associated pathways enriched in this list of repressed miR-124 targets.[25] Interestingly, fatty acid degradation and metabolism were the only two significantly enriched pathways (Table 6-2; $p < 0.05$). We then used qRT-PCR to validate miR-124-mediated repression of genes in the fatty acid β-oxidation pathway bearing putative miR-124-binding sites in their 3'UTR (Figure 2-2A). We analyzed the expression of HADH, HADHA, HADHB, PECR, ACADVL, ECI2, CPT1A, ACAA2, and ACADSB. Consistent with the microarray results, each of these genes' expression was found to be down-regulated by qRT-PCR (Figures 2-2A, 6-1, and 6-2). Notably, miR-124's repression of CPT1A expression is consistent with previous work demonstrating that this gene is a direct miR-124 target in prostate cancer cells.[26] Immunoblot analyses further confirmed similar reduction of HADHA and ECI2 protein levels (Figure 2-2B). Interestingly, serum starvation of Huh7.5 cells, which

promotes miR-124 expression, results in a significant decrease in ACADSB expression, consistent with physiologically relevant miR-124 repression of this gene during metabolic stress (Figure 6-3A). This is further supported by rescue of ACADSB expression during serum starvation by miR-124 inhibition (Figure 6-3B). The sum of miR-124's repressive effects on these individual genes should result in a greater overall effect of miR-124 on fatty acid oxidation.

Carnitine is a key cofactor that enables shuttling of acyl-CoAs into the mitochondria. Long-chain fatty acids are otherwise impermeable to the mitochondria. Closer examination of the microarray results revealed a down-regulation in the expression of SLC25A20, a gene encoding carnitine- acylcarnitine translocase, which mediates transport of acyl carnitines across the inner mitochondrial membrane; ALDH9A1, a gene encoding 4-trimethylaminobutyraldehyde dehydrogenase, which is proposed to be involved in the hepatic synthesis of carnitine, a key cofactor for the transfer of long-chain fatty acids to mitochondria for oxidation; and SLC22A5, a transporter for carnitine uptake from serum (Figures 6-1 and 6-2).[27] qRTPCR also validated the down-regulation of these three miR-124 targets in Huh7.5 cells transfected with miR-124 mimics (Figure 2-2C). Collectively, these data demonstrate that miR-124 is involved in the repression of carnitine homeostasis and fatty acid oxidation.

2.5.3 miR-124 Promotes Cellular TG Accumulation

Inhibition of fatty acid oxidation results in an accumulation of free fatty acids, which can be incorporated into TGs for storage. Therefore, we hypothesized that miR-124 overexpression would influence cellular TG levels. We assayed TG levels in control and miR-124-mimic-transfected Huh7.5 cells and observed a significant increase in cellular TG levels (Figure 2-3A), in line with miR-124's repression of fatty acid oxidation (Figure 2-2). Similarly, oil red O staining

revealed an increase in cellular lipid levels during miR-124 mimic transfection (Figure 2-3B). Collectively, our data demonstrate that miR-124 promotes hepatocellular TG accumulation.

2.5.4 miR-124 Inhibits Expression of Triglyceride Hydrolases

We sought to identify additional targets of miR-124, which could contribute to miR-124's induction of TG accumulation. Hydrolysis of TG stores mediates mobilization of fatty acids for very-low-density lipoprotein synthesis or as substrates for fatty acid oxidation. Therefore, repressed expression of TG hydrolases (TGHs) could also contribute to miR-124-induced increase in cellular TG levels. We noted that arylacetamide deacetylase (AADAC), an endoplasmic reticulum-localized carboxylester hydrolase that hydrolyzes TGs, was among the most highly miR-124-repressed genes in our microarray data (Table 6-1).[28]

Down-regulation at the transcriptional level was verified by qRT-PCR (Figure 2-4A), and immunoblot analysis confirmed that protein levels were also decreased in the miR-124-mimic-treated cells (Figure 2-4B). The microarray data also revealed decreased carboxylesterase 1 (CES1) and NR1H4 expression. CES1 is another hydrolase responsible for TG breakdown, whereas NR1H4 encodes for the farnesoid X receptor (FXR). Neither gene possesses miR-124-binding sites in their 3' UTR. FXR is a nuclear hormone receptor, which regulates the clearance of hepatic TGs, in part through induced expression of CES1.[28] qRT-PCR analysis validated an over 7.6-fold decrease in CES1 and an over 3.5-fold decrease in NR1H4 expression levels (Figure 2-4A). Surprisingly, we did not observe a down-regulation of CES1 protein expression levels; however, a recent study suggests that the half-life of the CES1 protein is approximately 96 hr.[29] This suggests that the timescale of our miR-124 overexpression experiments (72 hr) may not have been sufficient to enable observation of miR-124's repressive effect on CES1 expression.

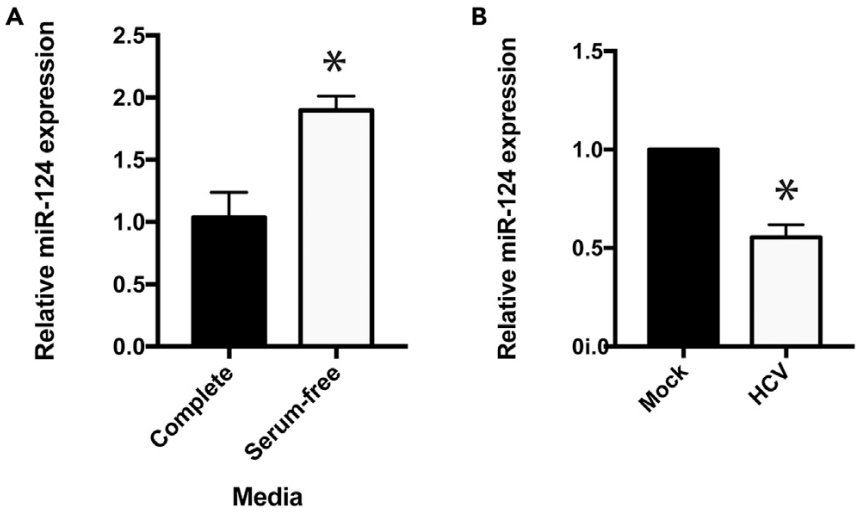

Figure 2-1. Serum Starvation and HCV Infection Modulate miR-124 Expression

(A) Huh7.5 cells were cultured in complete or serum-free media for 48 hr. qRT-PCR was performed to measure relative miR-124 expression (n = 3). (B) Huh7.5 cells were infected with HCV, and miR-124 expression levels relative to mock were measured 48 hr postinfection (n = 3). Data are represented as the mean G SEM (*p < 0.05).

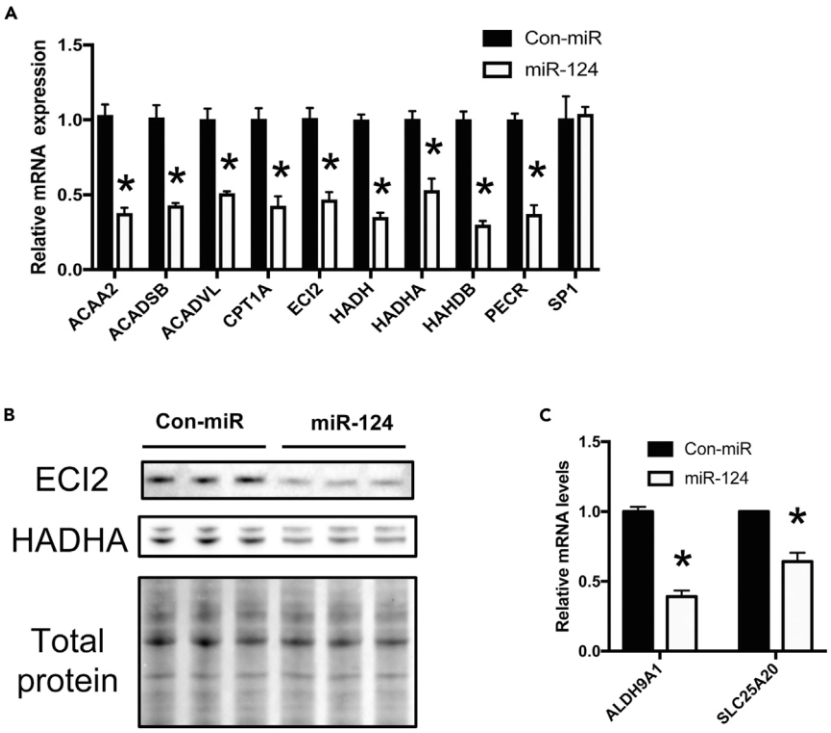

Figure 2-2. miR-124 Down-Regulates Fatty Acid Oxidation

(A) Relative mRNA expression levels of miR-124 predicted targets with roles in fatty acid degradation in Huh7.5 cells transfected with control (Con-miR) or miR-124 mimic, as measured by qRT-PCR (n > 5). (B) Immunoblot analysis of protein expression levels of ECI2 and HADHA (lower band) in miR-124- or control mimic- (Con-miR) transfected Huh7.5 cells. Three independent biological replicates are shown, and total protein detection serves as the loading control. The blot is cropped to emphasize relevant bands. (C) Relative mRNA expression levels of miR-124 predicted targets with roles in carnitine biosynthesis (n > 6). Data are represented as the mean G SEM (*p < 0.05). See also Tables 6-1 and 6-2.

Lastly, we observed miR-124-mediated repression of PNPLA2 expression in the microarray data. This miR-124 target gene encodes adipose triglyceride lipase (ATGL), a hepatic lipase responsible for mediating hepatic TG hydrolysis and channeling hydrolyzed fatty acids to β-oxidation.[30] This is consistent with our qRT-PCR data (Figure 2-4A), and previous reports demonstrating miR-124-mediated repression of PNPLA2 expression in adipocytes.[31] Collectively, concordant repression of TG hydrolysis and fatty acid oxidation should contribute to TG accumulation mediated by miR-124 overexpression in hepatic cells.

2.5.5 miR-124 Inhibits HCV Infection

We and others have identified several miRNAs that are differentially expressed during infection with HCV, promoting either pro- or antiviral environments via modulation of genes involved in lipid pathways.[9,10,32,33] We postulated, given HCV's strong reliance on hepatic lipid pathways to facilitate its life cycle, that miR-124, through regulation of TG homeostasis, could influence viral infectivity. miR-124 overexpression in Huh7.5 cells decreased viral infectivity and repressed the expression of miR-124 targets (Figure 6-4). This is consistent with a previous study demonstrating that decreased expression of AADAC impairs production of HCV.[34] Our work suggests that miR-124 inhibits HCV infection through inhibition of AADAC expression.

2.6 Discussion

miRNAs have emerged as a key regulatory layer in the maintenance of hepatic lipid homeostasis.[5] However, there are limited examples of miRNAs playing key roles in the regulation of TG catabolism. Hepatic miR-33 has been shown to regulate several key enzymes in the fatty acid oxidation pathway.[35] Herein, we identify a novel function for miR-124 in the regulation of

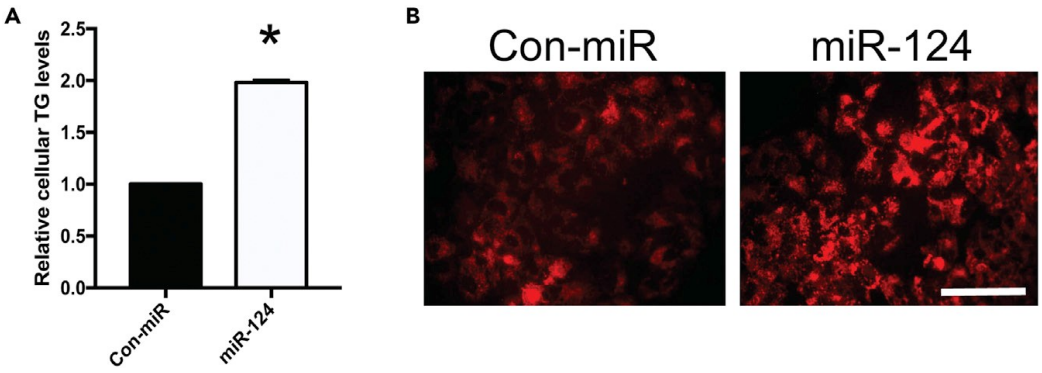

Figure 2-3. miR-124 Promotes Cellular Triglyceride Accumulation

(A) Relative cellular TG content in control and miR-124-mimic-transfected Huh7.5 cells as assessed by TG assays (n = 3). Data are representative of the mean G SEM (*$p < 0.05$). (B) Oil red O staining of cellular lipid droplet content in control and miR-124-mimic-transfected Huh7.5 cells. Cells were visualized using fluorescence microscopy. Scale bar, 100 μm.

TG catabolism via multiple key enzymes involved in fatty acid oxidation and TG hydrolysis. Through concerted targeting of multiple genes,miR-124 produces a cooperative inhibitory effect on lipid catabolism, resulting in hepatocellular TG accumulation (Figure 2-5). This highlights an emerging theme in miRNA regulation whereby miRNAs have evolved to target multiple genes in the same pathway to produce a greater overall regulatory effect.

Our work demonstrates that miR-124 suppresses the expression of several key enzymes in the mitochondrial β-oxidation pathway (ACADVL, ACADSB, HADHA, HADHB, HADH, and ACAA2). ACADVL encodes the mitochondrial membrane-bound long-chain acyl-CoA dehydrogenase (VLCAD), which is responsible for the first step of the mitochondrial fatty acid oxidation cycle for saturated long-chain fatty acids (14–20 carbons). VLCAD catalyzes the dehydrogenation of acyl-CoAs to trans-D2-enoyl-CoA. ACADSB performs an analogous dehydrogenation reaction for short/branched fatty acids. HADHA and HADHB form a hetero-octamer complex, called the mitochondrial trifunctional protein, responsible for catalyzing the last three steps of fatty acid oxidation for long-chain fatty acids. Specifically, HADHA is responsible for catalyzing trans-D2-enoyl CoA hydration to form L-3-hydroxyacyl-CoA, and the subsequent dehydrogenation to 3-ketoacyl CoA; then HADHB sequentially catalyzes long-chain keto-acyl-CoA thiolase activity producing an acetyl-CoA and an acyl-CoA. For short- and medium-chain fatty acids, HADH and ACAA2 catalyze the last two steps of the oxidation. For unsaturated fatty acids, cis-enoyl-CoA esters have to be transformed to trans configurations to enable their catabolism. ECI2 contributes to the catabolism of unsaturated fatty acids by catalyzing an isomerization of cis-D3 and trans-D3-enoyl CoA esters into trans-D2-enoyl-CoA esters. Fatty acid oxidation can also be catalyzed in the peroxisome, with the participation of a different set of enzymes, including PECR, which encodes a peroxisomal trans-D2-enoyl-CoA reductase.

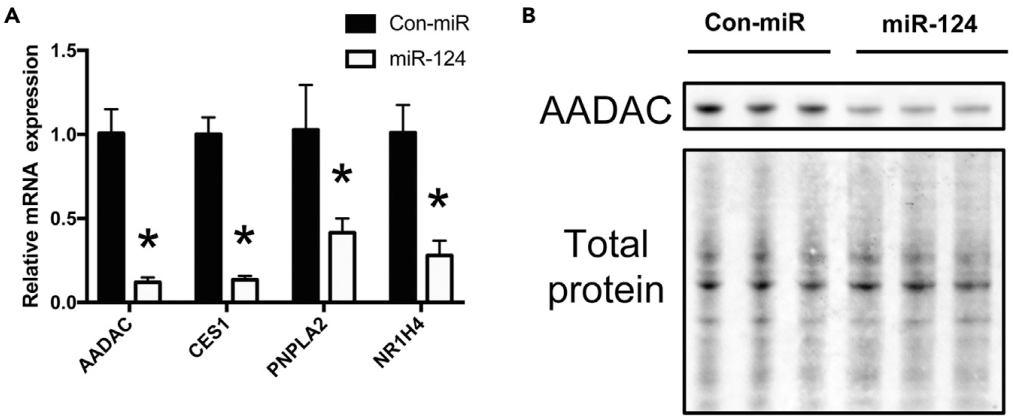

Figure 2-4. miR-124 Down-Regulates Genes associated with Triglyceride Hydrolysis

(A) Relative mRNA expression levels of PNPLA2, CES1, NR1H4, and AADAC in control and miR-124-mimic-transfected cells as assessed by qRT-PCR analysis ($n > 5$). Data are represented as the mean G SEM (*$p < 0.05$). (B) Immunoblot analysis of protein expression levels of AADAC in miR-124- or control mimic- (Con-miR) transfected Huh7.5 cells. Three independent biological replicates are shown, and total protein detection serves as loading control. Blot is cropped to emphasize relevant bands.

Collectively, our data highlight miR-124 as a regulator of multiple key nodes in both peroxisomal and mitochondrial β-oxidation.. Our data demonstrate that miR-124 down-regulates proteins responsible for carnitine uptake from plasma (SLC22A5), carnitine synthesis (ALDH9A1), and acyl-CoA conjugation of carnitine (CPT1A), as well as translocation of acyl-CoA-carnitine through the inner mitochondrial membrane (SLC25A20). As the CPT1A-catalyzed acyl transfer to carnitine represents one of the rate-limiting steps of fatty acid oxidation, this suggests that targeting of CPT1A by miR-124 should enable the miRNA to exert greater regulatory control over fatty acid oxidation.

A subset of the genes repressed by miR-124 do not possess canonical seed sites, suggesting a non-canonical or indirect mode of regulation. A previous study, which utilized Argonaute 2 (Ago2) co-immunoprecipitation followed by mRNA microarray analysis to identify miR-124 targets in HEK293 cells, suggested that miR-124-loaded Ago2 directly interacted with the 3' UTR of HADHB mRNA.[36] A subsequent study confirmed this interaction in mice brains using high-throughput sequencing of RNAs isolated by Ago cross-linking immunoprecipitation.[37] Close examination of the 3` UTR reveals a potential miR-124 ''G-bulge'' site (Figure 6-5), which is a recently described non-canonical miRNA-binding motif where a G nucleotide bulge is allowed in the mRNA (in the corresponding nucleotide position 5–6 of the miRNA).[38] Another potently repressed gene, AADAC, possesses no mRNA-binding sites in the 3' UTR to the best of our knowledge; however, examination of the open reading frame (ORF) reveals the presence of one canonical site. Typically, ORF-binding sites are less prone to miRNA regulation; however, if the sites are preceded by a stretch of rare codons, the recognition site may be functional.[39] Examination of the three codons upstream of the binding site reveal three rare codons (usage <12%; Figure 6-6), suggesting that miR-124 may regulate AADAC through a functional ORF-binding site. This

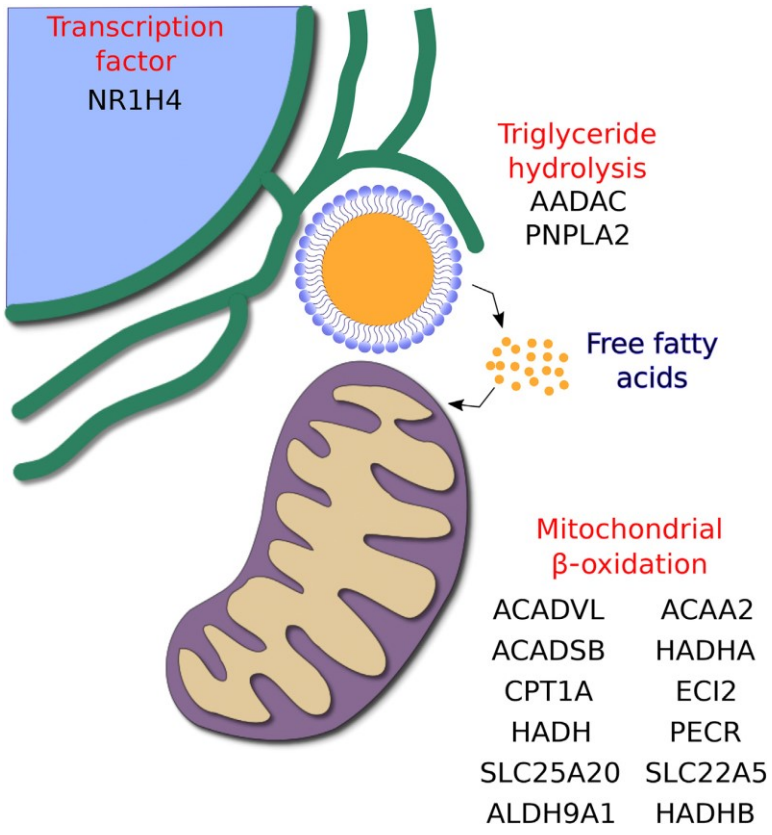

Figure 2-5. miR-124 Down-Regulates Fatty Acid and Triglyceride Catabolism.

Schematic depicting concerted regulation by miR-124 of genes involved in triglyceride hydrolysis and fatty acid catabolism.

implies that miR-124 regulates a subset of its metabolic gene targets using non-canonical mode of target recognition.

Several of the miR-124 targets have been established as targets of the transcription factor peroxisome proliferator-activated receptor α (PPAR-α), including HADHA, HADHB, ACAA2, ACADVL, SLC25A20, SLC22A5, and CPT1A.[40] This nuclear hormone receptor acts as a master transcriptional regulator of mitochondrial and peroxisomal fatty acid oxidation and is activated as part of the fasting response.[41] Although several of our described targets have been validated as direct targets of miR-124 in other systems, we postulate that decreased PPAR-α signalling is a major contributor to the observed reduction in fatty acid oxidation gene expression during miR-124 overexpression.

This is in line with decreased expression of the TGHs ATGL and CES1, which has previously been correlated with decreased PPAR-α activity.[42] Also, AADAC overexpression has been shown to promote fatty acid oxidation in rat hepatoma cells.[43] Therefore miR-124-mediated repression of these TGHs should result in an indirect repression of fatty acid oxidation.

Our miRNA expression analysis revealed that serum depletion activates miR-124 expression (Figure 2-1A). Interestingly, a recent study demonstrated that statin treatment of hepatoma cells induces miR-124 expression.[28] Together, these data suggest that metabolic stresses regulate miR-124 expression. In statin-treated mice, increased mitochondrial and peroxisomal fatty acid oxidation has been observed in the liver, suggesting that statin-induced miR-124 expression may serve to buffer this increase in fatty acid oxidation.[44]

Previous work suggested that miR-124 promotes hepatic TG synthesis through regulation of TRIB3 and enhanced hepatic lipogenesis.[16] We did not, however, observe increased expression

of lipogenic genes (SREBPs and FASN; Figures 6-1 and 6-5) or repression of TRIB3 (Figure 6-1). This could be a result of a variation in models used (Huh7.5 vs. mice), but our data strongly suggest that the observed miR-124-induced TG accumulation in Huh7.5 cells is due to decreased TG and fatty acid breakdown, as opposed to increased lipogenesis.

Also, miR-124 was previously identified as a broadly antiviral miRNA against murine cytomegalovirus, murine herpesvirus 68, and herpes simplex virus 1 during a genome-wide functional miRNA screen.[45] The same group later confirmed that the miRNA's antiviral activity extended to influenza A virus strains and respiratory syncytial virus.[46] In the latter study, the authors ascribed this antiviral activity, in part, to the regulation of p38 mitogen-activated protein kinase (MAPK) signalling.

Although we cannot exclude the contribution of the p38 MAPK signalling pathway to the observed anti-HCV effects of miR-124, given the strong dependence of HCV on hepatic lipid pathways, miR-124's regulation of hepatocellular metabolism likely contributes to the its influence on HCV. It is important to note that our previous work, using an HCV replicon model, suggests that miR-124 promotes HCV replication.[10] In contrast, this work employing a full-length virus (JFH-1) suggests that, in a model fully recapitulating the entire viral life cycle, miR-124 inhibits HCV infectivity. This is consistent with miR-124 regulation of AADAC, the only positive regulator of virion production identified among our miR-124 targets.[34]

Overall, our data highlight a novel functional role for miR-124 in hepatic TG catabolism. This metabolic stress-regulated miRNA concordantly regulates multiple nodes within the TG hydrolysis and fatty acid oxidation pathways, yielding a greater overall effect on TG homeostasis. It is interesting to note that there are several miRNAs that target metabolic pathways in the liver at different nodes. These miRNAs cooperate, often in a redundant fashion, to fine-tune metabolic

networks in the liver and manage the homeostatic response to multiple inputs (e.g., from the muscle and fat). Future work should examine the function of miR-124 in the context of systemic energy homeostasis.

2.7 Supplemental Information

Supplemental Information includes six figures and three tables and can be found in Chapter 6 of this thesis.

2.8 References

(1) Houten, S. M.; Wanders, R. J. A. A General Introduction to the Biochemistry of Mitochondrial Fatty Acid β-Oxidation. *J. Inherit. Metab. Dis.* **2010**, *33* (5), 469. https://doi.org/10.1007/S10545-010-9061-2.

(2) Mashek, D. G. Hepatic Fatty Acid Trafficking: Multiple Forks in the Road. *Adv. Nutr.* **2013**, *4* (6), 697. https://doi.org/10.3945/AN.113.004648.

(3) Ress, C.; Kaser, S. Mechanisms of Intrahepatic Triglyceride Accumulation. *World J. Gastroenterol.* **2016**, *22* (4), 1664–1673. https://doi.org/10.3748/WJG.V22.I4.1664.

(4) Chukkapalli, V.; Heaton, N. S.; Randall, G. Lipids at the Interface of Virus-Host Interactions. *Curr Opin Microbiol.* **2012**, *15* (4), 512–518. https://doi.org/10.1016/j.mib.2012.05.013.

(5) Moore, K. J.; Rayner, K. J.; Suárez, Y.; Fernández-Hernando, C. The Role of MicroRNAs

in Cholesterol Efflux and Hepatic Lipid Metabolism. *Ann. Rev. Nutr.* **2011**, *31*, 49–63. https://doi.org/10.1146/annurev-nutr-081810-160756.

(6) Pasquinelli, A. E. MicroRNAs and Their Targets: Recognition, Regulation and an Emerging Reciprocal Relationship. *Nat. Rev. Genet. 2012 134* **2012**, *13* (4), 271–282. https://doi.org/10.1038/NRG3162.

(7) Ben-Hamo, R.; Efroni, S. MicroRNA Regulation of Molecular Pathways as a Generic Mechanism and as a Core Disease Phenotype. *Oncotarget* **2015**, *6*, 1594–1604. https://doi.org/10.18632/oncotarget.2734.

(8) Li, Q.; Lowey, B.; Sodroski, C.; Krishnamurthy, S.; Alao, H.; Cha, H.; Chiu, S.; El-Diwany, R.; Ghany, M. G.; Liang, T. J. Cellular MicroRNA Networks Regulate Host Dependency of Hepatitis C Virus Infection. *Nat. Commun.* **2017**, *8* (1). https://doi.org/10.1038/S41467-017-01954-X.

(9) Singaravelu, R.; Chen, R.; Lyn, R. K.; Jones, D. M.; O'Hara, S.; Rouleau, Y.; Cheng, J.; Srinivasan, P.; Nasheri, N.; Russell, R. S.; et al. Hepatitis C Virus Induced Up-Regulation of MicroRNA-27: A Novel Mechanism for Hepatic Steatosis. *Hepatology* **2014**, *59* (1), 98–108. https://doi.org/10.1002/hep.26634.

(10) Singaravelu, R.; O'Hara, S.; Jones, D. M.; Chen, R.; Taylor, N. G.; Srinivasan, P.; Quan, C.; Roy, D. G.; Steenbergen, R. H.; Kumar, A.; et al. MicroRNAs Regulate the Immunometabolic Response to Viral Infection in the Liver. *Nat. Chem. Biol.* **2015**, *11* (12), 988–993. https://doi.org/10.1038/nchembio.1940.

(11) Singaravelu, R.; Quan, C.; Powdrill, M. H.; Shaw, T. A.; Srinivasan, P.; Lyn, R. K.; Alonzi, R. C.; Jones, D. M.; Filip, R.; Russell, R. S.; et al. MicroRNA-7 Mediates Cross-Talk between Metabolic Signaling Pathways in the Liver. *Sci. Rep.* **2018**, *8* (1), 361. https://doi.org/10.1038/s41598-017-18529-x.

(12) Esau, C.; Davis, S.; Murray, S. F.; Yu, X. X.; Pandey, S. K.; Pear, M.; Watts, L.; Booten, S. L.; Graham, M.; McKay, R.; et al. MiR-122 Regulation of Lipid Metabolism Revealed by in Vivo Antisense Targeting. *Cell Metab.* **2006**, *3* (2), 87–98. https://doi.org/10.1016/J.CMET.2006.01.005.

(13) Elmén, J.; Lindow, M.; Silahtaroglu, A.; Bak, M.; Christensen, M.; Lind-Thomsen, A.; Hedtjärn, M.; Hansen, J. B.; Hansen, H. F.; Straarup, E. M.; et al. Antagonism of MicroRNA-122 in Mice by Systemically Administered LNA-AntimiR Leads to up-Regulation of a Large Set of Predicted Target MRNAs in the Liver. *Nucleic Acids Res.* **2008**, *36* (4), 1153–1162. https://doi.org/10.1093/nar/gkm1113.

(14) Krützfeldt, J.; Rajewsky, N.; Braich, R.; Rajeev, K. G.; Tuschl, T.; Manoharan, M.; Stoffel, M. Silencing of MicroRNAs in Vivo with 'Antagomirs.' *Nat. 2005 4387068* **2005**, *438* (7068), 685–689. https://doi.org/10.1038/NATURE04303.

(15) Jopling, C. L.; Yi, M. K.; Lancaster, A. M.; Lemon, S. M.; Sarnow, P. Modulation of Hepatitis C Virus RNA Abundance by a Liver-Specific MicroRNA. *Science* **2005**, *309* (5740), 1577–1581. https://doi.org/10.1126/SCIENCE.1113329.

(16) Liu, X.; Zhao, J.; Liu, Q.; Xiong, X.; Zhang, Z.; Jiao, Y.; Li, X.; Liu, B.; Li, Y.; Lu, Y.

MicroRNA-124 Promotes Hepatic Triglyceride Accumulation through Targeting Tribbles Homolog 3. *Sci. Rep.* **2016**, *6* (October), 1–8. https://doi.org/10.1038/srep37170.

(17) Ning, B. F.; Ding, J.; Liu, J.; Yin, C.; Xu, W. P.; Cong, W. M.; Zhang, Q.; Chen, F.; Han, T.; Deng, X.; et al. Hepatocyte Nuclear Factor 4α-Nuclear Factor-KB Feedback Circuit Modulates Liver Cancer Progression. *Hepatology* **2014**, *60* (5), 1607–1619. https://doi.org/10.1002/HEP.27177.

(18) Sun, Y.; Pizzorusso, T.; Soreq, H.; Liu, L.; Liu, X.; Luo, Z.-M.; Guo, X.-M.; Su, D.-F. An Updated Role of MicroRNA-124 in Central Nervous System Disorders: A Review. *Front. Cell. Neurosci.* **2015**, *9*, 193. https://doi.org/10.3389/fncel.2015.00193.

(19) Singaravelu, R.; Srinivasan, P.; Pezacki, J. P. Armand-Frappier Outstanding Student Award — The Emerging Role of 25-Hydroxycholesterol in Innate Immunity. *Can. J. Microbiol.* **2015**, *61* (8), 521–530. https://doi.org/10.1139/CJM-2015-0292/ASSET/IMAGES/LARGE/CJM-2015-0292F2.JPEG.

(20) Vallianou, I.; Dafou, D.; Vassilaki, N.; Mavromara, P.; Hadzopoulou-Cladaras, M. Hepatitis C Virus Suppresses Hepatocyte Nuclear Factor 4 Alpha, a Key Regulator of Hepatocellular Carcinoma. *Int. J. Biochem. Cell Biol.* **2016**, *78*, 315–326. https://doi.org/10.1016/j.biocel.2016.07.027.

(21) Russell, R. S.; Meunier, J.-C.; Takikawa, S.; Faulk, K.; Engle, R. E.; Bukh, J.; Purcell, R. H.; Emerson, S. U. Advantages of a Single-Cycle Production Assay to Study Cell Culture-Adaptive Mutations of Hepatitis C Virus. *Proc. Natl. Acad. Sci. USA* **2008**, *105*, 4370–

4375. https://doi.org/10.1073/pnas.0800422105.

(22) Agarwal, V.; Bell, G. W.; Nam, J. W.; Bartel, D. P. Predicting Effective MicroRNA Target Sites in Mammalian MRNAs. *Elife* **2015**, *4* (e05005), 1–38. https://doi.org/10.7554/ELIFE.05005.

(23) Bonci, D.; Coppola, V.; Musumeci, M.; Addario, A.; Giuffrida, R.; Memeo, L.; D'Urso, L.; Pagliuca, A.; Biffoni, M.; Labbaye, C.; et al. The MiR-15a–MiR-16-1 Cluster Controls Prostate Cancer by Targeting Multiple Oncogenic Activities. *Nat. Med.* **2008**, *14* (11), 1271–1277. https://doi.org/10.1038/NM.1880.

(24) Hashimoto, Y.; Akiyama, Y.; Yuasa, Y. Multiple-to-Multiple Relationships between MicroRNAs and Target Genes in Gastric Cancer. *PLoS One* **2013**, *8* (5). https://doi.org/10.1371/JOURNAL.PONE.0062589.

(25) Chen, J.; Bardes, E. E.; Aronow, B. J.; Jegga, A. G. ToppGene Suite for Gene List Enrichment Analysis and Candidate Gene Prioritization. *Nucleic Acids Res.* **2009**, *37* (Web Server issue), W305. https://doi.org/10.1093/NAR/GKP427.

(26) Valentino, A.; Calarco, A.; Di Salle, A.; Finicelli, M.; Crispi, S.; Calogero, R. A.; Riccardo, F.; Sciarra, A.; Gentilucci, A.; Galderisi, U.; et al. Deregulation of MicroRNAs Mediated Control of Carnitine Cycle in Prostate Cancer: Molecular Basis and Pathophysiological Consequences. *Oncogene* **2017**, *36* (43), 6030–6040. https://doi.org/10.1038/onc.2017.216.

(27) Strijbis, K.; Vaz, F. M.; Distel, B. Enzymology of the Carnitine Biosynthesis Pathway.

IUBMB Life **2010**, *62* (5), 357–362. https://doi.org/10.1002/IUB.323.

(28) Lo, V.; Erickson, B.; Thomason-Hughes, M.; Ko, K. W. S.; Dolinsky, V. W.; Nelson, R.; Lehner, R. Arylacetamide Deacetylase Attenuates Fatty-Acid-Induced Triacylglycerol Accumulation in Rat Hepatoma Cells. *J. Lipid Res.* **2010**, *51* (2), 368. https://doi.org/10.1194/JLR.M000596.

(29) Phulukdaree, A.; Moodley, D.; Khan, S.; Chuturgoon, A. A. Atorvastatin Increases MiR-124a Expression: A Mechanism of Gamt Modulation in Liver Cells. *J. Cell. Biochem.* **2015**, *116* (11), 2620–2627. https://doi.org/10.1002/JCB.25209.

(30) Ross, M. K.; Borazjani, A.; Wang, R.; Crow, J. A.; Xie, S. Examination of the Carboxylesterase Phenotype in Human Liver. **2012**. https://doi.org/10.1016/j.abb.2012.04.010.

(31) Ong, K. T.; Mashek, M. T.; Bu, S. Y.; Greenberg, A. S.; Mashek, D. G. ATGL Is a Major Hepatic Lipase That Regulates TAG Turnover and Fatty Acid Signaling and Partitioning. *Hepatology* **2011**, *53* (1), 116. https://doi.org/10.1002/HEP.24006.

(32) Das, S. K.; Stadelmeyer, E.; Schauer, S.; Schwarz, A.; Strohmaier, H.; Claudel, T.; Zechner, R.; Hoefler, G.; Vesely, P. W. Micro RNA-124a Regulates Lipolysis via Adipose Triglyceride Lipase and Comparative Gene Identification 58. *Int. J. Mol. Sci.* **2015**, *16* (4), 8555–8568. https://doi.org/10.3390/IJMS16048555.

(33) Li, Q.; Lowey, B.; Sodroski, C.; Krishnamurthy, S.; Alao, H.; Cha, H.; Chiu, S.; El-Diwany, R.; Ghany, M. G.; Liang, T. J. Cellular MicroRNA Networks Regulate Host

Dependency of Hepatitis C Virus Infection. *Nat. Commun.* **2017**, *8* (1). https://doi.org/10.1038/s41467-017-01954-x.

(34) Shirasaki, T.; Honda, M.; Shimakami, T.; Horii, R.; Yamashita, T.; Sakai, Y.; Sakai, A.; Okada, H.; Watanabe, R.; Murakami, S.; et al. MicroRNA-27a Regulates Lipid Metabolism and Inhibits Hepatitis C Virus Replication in Human Hepatoma Cells. *J. Virol.* **2013**, *87* (9), 5270–5286. https://doi.org/10.1128/JVI.03022-12.

(35) Nourbakhsh, M.; Douglas, D. N.; Pu, C. H.; Lewis, J. T.; Kawahara, T.; Lisboa, L. F.; Wei, E.; Asthana, S.; Quiroga, A. D.; Law, L. M. J.; et al. Arylacetamide Deacetylase: A Novel Host Factor with Important Roles in the Lipolysis of Cellular Triacylglycerol Stores, VLDL Assembly and HCV Production. *J. Hepatol.* **2013**, *59* (2), 336–343. https://doi.org/10.1016/j.jhep.2013.03.022.

(36) Davalos, A.; Goedeke, L.; Smibert, P.; Ramirez, C. M.; Warrier, N. P.; Andreo, U.; Cirera-Salinas, D.; Rayner, K.; Suresh, U.; Pastor-Pareja, J. C.; et al. MiR-33a/b Contribute to the Regulation of Fatty Acid Metabolism and Insulin Signaling. *Proc. Natl. Acad. Sci.* **2011**, *108* (22), 9232–9237. https://doi.org/10.1073/pnas.1102281108.

(37) Karginov, F. V.; Conaco, C.; Xuan, Z.; Schmidt, B. H.; Parker, J. S.; Mandel, G.; Hannon, G. J. A Biochemical Approach to Identifying MicroRNA Targets. *Proc. Natl. Acad. Sci. U. S. A.* **2007**, *104* (49), 19291. https://doi.org/10.1073/PNAS.0709971104.

(38) Chi, S. W.; Zang, J. B.; Mele, A.; Darnell, R. B. Ago HITS-CLIP Decodes MiRNA-MRNA Interaction Maps. *Nature* **2009**, *460* (7254), 479.

https://doi.org/10.1038/NATURE08170.

(39) Chi, S. W.; Hannon, G. J.; Darnell, R. B.; Struct, N.; Biol, M. An Alternative Mode of MicroRNA Target Recognition HHS Public Access Author Manuscript. *Nat Struct Mol Biol* **2012**, *19* (3), 321–327. https://doi.org/10.1038/nsmb.2230.

(40) Gu, S.; Jin, L.; Zhang, F.; Sarnow, P.; Kay, M. A. The Biological Basis for MicroRNA Target Restriction to the 3' Untranslated Region in Mammalian MRNAs. *Nat Struct Mol Biol* **2009**, *16* (2), 144–150. https://doi.org/10.1038/nsmb.1552.

(41) Rakhshandehroo, M.; Knoch, B.; Müller, M.; Kersten, S. Peroxisome Proliferator-Activated Receptor Alpha Target Genes. *PPAR Res.* **2010**, *2010*, 612089. https://doi.org/10.1155/2010/612089.

(42) Kersten, S.; Seydoux, J.; Peters, J. M.; Gonzalez, F. J.; Desvergne, B.; Wahli, W. Peroxisome Proliferator–Activated Receptor α Mediates the Adaptive Response to Fasting. *J. Clin. Invest.* **1999**, *103* (11), 1489. https://doi.org/10.1172/JCI6223.

(43) Xu, J.; Li, Y.; Chen, W. D.; Xu, Y.; Yin, L.; Ge, X.; Jadhav, K.; Adorini, L.; Zhang, Y. Hepatic Carboxylesterase 1 Is Essential for Both Normal and Farnesoid X Receptor-Controlled Lipid Homeostasis. *Hepatology* **2014**, *59* (5), 1761. https://doi.org/10.1002/HEP.26714.

(44) Park, H.-S.; Jang, J. E.; Ko, M. S.; Woo, S. H.; Kim, B. J.; Kim, H. S.; Park, H. S.; Park, I.-S.; Koh, E. H.; Lee, K.-U. Statins Increase Mitochondrial and Peroxisomal Fatty Acid Oxidation in the Liver and Prevent Non-Alcoholic Steatohepatitis in Mice. *Diabetes*

Metab. J. **2016**, *40* (5), 376. https://doi.org/10.4093/dmj.2016.40.5.376.

(45) Santhakumar, D.; Forster, T.; Laqtom, N. N.; Fragkoudis, R.; Dickinson, P.; Abreu-Goodger, C.; Manakov, S. A.; Choudhury, N. R.; Griffiths, S. J.; Vermeulen, A.; et al. Combined Agonist-Antagonist Genome-Wide Functional Screening Identifies Broadly Active Antiviral MicroRNAs. *Proc. Natl. Acad. Sci.* **2010**, *107* (31), 13830–13835. https://doi.org/10.1073/pnas.1008861107.

(46) McCaskill, J. L.; Ressel, S.; Alber, A.; Redford, J.; Power, U. F.; Schwarze, J.; Dutia, B. M.; Buck, A. H. Broad-Spectrum Inhibition of Respiratory Virus Infection by MicroRNA Mimics Targeting P38 MAPK Signaling. *Mol. Ther. Nucleic Acids* **2017**, *7*, 256–266. https://doi.org/10.1016/J.OMTN.2017.03.008.

Chapter 3: A Bifunctional Nucleoside Probe for the Inhibition of the Human Immunodeficiency Virus-Type 1 Reverse Transcriptase

Initially published as Tyler A. Shaw, Christopher J. Ablenas, Geneviève F. Desrochers, Megan H. Powdrill, Didier A. Bilodeau, Jean-François Vincent-Rocan, Meijuan Niu, Anne Monette, Andrew J. Mouland, André M. Beauchemin, and John Paul Pezacki. (2020) A Bifunctional Nucleoside Probe for the Inhibition of the Human Immunodeficiency Virus-Type 1 Reverse Transcriptase. *Bioconjug Chem.* 31(5):1537-1544.

3.1 Statement of Contribution

Conceptualization, J.P.P., A.M.B.; Methodology, M.H.P., T.A.S., C.J.A, G.F.D, D.A.B; Formal Analysis, T.A.S., A.M.B and J.P.P.; Investigation, M.H.P., T.A.S., G.F.D., C.J.A., M.N., A.M, D.A.B; Writing – Original Draft, T.A.S., M.H.P, and J.P.P.; Review & Editing, T.A.S, M.H.P, A.M.B, and J.P.P.; Funding Acquisition, A.M.B, A.J.M., and J.P.P.; Supervision, A.M.B, A.J.M, and J.P.P.

3.1.1 Acknowledgements

The authors thank the Lady Davis Institute cell imaging and flow cytometry core facility, and Asianne Lee (University of Ottawa) for assistance with the synthesis and characterization of other structurally related probes. MHP and CJA are recipients of postdoctoral fellowship funding from the Canadian Network on Hepatitis C (CanHepC). This work was supported by the Natural Sciences and Engineering Council of Canada (NSERC) Discovery Grants to JPP (#298496) and Canadian Institutes of Health Research grants to AJM (#MOP-56974) and to JPP (#136807). GFD received funding from the Fonds de recherche du Québec – Nature et technologies (FRQNT).

JFVR thanks NSERC for a graduate scholarship and M.N. was supported by the Lady Davis Institute/Jewish General Hospital.

3.2 Summary

Nucleoside analogs have proven effective for the inhibition of viral polymerases and are the foundation of many antiviral therapies. In this work, the antiretroviral potential of 6-azauracil analogs was assessed using activity-based protein profiling techniques and functional assays. Probes based on the 6-azauracil scaffold were examined and found to bind to HCV polymerase and HIV-1 reverse transcriptase through covalent modification of residues near the active site. The modified sites on the HIV-1 RT were examined using a mass spectrometry approach, and it was discovered that the azauracil moieties modified the enzyme in proximity to its active site. However, these scaffolds gave little or no inhibition of enzyme activity. Instead, a bifunctional inhibitor was prepared using click chemistry to link the 6-azauracil moiety to azidothymidine (AzT) and the corresponding triphosphate (AzTTP). These bifunctional inhibitors were found to have potent inhibitory function through a mode of action that includes both alkylation and chain termination. An in vitro assay demonstrated that the bifunctional inhibitor was 23-fold more effective in inhibiting HIV-1 RT activity than the parent AzTTP. The bifunctional inhibitor was also tested in HIV-1 permissive T cells where it decreased Gag expression similarly to the front-line drug Efavirenz with no evidence of cytotoxicity. This new bifunctional scaffold represents an interesting tool for inhibiting HIV-1 by covalently anchoring a chain-terminating nucleoside analog in the active site of the reverse transcriptase, preventing its removal and abolishing enzymatic activity, and represents a novel mode of action for inhibiting polymerases including reverse transcriptases.

3.3 Introduction

The synthesis and characterization of nucleoside analogs has been an area of interest for the treatment of many diverse viruses, including those responsible for major pandemics, such as hepatitis C virus (HCV) and human immunodeficiency virus-type 1 (HIV-1).[1,2] In the case of retroviruses such as HIV-1, the target is their reverse transcriptase (RT), the enzyme responsible for the conversion of viral RNA into the viral DNA, which is incorporated into the host genome.[3] Viral polymerases represent a basic and essential component of the viral machinery not only for HIV-1, but throughout the entire viral kingdom.[4–6]As polymerases play a crucial role in the disparate life cycles of numerous viruses, the development of nucleoside analogs which mimic the natural substrates of these enzymes and disrupt their function has been an essential part of many antiviral strategies.[5,6]

Disruption of viral polymerases can be achieved through chain termination or mutation of the viral RNA/DNA. Chain terminations can be introduced using a nucleoside analog that lacks a 3' hydroxyl or sterically blocks the incorporation of the next nucleotide in the chain.[7,8] The 3' hydroxyl is required for the reaction with the incoming 5' phosphate of the next nucleotide in the extending RNA or DNA chain and the incorporation of an obligate chain terminator that lacks the 3' hydroxyl group results in the termination of the replication of the genetic material of the virus.[9] Zidovudine (azidothymidine or AzT, Figure 3-1) was the first antiretroviral drug and was used as a treatment for HIV-1 infections in 1987.[9] As a thymidine analog lacking a 3' hydroxyl group, AzT causes chain termination during the reverse transcription of proviral DNA.[9] Despite interactions with cellular polymerases and many side effects that have been associated with AzT, it remains a cornerstone in modern HIV-1 treatment regimens.[10] Nucleoside analogs as a class

have shown promise as anti-HIV-1 agents but resistant HIV-1 strains have arisen from patients and are predictive of rapid disease progression and death.[11] To prevent these resistant strains from developing, AzT has been combined with other non-thymidine RT inhibitors.[12] Current antiretroviral regimens against HIV-1 use a triple combination of AzT with a non-thymidine nucleoside analog and a protease inhibitor or non-nucleoside inhibitor of HIV-1 RT.[10]

Recently developed nucleoside inhibitors of HCV polymerase are designed as nonobligate chain terminators, as studies demonstrated that incorporation of obligate chain terminators can be reversed through pyrophosphorolysis.[13] The leading nonobligate chain terminator that has achieved success clinically in treating HCV infection is sofosbuvir. Sofosbuvir is a uridine analog that possesses a 3' hydroxyl and causes chain termination of the viral RNA by sterically blocking the incorporation of the next nucleotide in the replicating strand.[14,15] Therefore the development and characterization of novel nucleoside analogs and combinatorial approaches is of continued importance for HIV-1 and other antiviral therapies.[1,16]

Early studies of 6-azauracil demonstrated that it inhibited the growth of yeast and determined that this was achieved through the inhibition of transcriptional elongation by affecting GTP synthesis and depleting UTP pools.[17] While the literature doesn't suggest a direct interaction of 6-azauracil with polymerases, studies have demonstrated that uracil can be deleterious if incorporated into DNA.[18] Given the nucleotide-like structure of 6-azauracil and the lack of a 3' hydroxyl group, we hypothesize that RNA binding viral polymerases including HIV could incorporate azauracil probes instead of thymidine or uridine and the incorporation would result in chain termination.

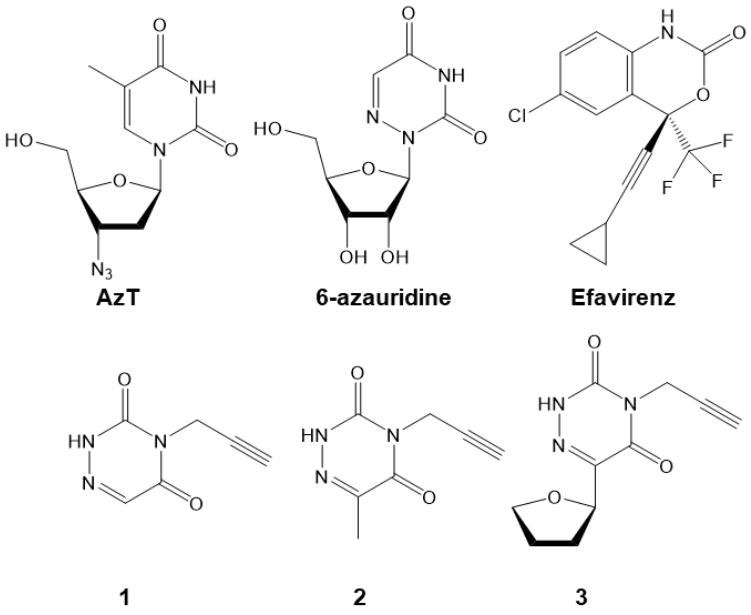

Figure 3-1. Structures of nucleoside analogs and non-nucleoside HIV-1 RT inhibitor.

Probes **1**, **2**, and **3** were previously synthesized based on the 6-azauridine scaffold. Zidovudine is a nucleoside inhibitor of HIV-1 RT and Efavirenz is a non-nucleoside inhibitor of HIV-1 RT.

The azauracil probes were previously synthesized and resemble 6-azauridine and 6-azauracil.[19] The azauracil scaffold was modified with the addition of an alkyne handle on the heterocyclic nitrogen at position 3 (Figure 3-1). Probe **3** is interesting in that it is a carbon-linked azauracil analog with different connectivity relative to 6-azauridine. The alkyne handle allows azide-alkyne cycloaddition reactions to be used to conjugate the probe to reporter groups used for affinity purification or chemoproteomic methods.[20–23] The probes can subsequently be functionalized using copper-catalyzed click chemistry, either with a fluorophore for visualization of the target during in gel fluorescence experiments or with biotin to selectively enrich targets from a complex proteome.[24–26]

3.4 Methods

3.4.1 In Vitro Labelling Experiments

Azauracil probes were prepared as previously described.[19] HIV-1 and HCV enzymes were a gift from Dr. Götte at the University of Alberta. Microfuge tubes containing 20 ug of each enzyme were incubated with 10 μM of probe **1**, **2**, or **3** for 1 hour at room temperature. Click mix containing 1 mM CuSO4, 1 mM TCEP, 100 μM TBTA, and 100 μM rhodamine azide was prepared in 1X PBS. The click mix was added to the probe reactions at a 1:1 ratio and incubated for 2 hours at room temperature in darkness. The reactions were then quenched at -80°C with 5 volumes of pre-chilled acetone for 1 hour and centrifuged at 14000 rpm for 15 minutes at 4°C. Pellets were dried, resuspended in 1X SDS loading buffer (50 mM Tris-HCl pH 6.8, 2% SDS, 10% glycerol, 100 mM DTT, 0.1% bromophenol blue), and run on a 10% stain free gel (Bio-Rad, Hercules, CA). Gels were imaged on an FMBIO Fluorescence Scanner (MiraiBio, Almeda, CA) or a ChemiDoc MP (Bio-Rad, Hercules, CA).

3.4.2 The [3+2] Huisgen Cycloaddition (Click) Reaction of AzTTP or AzT with Probe 3

The click reaction was prepared in 1X PBS using 5 mM Ascorbate, 10 mM CuSO4, 1 mM TBTA, 10 mM probe **3**, and 10 mM AzTTP or AzT. The components were reacted for 2 hours and excess copper was removed using Nickel NTA resin. The resin was washed with PBS, stripped three times with Ni^{2+} stripping buffer (20 mM NaHPO4 pH 7.4, 500 mM NaCl, 50 mM EDTA) and dried before adding the click reaction and collecting the reaction by centrifuging at 700 x g for 2 minutes. Both reactants matched exactly previously reported characterization, and after quantitative coupling via [3+2] Huisgen cycloaddition, the products **4** and **5** were characterized by NMR and ESI, supporting their structural assignment and purity. Spectral data for the products was also consistent with similar previously reported AzT "clicked" analogues.[41]

3.4.3 Protein Labelling for MS Preparation

10 µg of purified HIV-1 RT heterodimer was labelled with 10 µM of probe 1, 2, or 3 for 1 hour at room temperature. Excess probe was removed by a 15 minute acetone precipitation of the protein at -80°C, followed by centrifugation at 20 000 x g for 15 minutes. The pellet was resuspended in gel-loading buffer (0.1 M Tris pH 6.8, 10% glycerol, 4% SDS, 0.02% bromophenol blue, 30 mM DTT) and the protein separated on a 10% SDS-PAGE gel. The gel was stained by coomassie (1 g/L Brilliant blue R250, 10% glacial acetic acid, 50% MeOH) for 1 hour, destained in gel destaining solution (10% glacial acetic acid, 40% MeOH) and proteins were visualized on a ChemiDoc MP (Bio-Rad, Hercules, CA). Bands corresponding to p66 and p51 were excised and cut into 1 mm3 cubes. The bands were further destained in protein destain solution (50 mM ammonium bicarbonate, 50% acetonitrile) for 45 minutes. The gel was shrunk in acetonitrile and all liquid removed. Proteins were reduced in 10 mM DTT in 100 mM ammonium bicarbonate for

30 minutes at 56°C, after which the gel was shrunk in acetonitrile and all liquid was removed. Proteins were alkylated in 55 mM iodoacetamide in 100 mM ammonium bicarbonate for 20 minutes at room temperature in the dark, the gel shrunk in acetonitrile and all liquid removed. Proteins were incubated in trypsin buffer (13 ng/μL trypsin, 10% acetonitrile, 10 mM ammonium bicarbonate) at 4°C for 2 hours, then digested overnight at 37°C with end-over-end rotation. Extraction buffer (1.6% formic acid, 66% acetonitrile) was added and the samples incubated for 15 minutes at 37°C. The solution was removed and dried by vacuum centrifugation.

3.4.4 Mass Spectrometry Analysis

EASY nano-LC system coupled with Q Exactive Plus mass spectrometer (Thermo Scientific, San Jose, CA) were used for analysis of peptides with an Acclaim PepMap RSLC 75 μm ID x 150 mm length separation column (Thermo Scientific, San Jose, CA). Approximately 1 ug of peptides was injected and separated by the following gradient (A – 0.1 % formic acid in H_2O, B – 100 % acetonitrile, 0.1 % formic acid in H_20) with the flow of 300 nL/min: 0.0-73.0 min 5-40% B, 73.0-76.0 min 40-100% B, 76.0-85.0 min 100% B, 85.0-91.0 min 100-0% B, 91-100.0 min 0% B. Nano-ESI conditions: spray voltage in positive mode – 2100 V; ion transfer tube temperature – 250°C; S-lens RF level – 60. Full scan resolutions were set to 70 000 at m/z 200. Full scan target was 3 × 106 with a maximum fill time of 200 ms. Mass range was set to 375–1800 m/z. Target value for fragment scans was set at 1 × 105 and isolation width was set at 2 m/z. Resolution for HCD spectra was set to 17,500 at m/z 200 with and normalized collision energy was set at 30. All data was acquired in data depending mode using positive polarity. The raw data was processed using Proteome Discoverer (version 1.4.1.14, Thermo Scientific, San Jose, CA). MS2 spectra were searched with SEQUEST HT engine against a UniProt database for Homo

sapiens (Human) (http://www.uniprot.org). Peptides were generated from a tryptic digestion with up to two missed cleavages, carbamidomethylation of cysteines as fixed modifications, and oxidation of methionines, protein N-terminal acetylation, and modifications on cysteine, serine, threonine, or tyrosine residues corresponding to the exact mass of probes **1**, **2**, or **3** as variable modifications. Precursor mass tolerance was 10 ppm and product ions were searched at 0.6 Da tolerances. Peptide spectral matches (PSM) were validated using a target decoy validation with FDR of 1%. A minimum cross correlation (Xcorr) of above 1.00 was used to confirm peptide identity.

3.4.5 HIV-1 RT Activity Assay

The EnzChek Reverse Transcriptase Assay Kit (Thermo Fisher Scientific, Waltham, MA) was used to evaluate the activity of HIV-1 RT when treated with the probes and inhibitors. Reactions were performed in 96-well plates using the manufacturer's protocol with some modifications. The primer was added to the template using equal amounts of Component D and Component E and was incubated at room temperature for 1 hour. Once the primer and template were annealed, 199 volumes of Component F were added to introduce the nucleotides and factors required for reverse transcription. The final concentrations of the components of the reaction buffer and template mixture were 48 mM Tris-HCl pH 8.1, 6.4 mM MgCl2, 48 mM KCl, 10.4 mM DTT, 80 μM dNTP, 4 μM template, and 0.2 μM primer. The inhibitors were dissolved in DMSO and added at concentrations between 0.025 nM and 5 μM, with the concentration of DMSO not exceeding 1% in the reactions. A control reaction with only DMSO was performed in parallel and all reactions were incubated 20 minutes at room temperature before the addition of HIV-1 RT. The HIV-1 RT was added at a final concentration of 20 nM and reactions were incubated 45 minutes

before being quenched with Component G. PicoGreen working solution was prepared from Component A and Component B as per the manufacturer's protocol before being added to the reactions and incubating 5 minutes at room temperature on a shaker protected from light. Fluorescence was then measured using a Spectramax i3 (Molecular Devices, San Jose, CA) at an excitation wavelength of 480 nm and an emission wavelength of 520 nm. All reactions were performed in triplicate and fluorescence was normalized to DMSO control. Normalized data was plotted against the logarithm of inhibitor concentration and sigmoidal curves were fitted using Prism 7 (GraphPad, San Diego, CA).

3.4.6 HIV-1 Gag Imaging

Work with HIV-1 was performed under strict Public Health Agency of Canada guidelines under the Pathogen and Toxin License L-R3-01013-19 (Risk Group 3 Pathogens), and all personnel were extensively trained in safety precautions for the handling and disposing of infectious material. HEK293T, and SUP-T1 T cells were purchased from the American Type Culture Collection (ATCC). TZM-bl cells were obtained from NIH AIDS Reference and Reagent Program (ARRP). HEK293T and TZM-bl cells were grown and maintained in Dulbecco's modified Eagle medium (DMEM, Invitrogen) containing 10% fetal bovine serum (HyClone) and 1% penicillin-streptomycin (Life Technologies) at 37°C and 5% CO2. SUP-T1 cells were grown and maintained as suspension culture in RPMI 1640 (Life Technologies) supplemented with 10% FBS (Hyclone) and 1% penicillin/streptomycin (Life Technologies) at 37°C and 5% CO2. For virus production, wild type (WT) NL4.3 virus particles were prepared by transfection of HEK293T cells with pNL4.3 (ARRP) using the JetPrime transfection reagent (PolyPlus, VWR) following manufacturer's instructions. Viruses were pelleted from cell supernatants collected 48 hours post-

transfection, and filtered through a 0.22 μm filter (Pall) for centrifugation at 35,000 rpm for 1 hour at 4°C. Viruses were resuspended in D-PBS (Wisent), and viral titer was quantified using the X-gal infectivity assay using TZM-bl cells as described in.[44] For infection experiments, passage 3 SUP-T1 T cells in RPMI 1640 (Life Technologies) supplemented with 10% FBS (Hyclone) and 1% penicillin/streptomycin (Life Technologies) were treated with the nucleoside analogs for 1 hour at IC_{50} concentrations, following by infection with NL4.3 virus at a MOI of 3. Cells were collected 12 days later for immunofluorescence (IF) analysis of suspension cells, performed as described previously.[45]Briefly, sterile 18 mm No. 1 cover glasses (VWR), positively charged using 0.1 % poly-L-lysine solution (Sigma) overnight at 4°C, were washed with D-PBS, and placed into 12-well plates. 1 mL of cells (and supernatants) was deposited on top. Cells were allowed to settle onto and stick to covers glasses for 30 minutes at 37 °C and 5% CO2. Cells were washed with D-PBS and were fixed onto cover glasses using 4% paraformaldehyde (PFA) for 20 minutes. Fixed cells were washed with D-PBS, quenched using 0.1 M glycine for 10 minutes, washed with D-PBS, permeabilized using 0.2% Triton X-100 in D-PBS for 5 minutes, and were washed twice with D-PBS. Cells were blocked in 1X blocking solution (Roche) for 30 minutes. Cells were incubated with an anti-HIV-1-Gag primary antibody, mouse anti-p24 (1:250; Gag, NIH ARRP), in 1X blocking buffer for 1 hour at 37 °C. Cells were washed with D-PBS for 10 minutes prior to incubation with secondary antibody: Donkey anti-Mouse IgG (H+L) Highly Cross-Adsorbed, Alexa Fluor® 488 (1:500; Invitrogen-Thermo Fisher Scientific #A-21202) for 1 hour at 37 °C. Cells were washed with D-PBS for 20 minutes, dried, and mounted onto glass slides (Thermo Scientific) using ProLong Gold Antifade Reagent with DAPI (Life Technologies). For IF imaging of slides, laser confocal microscopy was performed (n=35 per treatment group) using a Leica DM16000B microscope equipped with a WaveFX spinning disk confocal head (Quorum

Technologies) and HCX PL APO / 40X, Oil / 0.75-1.25 NA CS and HCX PL APO / 63X, Oil / 0.60-1.40 NA BL objectives, and images were acquired by a Hamamatsu EM-charge coupled device digital camera. For multi-color image capture, AlexaFluor-488 conjugated secondary antibody emission was captured by 500–550 nm, bandpass filter, followed by capture of (4′,6-diamidino-2-phenylindole) DAPI emission using 435–485 nm bandpass filter. Images were recorded from laser-scanned cell focal layers with a thickness of 1 μm, and digitized at a resolution of 1024 × 1024 pixels. Raw .liff image files were exported by Volocity software (Perkin Elmer) for import into Imaris software v. 8.1.2 (Bitplane/Andor) used for image montage and analysis. Imaris-generated .csv file exports of quantitative Gag mean fluorescence intensity (MFI) were imported into Excel (Microsoft), and retabulated for statistical analysis using GraphPad v6.1 (Prism), also generating graphical outputs. P-values of less than 0.05 were considered statistically significant.

3.5 Results and Discussion

The ability of the probes to covalently labell the HIV-1 reverse transcriptase or the HCV polymerase or helicase was investigated in an initial fluorescence-based interaction screen. Purified HIV-1 RT was incubated with **1**, **2**, **3**, or vector alone. Heat denatured HIV-1 RT was incubated with **3** in parallel. Click chemistry was used for the azide-alkyne cycloaddition of a rhodamine fluorophore and the labelled enzymes were resolved on SDS-PAGE (Figure 3-2A).

The probes labelled the HIV-1 RT and the no probe and heat denatured controls confirmed that labelling was specific to the structure of HIV-1 RT and the reaction of the probes with the enzyme. In a subsequent experiment, HIV-1 RT and HCV NS5b polymerase and NS3h helicase domains were reacted with **1** or **3.** The HIV-1 RT mutants and both HCV enzymes were labelled

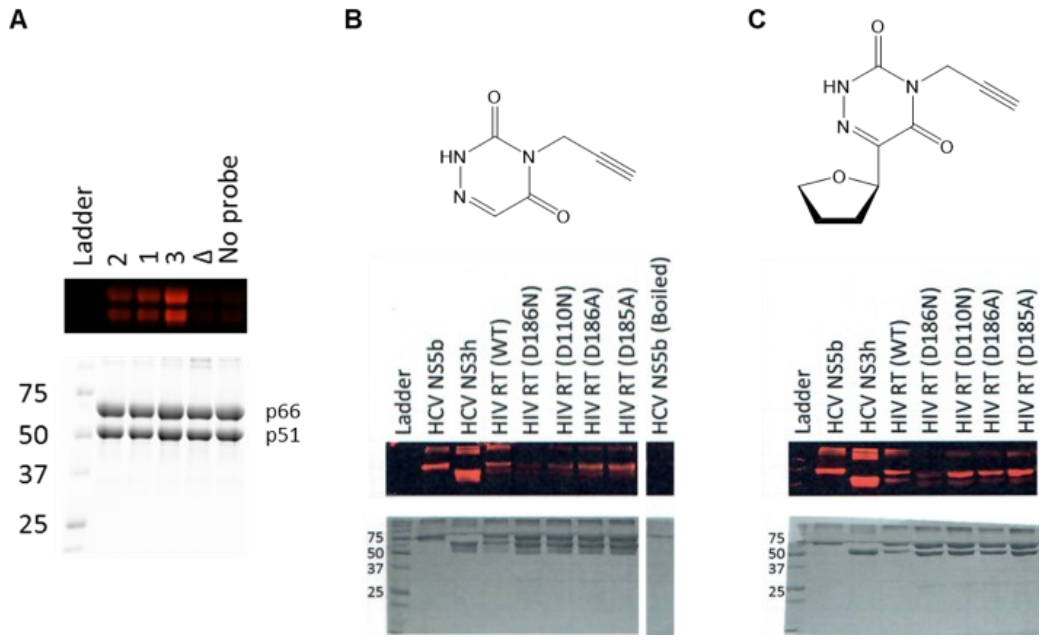

Figure 3-2. **Azauracil probes label HIV-1 and HCV polymerases and the HCV helicase.**

Purified HIV-1 and HCV NS5b polymerase and NS3h helicase enzymes were reacted with azauracil probes and click chemistry was used to attach a rhodamine azide fluorophore to the labelled enzymes. A) HIV-1 RT with probes **1**, **2**, and **3**. B) HIV-1 RT, HIV-1 RT mutants, HCV polymerase, and HCV helicase with probe **1**. C) HIV-1 RT, HIV-1 RT mutants, HCV polymerase, and HCV helicase with probe **3**. The enzymes were separated by SDS-PAGE and fluorescence was visualized with excitation at 530 nm and emission at 605 nm for rhodamine (top) or using the stain free channel for total protein (bottom).

by the probes (Figures 3-2B and C). Notably, **1** and **3** displayed better labelling of the p66 subunit than the p51 subunit of HIV-1 RT and the mutants were labelled less efficiently than the wildtype in both cases, with minimal labelling of the D186N mutant by either probe. The experiment was also performed on a heat denatured sample of HCV NS5b to see the specificity of the reaction. The heat denatured sample of HCV polymerase was not labelled by **1**, suggesting that the structure of the protein is important for the labelling reaction. Interestingly, the active site mutants displayed less labelling than the wildtype. This could be due to the magnesium binding role of the aspartic acid residues in the active site.[27] D186, D185, and D110 in concert with a pair of magnesium ions are responsible for the coordination of the incoming nucleotide commensurate with changes in protein structure and accessibility. D185 and D110 bind a magnesium ion first, and in a second step all three residues bind a magnesium ion that is carried into the active site with the incoming nucleotide. The pair of magnesium ions facilitate the coordination of the nucleotide and position it for the polymerase activity. In the absence of the aspartic acid residues the activity of HIV-1 RT is abolished. In the following experiment, the mutant enzymes displayed less labelling with the nucleoside probes, potentially due to the inability of the enzyme to coordinate with the incoming nucleoside probe and access target residues near the active site.

A mass spectrometry approach was used to determine the residues of HIV-1 RT that react with the probes. Probe-labelled p66 and p51 subunits of HIV-1 RT were digested in-gel by trypsin and analyzed by LC-MS/MS (Table 7-1). The resulting spectra were then searched for peptides with masses consistent with labelling of probes **1**, **2**, or **3** on cysteine, serine, threonine, or tyrosine residues. The same analyses were performed on unlabelled HIV-1 RT p66 and p51 subunits and only putative probe-labelled peptides found exclusively in the labelled samples were retained

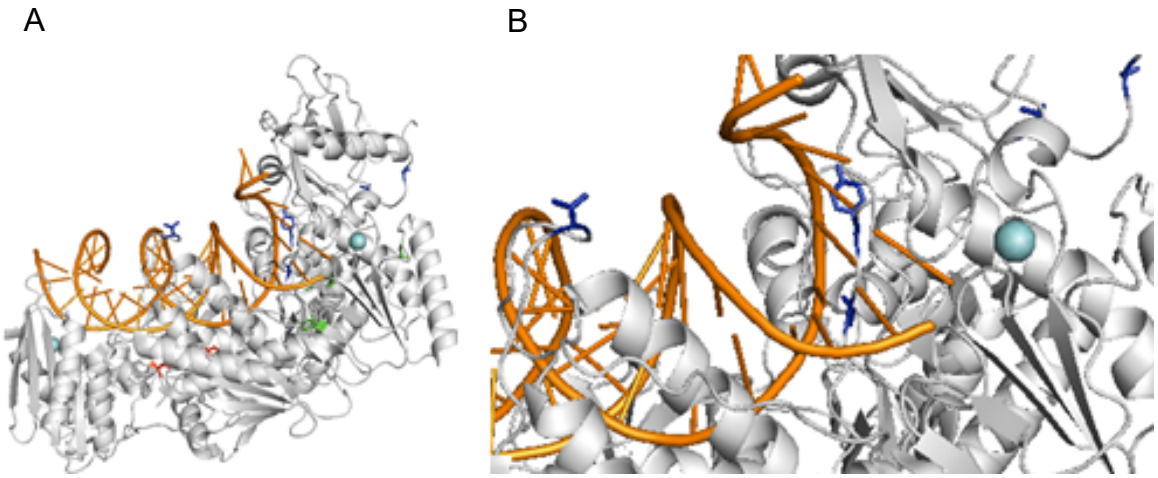

Figure 3-3. **HIV-1 RT labellng by azauracil probes.**

The 5TXL crystal structure was used to annotate probe adducts. A) HIV-1 RT with all modified sites indicated. B) HIV-1 RT template binding cleft with probe **3** adducts indicated. Red indicates probe **1**, green indicates probe **2**, and blue indicates probe **3**. Cyan indicates magnesium ions in polymerase and Rnase H active sites.

(Table 6-2 and 6-3). The probe adduct sites were then annotated on the 5TXL crystal structure of HIV-1 RT to identify any adducts in proximity to the active site (Figure 3-3).[28]

It was discovered that probe **3** formed an adduct with threonine 290 of the p66 subunit, while probe **2** formed an adduct with tyrosine 232; both residues in proximity to the RNA binding cleft of the reverse transcriptase. These peptides are the only probe-labelled peptides to possess an X-correlation score of over 1.5, suggesting that probe labelling of HIV-1 RT displays a selectivity towards the RNA-binding cleft over the remainder of the protein.

The azauracil subunit could form covalent modifications of enzymes via two potential mechanisms. The reaction of the C5 carbonyl or ring opening at the C3-N4 bond have been reported, and the underlying hypothesis is that such reactions of the azauracil subunit would be favored in enzymes through temporary intramolecularity and stabilization of key intermediates. For example, the C5 carbonyl of the azauracil has been shown to engage in condensation reactions with proximal nitrogen nucleophiles and the carbonyl oxygen can also react with a proximal electrophile.[29,30] The second mechanism would involve using the azauracil as a cyclic "NNCO" electrophile, in analogy with the reactivity of oxadiazolones.[31] Thus it is likely that covalent modification occurs according to Eq. 3-1.

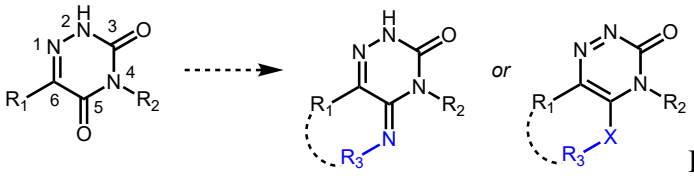

Eq. 3-1

The interaction of the azauracil moiety in compound **3** with viral enzymes has not been described previously and these observations suggest a novel mode of action. The scaffolds studied here

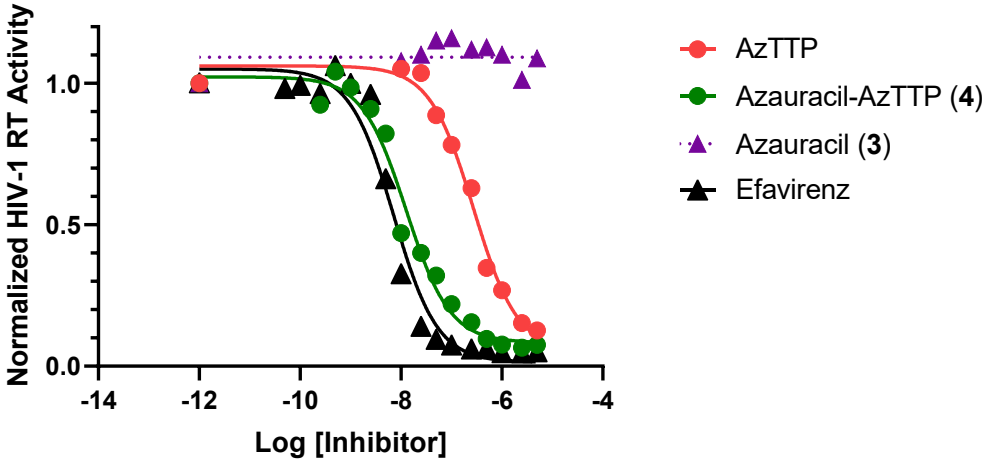

Figure 3-4. Azauracil does not affect HIV-1 RT activity but increases the potency of AzTTP.

HIV-1 RT activity was assessed with each inhibitor and with DMSO using the EnzChek Reverse Transcriptase Kit. Experiments were performed in triplicate and normalized to a DMSO control reaction. Inhibitor concentrations are in M.

contain alkyne handles that have the potential for bioorthogonal reactions with other probes to introduce new functionalities with bifunctional properties.

Bifunctionality is desirable as it increases the potency and binding strength of an inhibitor or drug for its target through the introduction of additional moieties that target the enzyme.[32–34] Inspired by bifunctional strategies employed in PROTACS, ligand-directed covalent modifiers, and others,[35–41] we constructed a bifunctional probe using a simple click reaction for the *in vitro* conjugation of the alkyne group of **3** to the azide group of AzTTP (Scheme 3-1). Following the click reaction, excess copper was removed using stripped Ni-NTA resin. The resulting azauracil-AzTTP (**4**) and **3** were then tested against HIV-1 RT activity using an *in vitro* assay. The inhibitory potential of **3** and **4** were compared to AzTTP and efavirenz, established nucleoside and non-nucleoside inhibitors of HIV-1 RT. While AzTTP and efavirenz were both potent inhibitors of HIV-1 RT, compound **3** didn't display any inhibition of the enzyme (Figure 3-4).

The average of three experiments was subjected to non-linear curve fitting to generate sigmoidal curves from the activity assay and IC_{50} values were calculated. The *in vitro* assay yielded an IC_{50} of 270 ± 3.7 nM for AzTTP and 7.2 ± 0.5 nM for efavirenz. Conjugating probe **3** to AzTTP greatly increased the inhibitory effect of AzTTP against HIV-1 RT and resulted in an IC_{50} of 12 ± 0.7 nM, a 23-fold increase in potency. The relative IC_{50} values that were obtained for AzTTP and efavirenz are in line with previous reports for similar assays.[42,43] The observed increase in HIV-1 RT inhibition suggests that conjugating an azauracil probe to AzTTP produces a more potent bifunctional inhibitor. Other derivatives of AzT have been synthesized but none showed antiviral potentcy, in contrast to the bifunctional inhibitors made herein.[41] The bifunctional inhibitors in the current study lack the 3' hydroxyl group that is required for phosphodiester linkages. In this case,

Scheme 3-1. Click chemistry was used to conjugate probe 3 to AzT or AzTTP. Probe 3 was reacted with azidothymidine (AzT) or triphosphate (AzTTP) for 1 hour under click conditions before removing excess copper using nickel NTA resin. Syntheses were conducted with TCEP or ascorbate as the reducing agent. TCEP = tris(2-carboxyethyl)phosphine, TBTA = tris[(1-benzyl-1H-1,2,3-triazol-4-yl)methyl]amine.

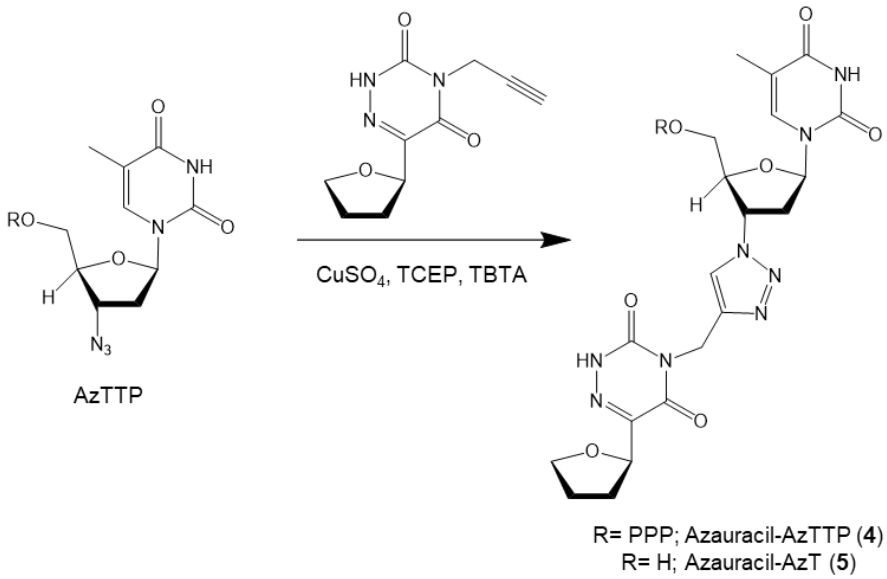

the AzTTP is incorporated into the reverse transcribed viral DNA product while the azauracil moiety covalently binds HIV-1 RT and cannot undergo further chain extension due to the lack of a 3' hydroxyl group. AzTTP acts as an obligate chain terminator by covalently binding to the previous nucleotide and preventing the extension of the viral DNA intermediate needed for integration by the viral integrase, while the azauracil moiety presumably covalently bonds the chain terminated DNA fragment to the enzyme and blocks further enzyme function (Scheme 3-2).

The bifunctional inhibitor was then examined against a cell culture model of HIV-1. Two of the rate-limiting steps of zidovudine's mode of action include the transport of the drug into the cell and the phosphorylation of the drug by host kinases and/or phosphotransferases.[1] A non-phosphorylated form of the bifunctional inhibitor (**5**) was also synthesized to test for how these two processes might affect the bifunctional inhibitor in cell culture and its effects on live virus**.** To determine if the bifunctional inhibitors are active against live virus, we conducted experiments in T cell culture. SUP-T1 cells were infected with HIV-1, treated with drugs and then at 12 days they were fixed and stained for Gag expression (Figure 3-5). In this experiment, Gag expression represents the replication of the viral RNA, and thereby the fitness of the virus. While the azauracil **3** only modestly decreased Gag expression, both forms of the bifunctional inhibitor decreased its expression to similar levels obtained with zidovudine or efavirenz. No toxicity was observed over 12 days of treatment. The antiviral activity of the bifunctional inhibitors demonstrates increased potency carries through to live virus experiments. The modification of zidovudine with an azauracil does not hinder its antiretroviral activity but increases its potency by introducing a covalent linkage to the enzyme. The additional covalent linkage could be pivotal in preventing pyrophosphorolysis of the chain terminator.

Scheme 3-2. Chain termination and crosslinking of HIV-1 RT with azauracil-AzTTP. Reverse transcriptase catalyzes the reaction of the 3' hydroxyl group of the last nucleotide in the chain with the 5' phosphate group of the incoming nucleotide. The incorporation of azauracil-AzTTP in place of a nucleotide causes chain termination of the DNA strand and covalent modification of the reverse transcriptase. The result is a chain terminated DNA and a covalently modified reverse transcriptase. Rectangles represent the RNA/DNA bases, the circles represent phosphate groups or phosphodiester linkages, and the pentagon represents the triazine linkage.

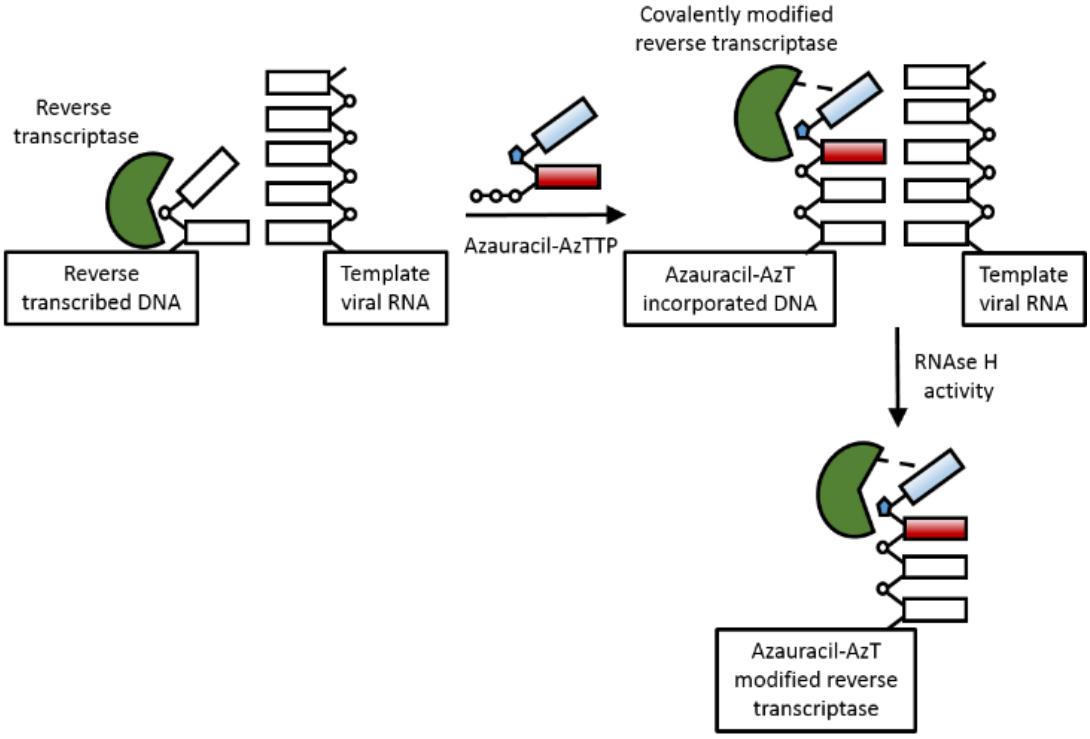

The bifunctional probes presented herein introduce a new class of probes for HIV-1 RT that covalently modify the enzyme without disrupting its activity. The bifunctional nature of the probes allows bioorthogonal conjugation with chemical biology tools or a nucleoside analog for the inhibition of the enzyme. Previous studies demonstrated that inhibiting HIV-1 RT with obligate chain terminators can be reversed through pyrophosphorolysis.[16] By linking the azauracil scaffold to a nucleoside inhibitor, the bifunctional inhibitor is anchored in the active site through a covalent bond of the 6-azauracil moiety with the enzyme's substrate binding cleft, preventing pyrophosphorolysis of the nucleoside analog, making the chain termination irreversible and thereby inactivating the enzyme.

The antiretroviral potential of 6-azauracil analogs was assessed herein using activity-based protein profiling techniques and functional assays. While probes based on the 6-azauracil scaffold were found to be covalent modifiers at residues near the active site, they did not inhibit RT activity. However, a bifunctional inhibitor, prepared using the bioorthogonal [3+2] Huisgen reaction was found to have potent inhibitory function, increasing the potency of AzTTP against HIV-1 RT *in vitro* by approximately 23-fold. The antiretroviral activity of the bifunctional inhibitor was also confirmed in T cell culture with decreased Gag expression. This new scaffold is established as a tool for probing HIV-1 RT through dual modes of action including covalent anchoring and chain-termination. Taken together, these data confirm a new chemical biology strategy for more efficient targeting of nucleotide polymerases.

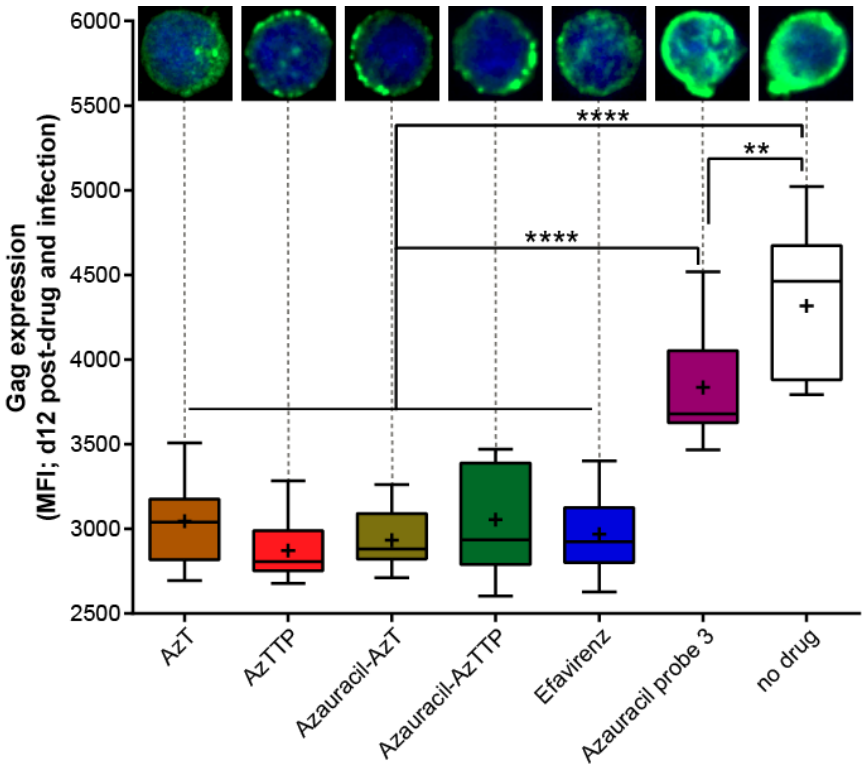

Figure 3-5. Bifunctional azauracil inhibitors decrease Gag expression in cell culture.

Cellular Gag expression (*green*) assessed 12 days following (post) drug treatments and infection of SUP-T1 cells by WT NL4.3 virus. DAPI was used to stain cellular DNA. Data are presented as box and whiskers plots, where horizontal lines indicate median, plus symbol indicates mean, and whiskers are minimum to maximum. Corresponding representative IF images are aligned at top of each treatment. MFI, mean fluorescence intensity; d, day; **, $p < 0.01$****; $p < 0.0001$.

3.6 References

(1) Cihlar, T. and Ray, A. S. Nucleoside and nucleotide HIV reverse transcriptase inhibitors: 25 years after zidovudine. *Antiviral Res.* **2010**, 85(1), 39–58. https://10.1016/J.ANTIVIRAL.2009.09.014.

(2) Feld, J. Interferon-Free Strategies with a Nucleoside/Nucleotide Analogue. *Semin. Liver Dis.* **2014**, 34(1), 37–46. https://10.1055/s-0034-1371009.

(3) Hu, W.-S. and Hughes, S. H. HIV-1 reverse transcription. *Cold Spring Harb. Perspect. Med.* **2012**, 2(10), 1–22. https://10.1101/cshperspect.a006882

(4) Suzuki, T. Hepatitis C Virus Replication. In *Organelle Contact Sites: From Molecular Mechanism to Disease*, Vol. 997; Springer, **2017**; pp. 199–209. https://doi.org/10.1007/978-981-10-4567-7_15.

(5) Rice, C. M. New insights into HCV replication: potential antiviral targets. *Top. Antivir. Med.*, **2011**, 19(3), 117–20.

(6) Frick, D. N. HCV Helicase: Structure, Function, and Inhibition. In *Hepatitis C Viruses: Genomes and Molecular Biology*; Horizon Bioscience, **2006**; pp. 207–244.

(7) Menéndez-Arias, L. Mechanisms of resistance to nucleoside analogue inhibitors of HIV-1 reverse transcriptase. *Virus Res.*, **2008**, 134, 124–146. https://doi.org/10.1016/j.virusres.2007.12.015

(8) Eltahla, A. A.; Luciani, F.; White, P. A.; Lloyd, A. R. and Bull, R. A. Inhibitors of the Hepatitis C Virus Polymerase; Mode of Action and Resistance. *Viruses* **2015**, 7(10), 5206–5224. https://doi.org/10.3390/v7102868.

(9) Quan, Y.; Rong, L.; Liang, C. and Wainberg, M. A. Reverse transcriptase inhibitors can selectively block the synthesis of differently sized viral DNA transcripts in cells acutely infected with human immunodeficiency virus type 1. *J. Virol*. **1999**, 73(8), 6700–6707.https://10.1128/JVI.73.8.6700-6707.1999.

(10) Gardner, K.; Hall, P. A.; Chinnery, P. F. and Payne, B. A. I. HIV Treatment and Associated Mitochondrial Pathology: Review of 25 Years of in Vitro, Animal, and Human Studies, *Toxicol. Pathol.* **2014**, 42, 811–822. https://doi.org/10.1177/0192623313503519.

(11) D'Aquila, R. T.; Johnson, V. A.; Welles, S. L.; Japour, A. J.; Kuritzkes, D. R.; DeGruttola, V.; Reichelderfer, P. S.; Coombs, R. W.; Crumpacker, C. S.; Kahn, J. O.; et al., Zidovudine resistance and HIV-1 disease progression during antiretroviral therapy. *Ann. Intern. Med.* **1995**, 122(6), 401–408. https://doi.org/10.7326/0003-4819-122-6-199503150-00001.

(12) Kumar, P. N. and Patel, P. Lamivudine for the treatment of HIV. *Expert Opin. Drug Metab. Toxicol.* **2009**, 6(1), 105–114. https://doi.org/10.1517/17425250903490418.

(13) Deval, J.; Powdrill, M. H.; D'Abramo, C. M.; Cellai, L. and Götte, M. Pyrophosphorolytic excision of nonobligate chain terminators by hepatitis C virus NS5B

polymerase. *Antimicrob. Agents Chemother.* **2007**, 51(8), 2920–2928. https://doi.org/10.1128/AAC.00186-07.

(14) Fung, A.; Jin, Z.; Dyatkina, N.; Wang, G.; Beigelman, L. and Deval, J. Efficiency of Incorporation and Chain Termination Determines the Inhibition Potency of 2'-Modified Nucleotide Analogs against Hepatitis C Virus Polymerase, *Antimicrob. Agents Chemother.* **2014**, 58(7), 3636–3645. https://doi.org/10.1128/AAC.02666-14.

(15) Ma, H.; Jiang, W.-R.; Robledo, N.; Leveque, V.; Ali, S.; Lara-Jaime, T.; Masjedizadeh, M.; Smith, D. B.; Cammack, N.; Klumpp, K. et al. Characterization of the Metabolic Activation of Hepatitis C Virus Nucleoside Inhibitor-D-2-Deoxy-2-fluoro-2-C-methylcytidine (PSI-6130) and Identification of a Novel Active 5-Triphosphate Species. *J. Biol. Chem.* **2007**, 282(41), 29812–29820. https://10.1074/jbc.M705274200.

(16) Esposito, F.; Corona, A. and Tramontano, E. HIV-1 Reverse Transcriptase Still Remains a New Drug Target: Structure, Function, Classical Inhibitors, and New Inhibitors with Innovative Mechanisms of Actions. *Mol. Biol. Int.* **2012**, 2012, 1–23. https://doi.org/10.1155/2012/586401.

(17) Zhou, H.; Liu, Q.; Shi, T.; Yu, Y. and Lu, H. Genome-wide screen of fission yeast mutants for sensitivity to 6-azauracil, an inhibitor of transcriptional elongation. *Yeast* **2015**, 32(10), 643–655. https://doi.org/10.1002/yea.3085.

(18) Priet, S.; Sire, J. and Quérat, G. Uracils as a Cellular Weapon Against Viruses and Mechanisms of Viral Escape. *Curr. HIV Res.* **2005**, 4(1), 31–42. https://doi.org/10.2174/157016206775197673.

(19) Vincent-Rocan, J.-F.; Ivanovich, R. A.; Clavette, C.; Leckett, K.; Bejjani, J. and Beauchemin, A. M. Cascade reactions of nitrogen-substituted isocyanates: a new tool in heterocyclic chemistry. *Chem. Sci.*, **2016**, 7(1), 315–328. https://doi.org/10.1039/C5SC03197D.

(20) Kolb, H. C.; Finn, M. G. and Sharpless, K. B. Click Chemistry: Diverse Chemical Function from a Few Good Reactions. *Angew. Chemie Int. Ed.* **2001**, 40(11), 2004–2021. https://doi.org/10.1002/1521-3773(20010601)40:11<2004::AID-ANIE2004>3.0.CO;2-5.

(21) Rostovtsev, V. V.; Green, L. G.; Fokin, V. V. and Sharpless, K. B. A stepwise huisgen cycloaddition process: Copper(I)-catalyzed regioselective "ligation" of azides and terminal alkynes. *Angew. Chemie Int. Ed.* **2002**, 41(14), 2596–2599. https://10.1002/1521-3773(20020715)41:14<2596::AID-ANIE2596>3.0.CO;2-4.

(22) Tornøe, C. W.; Christensen, C. and Meldal, M. Peptidotriazoles on Solid Phase: [1,2,3]-Triazoles by Regiospecific Copper(I)-Catalyzed 1,3-Dipolar Cycloadditions of Terminal Alkynes to Azides. *J. Org. Chem.* **2002**, 67(9), 3057–3064. https://doi.org/10.1021/jo011148j.

(23) Worrell, B. T.; Malik, J. A. and Fokin, V. V. Direct evidence of a dinuclear copper intermediate in Cu(I)-catalyzed azide-alkyne cycloadditions. *Science* **2013**, 340(6131), 457–60. https://doi.org/10.1126/science.1229506.

(24) McKay, C. S and Finn, M. G. Click Chemistry in Complex Mixtures: Bioorthogonal Bioconjugation. *Chem. Biol.* **2014**, 21(9), 1075–1101. https://doi.org/10.1016/J.CHEMBIOL.2014.09.002

(25) Desrochers, G. F. and Pezacki, J. P. ABPP and Host–Virus Interactions. In *Current Topics in Microbiology and Immunology*, Vol. 420; Springer International Publishing, **2019**; pp. 131–154. https://doi.org/10.1007/82_2018_139.

(26) Moellering, R. E. and Cravatt, B.F. How chemoproteomics can enable drug discovery and development. *Chem. Biol.* **2012**, 19(1), 11–22. https://doi.org/10.1016/j.chembiol.2012.01.001.

(27) Goldschmidt, V.; Didierjean, J.; Ehresmann, B.; Ehresmann, B.; Isel, C. and Marquet, R. Mg2+ dependency of HIV-1 reverse transcription, inhibition by nucleoside analogues and resistance. *Nucleic Acids Res.* **2006**, 34(1), 42–52. https://doi.org/10.1093/nar/gkj411.

(28) Das, K.; Martinez, S. E. and Arnold, E. Structural Insights into HIV reverse transcriptase mutations Q151m and Q151m complex that confer multinucleoside drug resistance. *Antimicrob. Agents Chemother.* **2017**, 61(6), e00224-17. https://doi.org/10.1128/AAC.00224-17

(29) Hlaváč, J. and Slouka, J. Cyclocondensation Reactions of Heterocyclic Carbonyl Compounds. [1]. Synthesis of 2,6-bs(6-azauracil-5-yl)aniline and its Use for Synthesis of Some Other Polynuclear 1,2,4-Triazines. *J. Heterocycl. Chem.* **1997**, 34, 917.

(30) Lakner, F. J.; Xia, H.; Pervin, A.; Hammaker, J. R.; Jahangiri, K. G.; Dalton, M. K.; Khvat, A.; Kiselyov, A. and Ivachtchenko, A. V. A novel mesoionic ring system: Unusual cyclization of thio- and amino-acid derivatives of 6-azauracil. *Tetrahedron Lett.* **2005**, 46(32), 5325–5328. https://doi.org/10.1016/j.tetlet.2005.06.032.

(31) Saegusa, Y.; Harada, S. and Nakamura, S. J. Ring-opening reaction of 1,3,4-oxadiazolone and 1,3,4-oxadiazolinethione: Reaction of 2-phenyl-1,3,4-oxadiazolin-5-one and 2-phenyl-1,3,4-oxadiazoline-5-thione with amines. *Heterocycl. Chem.* **1988**, 25(5), 1337–1342. https://doi.org/10.1002/jhet.5570250513.

(32) Jencks, W. P. On the attribution and additivity of binding energies (proteins/ligands/entropy/enzymes). *Proc. Natl. Acad. Sci. U. S. A.* **1981**, 78(7), 4046–4050. https://doi.org/10.1073/pnas.78.7.4046.

(33) Iyidogan, P.; Sullivan, T. J.; Chordia, M. D.; Frey, K. M. and Anderson, K. S. Design, Synthesis, and Antiviral Evaluation of Chimeric Inhibitors of HIV Reverse Transcriptase. *ACS Med. Chem. Lett.* **2013**, 4(12), 1183–1188. https://doi.org/10.1021/ml4002979.

(34) Bailey, C. M.; Sullivan, T. J.; Iyidogan, P.; Tirado-Rives, J.; Chung, R.; Ruiz-Caro, J.; Mohamed, E.; Jorgensen, W. L.; Hunter, R. et al. Bifunctional inhibition of human immunodeficiency virus type 1 reverse transcriptase: mechanism and proof-of-concept as

a novel therapeutic design strategy. *J. Med. Chem.* **2013**, 56(10), 3959–3968. https://doi.org/10.1021/jm400160s.

(35) Paiva, S. L. and Crews, C. M. Targeted protein degradation: elements of PROTAC design. *Curr. Opin. Chem. Biol.* **2019**, 50, 111–119. https://doi.org/10.1016/j.cbpa.2019.02.022.

(36) Smith, B. E.; Wang, S. L.; Jaime-Figueroa, S.; Harbin, A.; Wang, J.; Hamman, B. D. and Crews, C. M. Differential PROTAC substrate specificity dictated by orientation of recruited E3 ligase. *Nat. Commun.* **2019**, 10(1), 131. https://doi.org/10.1038/s41467-018-08027-7

(37) Cromm, P. M. and Crews, C. M. Targeted Protein Degradation: from Chemical Biology to Drug Discovery. *Cell Chem. Biol.* **2017**, 24, 1181–1190. https://doi.org/10.1016/j.chembiol.2017.05.024.

(38) Tamura, T.; Ueda, T.; Goto, T.; Tsukidate, T.; Shapira, Y.; Nishikawa, Y.; Fujisawa, A. and Hamachi, I. Rapid labelling and covalent inhibition of intracellular native proteins using ligand-directed N-Acyl-N-Alkyl sulfonamide. *Nat. Commun.* **2018**, 9(1), 1870. https://doi.org/10.1038/s41467-018-04343-0.

(39) Takaoka, Y.; Ojida, A. and Hamachi, I. Protein organic chemistry and applications for labeling and engineering in live-cell systems. *Angew. Chem. Int. Ed. Engl.* **2013**, 52(15), 4088–106. https://doi.org/10.1002/anie.201207089.

(40) Ciubotaru, M.; Musat, M. G.; Surleac, M.; Ionita, E.; Petrescu, A. J.; Abele, E. and Abele, R. The Design of New HIV-IN Tethered Bifunctional Inhibitors Using Multiple Microdomain Targeted Docking. *Curr. Med. Chem.* **2019**, 26(15), 2574–2600. https://doi.org/10.2174/0929867325666180406114405.

(41) Zhou, L.; Amer, A.; Korn, M.; Burda, R.; Balzarini, J.; De Clercq, E.; Kern, E. R. and Torrence, P. F. Synthesis and antiviral activities of 1,2,3-triazole functionalized thymidines: 1,3-Dipolar cycloaddition for efficient regioselective diversity generation. *Antivir. Chem. Chemother.* **2005**, 16(6), 375–383. https://doi.org/10.1177/095632020501600604.

(42) King, R. W.; Klabe, R. M.; Reid, C. D. and Erickson-Viitanen, S. K. Potency of Nonnucleoside Reverse Transcriptase Inhibitors (NNRTIs) Used in Combination with Other Human Immunodeficiency Virus NNRTIs, NRTIs, or Protease Inhibitors. *Antimicrob. Agents Chemother.* **2002**, 46(6), 1640–1646. https://doi.org/10.1128/AAC.46.6.1640-1646.2002.

(43) Baba, M.; De Clercqt, E.; Tanakat, H.; Ubasawa, M.; Takashima, H.; Sekiya, K.; Nitta, I.; Umezu, K.; Nakashimat, H.; Mori, S.; Shigeta, S. et al., Potent and selective inhibition of human immunodeficiency virus type 1 (HIV-1) by 5-ethyl-6-phenylthiouracil derivatives through their interaction with the HIV-1 reverse transcriptase. *Proc. Natl. Acad. Sci. USA* **1991**, 88, 2356–2360. https://doi.org/10.1073/pnas.88.6.2356.

(44) Xing, L.; Wang, S.; Hu, Q.; Li, J. and Zeng, Y. Comparison of three quantification methods for the TZM-bl pseudovirus assay for screening of anti-HIV-1 agents. *J. Virol. Methods* **2016**, 233, 56–61. https://doi.org/10.1016/j.jviromet.2016.03.008.

(45) Monette, A.; Ajamian, L.; López-Lastra, M. and Mouland, A. J. Human immunodeficiency virus type 1 (HIV-1) induces the cytoplasmic retention of heterogeneous nuclear ribonucleoprotein A1 by disrupting nuclear import. Implications for HIV-1 gene expression. *J. Biol. Chem.* **2009**, 284(45), 31350–31362. https://doi.org/10.1074/jbc.M109.048736.

Chapter 4: Reactivity of N-acyl hydrazone probes with the mammalian proteome

Initially published as Tyler A. Shaw, Megan H. Powdrill, Allison R. Sherratt, Keira Garland, Bin-Jie Li, André M. Beauchemin, and John Paul Pezacki. (2021) Reactivity of N-acyl Hydrazone Probes with the Mammalian Proteome. *RSC Med. Chem.* 12:797-803.

4.1 Statement of Contribution

JPP and AMB conceived of the project and directed the work. TS conducted the majority of the experiments, interpretations and drafted the manuscript. MHP and ARS helped with proteomics and performed some biochemical assays. KG and B-JL synthesized probes and performed reactivity studies. The other authors contributed to data collection and interpretation. The manuscript was written through contributions of all authors. All authors have given approval to the final version of the manuscript.

4.1.1Acknowledgements

Thanks to Dr. Dennis Öczelik for technical help. We'd like to thank Dr. Linda Chelico for supplying us with purified APOBEC proteins. The authors thank the Natural Sciences and Engineering Research Council of Canada (NSERC) and the University of Ottawa for financial support of this work. Bin-Jie Li thanks the China Scholarship Council for a graduate scholarship.

4.2 Summary

Small molecule probes with distinct reactivities are useful tools for the identification and characterization of protein modifications and function. Herein, we show that hydrazone probes with an N-carbamate structural motif react differently from N-carbamates within the human

proteome. Mass spectrometry analysis of probe-treated mammalian cell lysates identified several proteins that were covalently modified by the hydrazone probes, including the cytidine deaminase APOBEC3A. We used this enzyme as a model to explore the reactivity of the probes with amino acid residues using LC-MS/MS. Both reactive serine and cysteine residues outside of the enzyme active site were covalently modified. A 1-napthol leaving group provided the most extensive reactivity. These results confirm a unique chemotype for hydrazone probes which can be further optimized to target distinct targets of the human proteome.

4.3 Introduction

Small molecule probes are one of many functional proteomics tools that have contributed to an understanding of the complex biological functions and mechanisms of the human proteome. Many classes of enzymes or individual proteins can be examined using existing probes, including kinases, phosphatases, hydrolases and proteases; however, not all proteins within these classes can be studied using established probes and many classes of enzymes are not targeted at all.[1–3] The development of probes with new chemotypes and novel reactivities, such as electrophilic probes that permit the study of nucleophilic protein modifications or co-factors, provide new opportunities to elucidate functions of proteins not accessible with current probes.[4] In establishing new probe chemotypes, researchers hope to discover previously unreported reactivities that allow the study of proteins involved in pathological processes. For example, a fluorophosphonate (FP) probe was developed and used extensively to target the serine hydrolase subfamily and the carbamate chemotype was found to be more specific to particular serine hydrolases within this subfamily.[5,6] Serine hydrolases are important biological targets to study as they are involved in

neurodegenerative and metabolic disease and probes are being modified to target specific enzymes within this class for study or inhibition.[7–9]

One of our groups has previously studied hydrazone derivatives of carbamate probes which possess leaving groups directly linked to the carbonyl group, and used their ability to act as precursors to rare nitrogen-substituted isocyanates.[10] From a synthetic perspective, these carbamate-hydrazone hybrids exhibited rich reactivity and engaged in a variety of reactions, providing products incorporating the NNCO motif that is present in over 50 pharmaceuticals and agrochemicals.[11] However, to our knowledge the biological activity and specificity of such carbamate-hydrazone hybrids has not been evaluated. Given that these hybrids differ from carbamates by possessing an additional nitrogen atom, modifying their hydrogen-bonding ability and the electrophilicity of their carbonyl, we hypothesized that such carbamate-hydrazone hybrids would display different specificity but could similarly be used to monitor the activity of serine hydrolases in the complex human proteome.

In order to compare the reactivities of carbamate scaffolds with those of N-acyl hydrazones, we designed probes to have the same leaving groups as previous carbamate inhibitors.[6] Modification of the leaving group on these molecules was shown to have a significant influence on both potency and selectivity.[12] Particularly, naphthyl leaving groups were shown to be selective for AADACL1 and FAAH2.[6] Since hydrazone probes can react at either of two electrophilic sites (Scheme 4-2), we hypothesized that leaving group structure may be important for carbonyl addition reactions. Probes were designed to contain alkyne groups for further modification after

Scheme 4-1. Structural comparison of traditional carbamate and N-acyl hydrazone scaffolds used in this study.

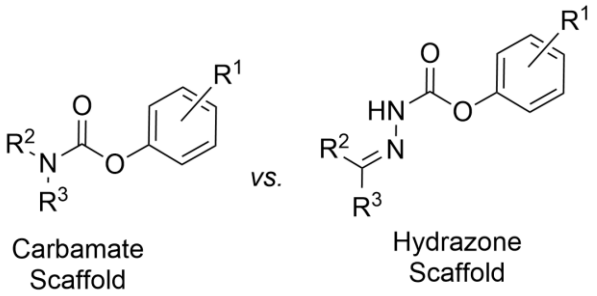

Carbamate Scaffold

Hydrazone Scaffold

Scheme 4-2. Mechanisms for enzyme active site modifications by nucleophilic residues in serine hydrolases.

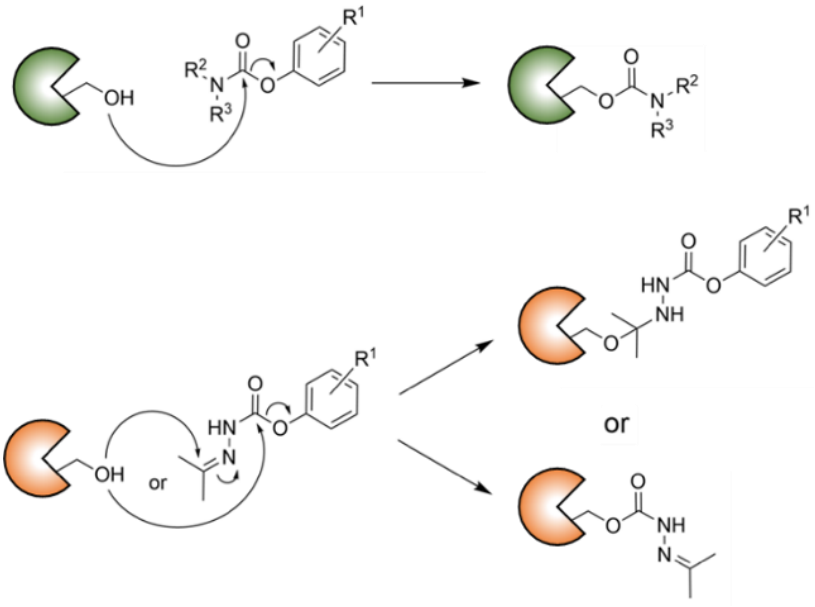

incubation with human cell proteomes. The alkyne group allows a traditional activity-based protein profiling (ABPP) approach to be used, employing azide-alkyne cycloaddition to conjugate the probe-labelled proteome with click chemistry to add a fluorophore for visualization of proteins on SDS-PAGE or biotin azide to selectively enrich proteins from a complex proteome.[17–19] Herein, we show that carbamate-hydrazone hybrid probes display a unique reactivity profile, demonstrating that they were not targeting the active site of serine hydrolases despite structural similarities to probes with carbamate scaffolds. Using a combination of in-gel proteome labelling and LC-MS/MS, we identify targets within the human proteome modified by these probes, and establish their mechanism of reaction.

4.4 Methods

4.4.1 Cell Culture and Labelling

Cell lines were maintained in Dulbecco's Modified Eagle Medium (DMEM) supplemented with 10 % fetal bovine serum (FBS) at 37 °C and 5 % CO_2. MCF-7 cells were also supplemented with 10% insulin. For *in vitro* labelling studies, cells were seeded at a density of 2.5 x 10^6 cells/10 cm plate, incubated overnight, the medium was removed, and cells were washed twice with phosphate buffered saline (PBS). Cells were harvested in ice-cold PBS containing 1 % Triton X-100 and briefly sonicated. The soluble proteome was collected following centrifugation at 14,000 x g for 15 min at 4 °C. The soluble proteome was incubated with 10 uM of the different probes for 1 h at room temperature. Protein concentrations were quantified using a Bio-Rad DC protein assay. For all reactions, samples were diluted to a concentration of 1 mg/mL and 70 µg of protein from each condition was removed for a copper-catalyzed click reaction with rhodamine azide. The click reaction was performed in PBS containing 1 mM freshly prepared tris(2-carboxyethyl)phosphine

(TCEP), 100 μM tris(benzyltriazolylmethyl)amine (TBTA), 1 mM $CuSO_4$, and 100 μM rhodamine azide. Following a 1 h incubation at room temperature on a rotator, the reaction was quenched by acetone precipitation. Samples were resolved by 12 % SDS-PAGE and visualized using in-gel fluorescence scanning on a ChemiDoc MP system (Bio-Rad).

4.4.2 Mass Spectrometry

Streptavidin enrichment, sample processing and mass spec identification of hydrazone-labelled proteins was performed as previously described.[23] To identify specific residues modified by the hydrazone probes, purified APOBEC3A (a kind gift from Linda Chelico at the University of Saskatchewan) was incubated for 1 h at room temperature with 10 μM of designated probe. Samples were reduced with 20 mM DTT and heated to 65 °C for 30 min. Subsequently, 25 mM iodoacetamide was added and samples rotated in the dark for 45 min at room temperature. Samples were buffer exchanged into 100 mM triethylammonium bicarbonate (TEAB) using Bio-Rad P-6 columns and the volume adjusted to 100 μL in TEAB buffer. Samples were digested using trypsin (10 ng/μL) overnight at 37 °C then loaded onto a BioSpin C18 column, centrifuged at 1,500 x g for 1 min, washed twice with 0.5 % trifluoroacetic acid (TFA) in 5 % acetonitrile (ACN), and eluted with 70 % ACN. Peptides were vacuum dried.

4.5 Results

In an effort to expand the toolkit of probes available for functional proteomics, and to understand the biochemistry of N-acyl hydrazones that have structural and chemical similarities to carbamate scaffolds, we designed a series of N-acyl-hydrazone probes with different ring structures (Probes A-C; Scheme 4-3), which serve as leaving groups following nucleophilic displacement. Probe D contains a methyl group on the hydrazone nitrogen bearing the acyl group

to help probe the importance of the N-H group on reactivity and specificity (Probe D; Scheme 4-3).

To examine the protein targets of our probes, we utilized a profiling approach consisting of in-gel fluorescence assays to obtain a visual profile of the targets combined with LC-MS/MS to identify the labelled proteins. We performed a preliminary screen of our probes in human cell lines including the hepatocellular carcinoma Huh7 cell line, MCF7 breast adenocarcinoma cells, A549 lung carcinoma cells as well as Vero African green monkey fibroblast-like kidney cells. Proteomes from these cell lines were incubated with hydrazone probes, labelled with a fluorophore using click chemistry, resolved by SDS-PAGE and visualized by fluorescent scanning. We observed different banding patterns within each cell line, illustrating the unique natures of their protein profiles (Figure 4-1). The proteome of the MCF7 cell line displays the most extensive reactivity with the probes, while Vero cells show the lowest reactivity, based on the number of bands visible and the intensity of the bands. Targets of probe B displayed significantly higher levels of labelling as compared to both probe A and probe C. Since 1-naphtol is the best leaving group, it is expected that probe B would be the most reactive. The presence of the methyl group adjacent to the hydrazone moiety (probe D) further decreases labelling, as an isocyanate intermediate cannot form and internal proton transfer is not possible with this chemical moiety.[20]

To determine if N-acyl hydrazone probes react similarly to carbamate analogs, we examined their ability to label serine hydrolases, a common target of carbamate inhibitors. We compared the labeling patterns with the well-established fluorphosphonate (FP) probe.[21,22] A visual comparison the labelling of hydrozones to that of FP interestingly shows that the hydrazone-

Scheme 4-3. Structure of hydrazone probes used in this study. The targeting region of the probes contains a hydrazone, while the leaving groups include phenol (Probes A, D) or naphtol (Probes B, C). Probe D has a phenol leaving group identical to that on probe A but contains an additional methyl group preventing acid-base chemistry at that location.

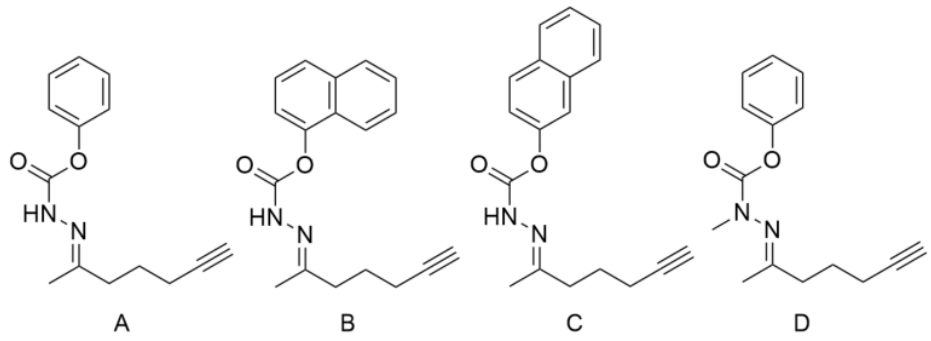

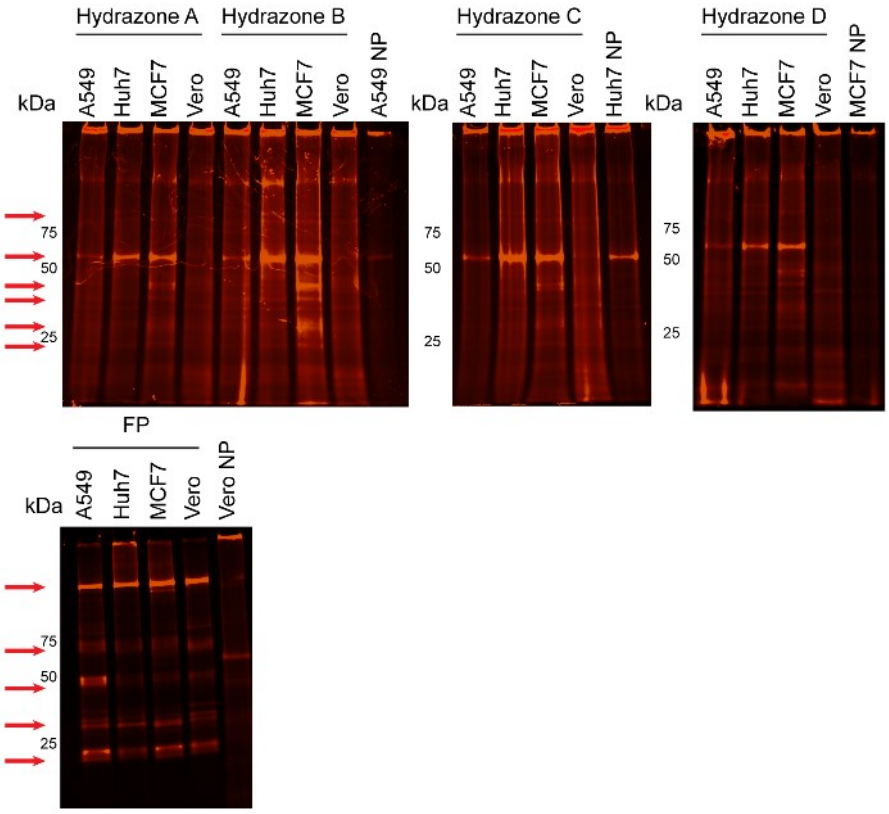

Figure 4-1. In gel labelling of hydrazone targets.

Proteomes from designated cell lines were incubated with hydrazone probes A through D or FP. After a copper-catalyzed click reaction with rhodamine azide, samples were resolved on 12% polyacrylamide gels. The red arrows highlight some of the bands representing labelled proteins. The no probe (NP) samples were subjected to the click reaction but were not incubated with probe.

labelled proteome is distinctly labelled, as evidenced by significantly different banding patterns (Figure 4-1). Further quantification of the labelled proteomes with probes A-D confirmed that they do not appreciably label serine hydrolases despite their chemical similarity to carbamates.

Based on the in-gel labelling profiles of the hydrazone probes as compared to the FP probe, we observe that the targets of the hydrazones are distinct from the FP targets. To compare and contrast the targets of probe A and FP, Huh7 lysates were incubated with each probe and labelled proteins tagged with biotin azide by copper-catalyzed cycloaddition. The labelled proteomes were enriched via streptavidin pulldown, digested with trypsin, subjected to LC-MS/MS analysis, and classified into protein families using PANTHER (Figure 4-2).[23,24] Mass spectrometry demonstrated that the hydrazone probe had a preference for nucleic acid binding proteins and transporter proteins (Figure 4-2A). The targets of both probes were then cross-referenced, and 47 proteins, out of a total of 183 (FP) and 835 (Probe A), were labelled by both probes.

To identify putative targets of the hydrazone probes, Huh7 lysates labelled with probes A-C were subjected to mass spectrometry analysis as described above.[23,24] As shown in Table 8-1, the protein reactivity of probe B was more extensive than that of probes A or C, consistent with the in-gel fluorescence shown in Figure 4-1. The targets pulled down by the different probes had very limited overlap, with only non-specific proteins such as actin showing up in each profile. One protein identified as a target of probe A, APOBEC3A, is a cytidine deaminase that plays an important role during viral infection and in many cancers.[25,26] This protein was chosen as a model to establish the specific amino acids modified by the hydrazone probes.

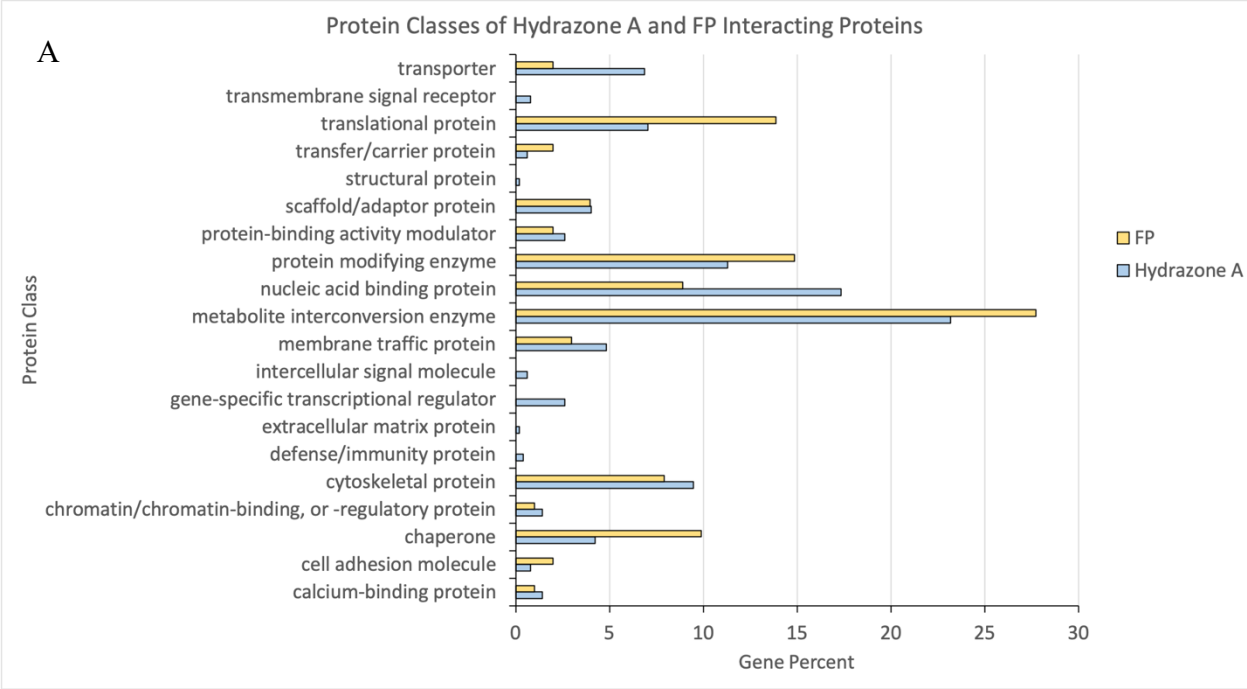

Figure 4-2. Interacting protein classes of FP and hydrazone probe A.

Huh7 lysates were incubated with each probe, reacted with biotin azide, and subjected to streptavidin enrichment. The enriched proteome was trypsin digested and submitted for mass spectrometry. Protein targets were classified using PANTHER. A) bar chart of classes of protein targets B) venn-diagram showing overlapping targets of both probes.

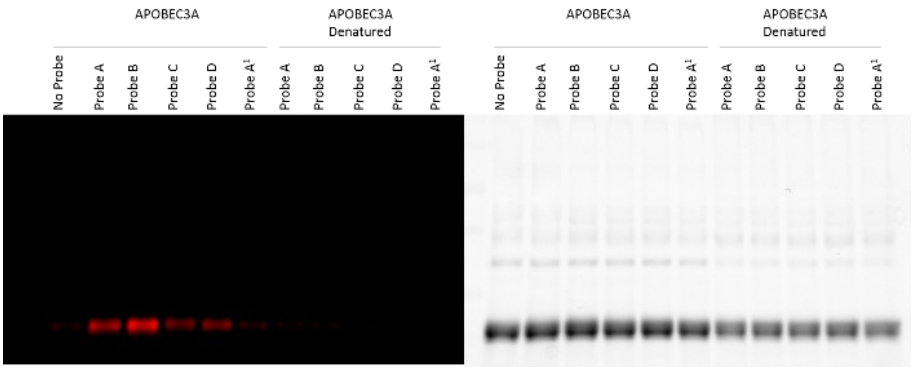

Figure 4-3. Labelling of purified APOBEC3A.

Fluorescence (left) and whole protein stain-free (right) scans for each gel are shown. Probe A^1 is structurally similar to probe A but lacks the alkyne group.

To examine the mechanism of probe reactivity with protein targets, we incubated purified APOBEC3A with our probes. We first used in-gel fluorescence to confirm *in vitro* targeting of APOBEC3A by the hydrazone probes (Figure 4-3). Probe D labelled APOBEC3A to a slightly lesser degree than probe A, indicating that the methyl group has a minor effect on the reactivity. Heat denaturation of the samples prevented probe binding, suggesting that there is a structural requirement for probe binding.

We performed LC-MS/MS analysis of probe A-labelled APOBEC3A proteins to identify the amino acids targeted by the probe. (Table 8-2, and Table 8-3). The adducts observed by MS are displayed on a crystal structure of APOBEC3A (5KEG),[27] in Figure 4-4. We observe modification of nucleophilic cysteine and serine residues. A single cysteine residue, C34, was discovered with a cross correlation score greater than 2.0 in three independent trials of the experiment. This suggests that C34 reacts with probe A. However, the adduct that was discovered is not located near the enzyme active site, indicating that the enzyme is not targeted through an activity-based mechanism, but instead react with reactive cysteine and serine nucleophilic residues in an affinity-dependent manner.

To provide further support for the adducts observed by LC-MS/MS, we also observed the reactions of hydrazone probes with biological nucleophiles via NMR (Figures 8-1, 8-2). Hydrazone A was tested with N-acetyl cysteine and yielded the same adduct discovered in the LC-MS/MS experiments. These results provided not only chemical confirmation of protein modification, but also demonstrated the possibility of intramolecular exchange of the adduct following initial labelling. NMR experiments (Figures 8-1, 8-2) confirmed that a nucleophilic thiol can react with the hydrazone moiety to form the adduct shown in Eq. 4-1 and can be exchanged with other

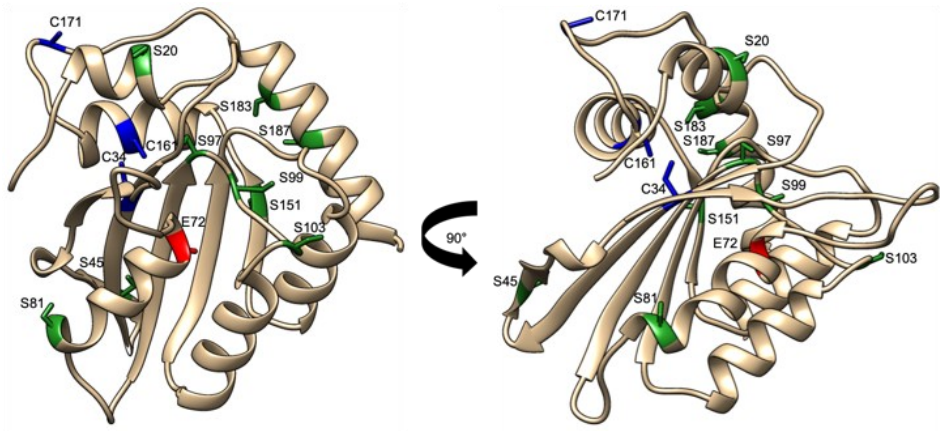

Figure 4-4. Modification sites on APOBEC3A with hydrazone probe A.

Ribbon structure of APOBEC3A (PDB 5KEG). The active site E72 is mutated to A72 in this structure (shown in red). Cystine residues modified by probe A are shown in blue and serine residues are shown in green.

nucleophilic residues such as primary amines or alcohols to form an analogous product demonstrated in Eq. 4-2.

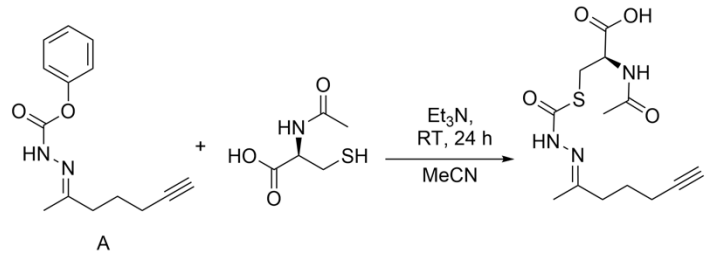

Eq.4-1

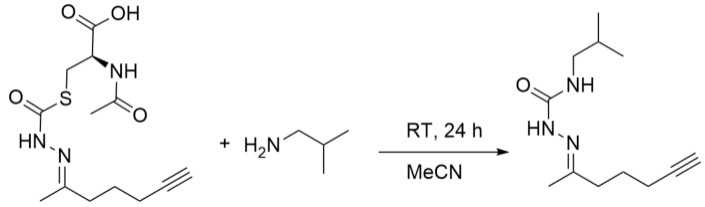

Eq. 4-2

This chemical exchange may explain why we see multiple residues labelled for APOBEC3A. We postulate that a kinetic product is formed first with the nucleophilic cysteine residue and then exchanges to the thermodynamically more stable serine adducts. This observation of chemical exchange suggests that an initial adduct could form with cysteine thiols and undergo intramolecular exchange to proximal residues and explains the variation of adducts seen in the mass spectrometry experiments. Deamination assays confirmed that the probes reacted with residues outside of the enzyme active site. The assays were performed with purified ABOPEC proteins labelled by probe A alone, or labelled by Probe A and conjugated to a biotin. Probe A did not inhibit APOBEC deamination activity (Figure 8-3), confirming that it binds outside of the active site. Even with the addition of a bulky biotin group on the probe, the activity of the APOBEC enzymes was not affected and therefore it was concluded that the probe must bind to APOBEC proteins through an affinity-based mechanism. Having established that hydrazone probes have an affinity-based interaction with APOBEC3A, we then sought to use probe A to pull down the

deaminase from MCF-7 or A549 cells stimulated with interferon gamma (Figure 4-5). Unfortunately A3A was not present in the pulldowns, regardless of interferon stimulation, indicating that the protein was not present in high enough concentration in these cell types as compared with human hepatoma cells. These additional pulldowns were then classified using PANTHER to compare the proteins that reacted with the probes in each cell type.

4.6 Discussion

In this study, we have developed a series of hydrazone probes with varying oxygen-substituted structures that are expected to serve as leaving groups upon formation of a covalent enzyme-probe adduct. Previous work with probes based on a carbamate scaffold has shown that the structure of the leaving group makes a significant contribution to potency and selectivity[6,12]. Particularly, naphthyl leaving groups were shown to be selective for AADACL1 and FAAH2.[6] Carbamates have been demonstrated to target a distinct group of serine hydrolases. Serine hydrolases play important roles in a variety of disease states and, therefore, carbamates can serve as useful tools to study their activity. However, in comparing profiles with those obtained using carbamate probes we discovered that structurally similar N-acyl hydrazones target different enzymes are less selective and more reactive generally.[6] Despite some structural similarities of our probes with carbamates, the compounds developed for our study modified both serine and cysteine moieties. In agreement with previous work showing that the leaving group structure can greatly affect probe specificity, we found that slight changes in the naphthyl structures of probe B and probe C had a significant impact on specificity.[6] Fine tuning of the leaving group may help to target the probe to specific residues and limit cross-reactivity. Future work will examine these selectivity profiles against mammalian proteomes.

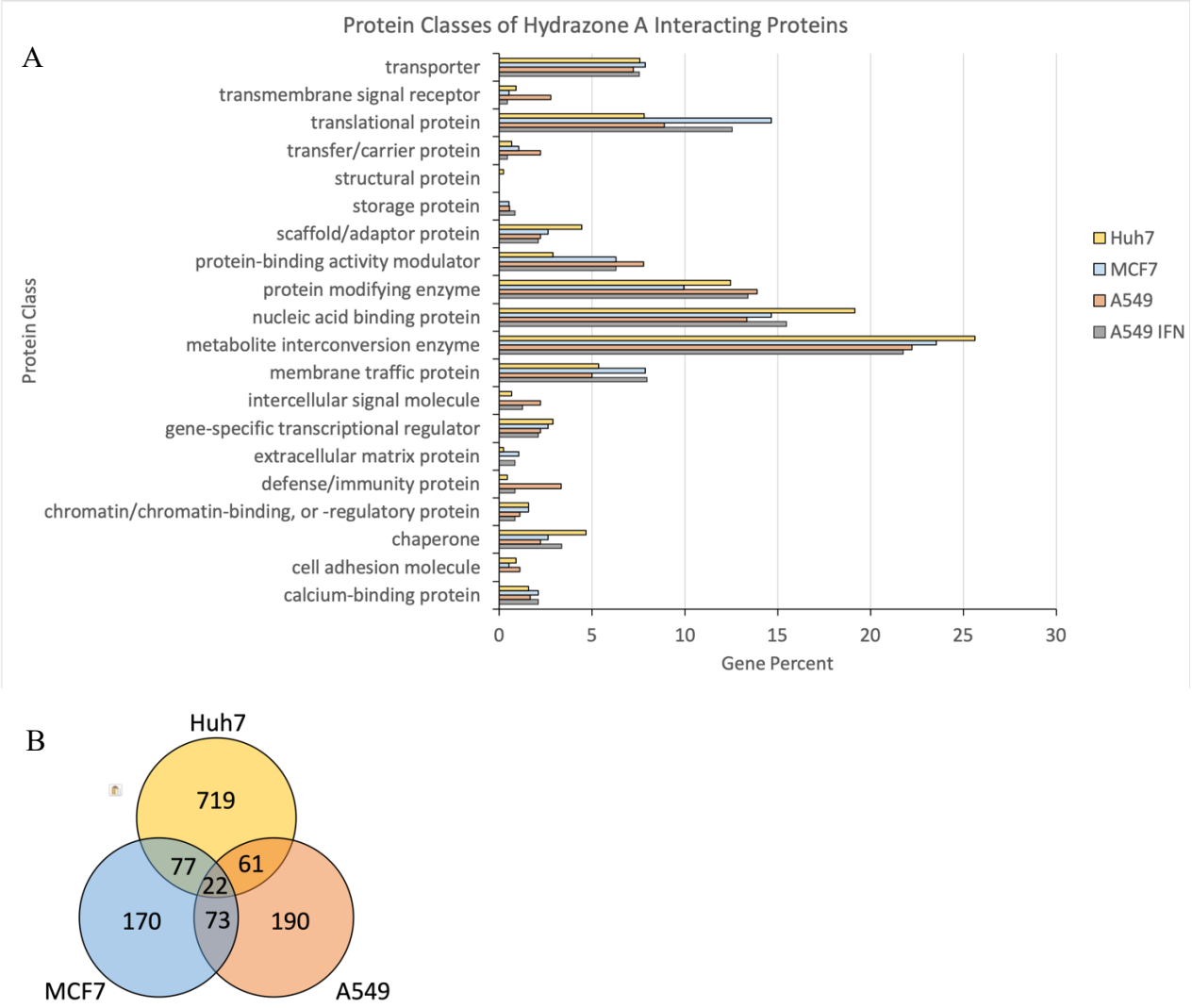

Figure 4-5. Comparison of Hydrazone A targets in various cell lines.

Lysates were incubated with each probe, tagged with biotin azide and subjected to streptavidin enrichment. The enriched proteome was digested with trypsin and submitted for mass spectrometry. Protein targets were classified using PANTHER. A) bar chart of classes of protein targets B) Venn diagram of overlapping targets in each cell line.

4.7 References

(1) Benns, H. J.; Wincott, C. J.; Tate, E. W.; Child, M. A. Activity- and Reactivity-Based Proteomics: Recent Technological Advances and Applications in Drug Discovery. In *Current Opinion in Chemical Biology*, Elsevier Ltd, **2021**; pp 20–29. https://doi.org/10.1016/j.cbpa.2020.06.011.

(2) Deng, H.; Lei, Q.; Wu, Y.; He, Y.; Li, W. Activity-Based Protein Profiling: Recent Advances in Medicinal Chemistry. *Eur. J. Med. Chem.* **2020**, 191. https://doi.org/10.1016/j.ejmech.2020.112151.

(3) Bachovchin, D. A.; Brown, S. J.; Rosen, H.; Cravatt, B. F. Substrate-Free High-Throughput Screening Identifies Selective Inhibitors for Uncharacterized Enzymes. *Nat. Biotechnol.* **2009**, *27* (4), 387–394. https://doi.org/10.1038/nbt.1531.

(4) Matthews, M. L.; He, L.; Horning, B. D.; Olson, E. J.; Correia, B. E.; Yates, J. R.; Dawson, P. E.; Cravatt, B. F. Chemoproteomic Profiling and Discovery of Protein Electrophiles in Human Cells. *Nat. Chem.* **2017**, *9* (3), 234–243. https://doi.org/10.1038/nchem.2645.

(5) Li, W.; Blankman, J. L.; Cravatt, B. F. A Functional Proteomic Strategy to Discover Inhibitors for Uncharacterized Hydrolases. *J. Am. Chem. Soc.* **2007**, *129* (31), 9594–9595. https://doi.org/10.1021/ja073650c.

(6) Bachovchin, D. A.; Ji, T.; Li, W.; Simon, G. M.; Blankman, J. L.; Adibekian, A.; Hoover, H.; Niessen, S.; Cravatt, B. F. Superfamily-Wide Portrait of Serine Hydrolase Inhibition

Achieved by Library-versus-Library Screening. *Proc. Natl. Acad. Sci. U. S. A.* **2010**, *107* (49), 20941–20946. https://doi.org/10.1073/pnas.1011663107.

(7) Chang, J. W.; Nomura, D. K.; Cravatt, B. F. A Potent and Selective Inhibitor of KIAA1363/AADACL1 That Impairs Prostate Cancer Pathogenesis. *Chem. Biol.* **2011**, *18* (4), 476–484. https://doi.org/10.1016/j.chembiol.2011.02.008.

(8) Niphakis, M. J.; Cognetta, A. B.; Chang, J. W.; Buczynski, M. W.; Parsons, L. H.; Byrne, F.; Burston, J. J.; Chapman, V.; Cravatt, B. F. Evaluation of NHS Carbamates as a Potent and Selective Class of Endocannabinoid Hydrolase Inhibitors. *ACS Chem. Neurosci.* **2013**, *4* (9), 1322–1332. https://doi.org/10.1021/cn400116z.

(9) Viader, A.; Ogasawara, D.; Joslyn, C. M.; Sanchez-Alavez, M.; Mori, S.; Nguyen, W.; Conti, B.; Cravatt, B. F. A Chemical Proteomic Atlas of Brain Serine Hydrolases Identifies Cell Type-Specific Pathways Regulating Neuroinflammation. *Elife* **2016**, *5*, e12345. https://doi.org/10.7554/eLife.12345.

(10) Garland, K.; Gan, W.; Depatie-Sicard, C.; Beauchemin, A. M. A Practical Approach to Semicarbazone and Hydrazone Derivatives via Imino-Isocyanates. *Org. Lett.* **2013**, *15* (16), 4074–4077. https://doi.org/10.1021/ol4016089.

(11) Vincent-Rocan, J.-F.; Ivanovich, R. A.; Clavette, C.; Leckett, K.; Bejjani, J.; Beauchemin, A. M. Cascade Reactions of Nitrogen-Substituted Isocyanates: A New Tool in Heterocyclic Chemistry. *Chem. Sci.* **2016**, *7* (1), 315–328. https://doi.org/10.1039/C5SC03197D.

(12) Armand Cognetta III, A. B.; Niphakis, M. J.; Lee, H.-C.; Martini, M. L.; Hulce, J. J. Selective N-Hydroxyhydantoin Carbamate Inhibitors of Mammalian Serine Hydrolases. *Chem. Biol.* **2015**, *22*, 928–937. https://doi.org/10.1016/j.chembiol.2015.05.018.

(13) Kolb, H. C.; Finn, M. G.; Sharpless, K. B. Click Chemistry: Diverse Chemical Function from a Few Good Reactions. *Angew. Chemie Int. Ed.* **2001**, *40* (11), 2004–2021. https://doi.org/10.1002/1521-3773(20010601)40:11<2004::AID-ANIE2004>3.0.CO;2-5.

(14) Rostovtsev, V. V.; Green, L. G.; Fokin, V. V.; Sharpless, K. B. A Stepwise Huisgen Cycloaddition Process: Copper(I)-Catalyzed Regioselective "Ligation" of Azides and Terminal Alkynes. *Angew. Chemie Int. Ed.* **2002**, *41* (14), 2596–2599. https://doi.org/10.1002/1521-3773(20020715)41:14<2596::AID-ANIE2596>3.0.CO;2-4.

(15) Tornøe, C. W.; Christensen, C.; Meldal, M. Peptidotriazoles on Solid Phase: [1,2,3]-Triazoles by Regiospecific Copper(I)-Catalyzed 1,3-Dipolar Cycloadditions of Terminal Alkynes to Azides. *J. Org. Chem.* **2002**, *67* (9), 3057–3064. https://doi.org/10.1021/jo011148j.

(16) Worrell, B. T.; Malik, J. A.; Fokin, V. V. Direct Evidence of a Dinuclear Copper Intermediate in Cu(I)-Catalyzed Azide-Alkyne Cycloadditions. *Science* **2013**, *340* (6131), 457–460. https://doi.org/10.1126/science.1229506.

(17) McKay, C. S.; Finn, M. G. Click Chemistry in Complex Mixtures: Bioorthogonal Bioconjugation. *Chem. Biol.* **2014**, *21* (9), 1075–1101. https://doi.org/10.1016/J.CHEMBIOL.2014.09.002.

(18) Desrochers, G. F.; Pezacki, J. P. ABPP and Host–Virus Interactions. In *Current Topics in Microbiology and Immunology*; Springer International Publishing, **2019**; Vol. 420, pp 131–154. https://doi.org/10.1007/82_2018_139.

(19) Moellering, R. E.; Cravatt, B. F. How Chemoproteomics Can Enable Drug Discovery and Development. *Chem. Biol*. **2012**, 19(1), 11–22. https://doi.org/10.1016/j.chembiol.2012.01.001.

(20) Vincent-Rocan, J. F.; Beauchemin, A. M. N -Isocyanates, N -Isothiocyanates and Their Masked/Blocked Derivatives: Synthesis and Reactivity. *Synth.* **2016**, *48* (21), 3625–3645. https://doi.org/10.1055/s-0036-1588066.

(21) Liu, Y.; Patricelli, M. P.; Cravatt, B. F. Activity-Based Protein Profiling: The Serine Hydrolases. *Proc. Natl. Acad. Sci. U. S. A.* **1999**, *96* (26), 14694–14699. https://doi.org/10.1073/pnas.96.26.14694.

(22) Wang, C.; Abegg, D.; Dwyer, B. G.; Adibekian, A. Discovery and Evaluation of New Activity-Based Probes for Serine Hydrolases. *ChemBioChem* **2019**, *20* (17), 2212–2216. https://doi.org/10.1002/cbic.201900126.

(23) Nasheri, N.; McKay, C. S.; Fulton, K.; Twine, S.; Powdrill, M. H.; Sherratt, A. R.; Pezacki, J. P. Hydrophobic Triaryl-Substituted β-Lactams as Activity-Based Probes for Profiling Eukaryotic Enzymes and Host-Pathogen Interactions. *ChemBioChem* **2014**, *15* (15), 2195–2200. https://doi.org/10.1002/cbic.201402097.

(24) Mi, H.; Muruganujan, A.; Ebert, D.; Huang, X.; Thomas, P. D. PANTHER Version 14: More Genomes, a New PANTHER GO-Slim and Improvements in Enrichment Analysis Tools. *Nucleic Acids Res.* **2019**, *47* (D1), D419–D426. https://doi.org/10.1093/nar/gky1038.

(25) Adolph, M. B.; Love, R. P.; Feng, Y.; Chelico, L. Enzyme Cycling Contributes to Efficient Induction of Genome Mutagenesis by the Cytidine Deaminase APOBEC3B. *Nucleic Acids Res.* **2017**, *45* (20), 11925–11940. https://doi.org/10.1093/nar/gkx832.

(26) Feng, Y.; Baig, T. T.; Love, R. P.; Chelico, L. Suppression of APOBEC3-Mediated Restriction of HIV-1 by Vif. *Front. in Microbiol*. **2014**, 5, 450 https://doi.org/10.3389/fmicb.2014.00450.

(27) Kouno, T.; Silvas, T. V.; Hilbert, B. J.; Shandilya, S. M. D.; Bohn, M. F.; Kelch, B. A.; Royer, W. E.; Somasundaran, M.; Yilmaz, N. K.; Matsuo, H.; et al. Crystal Structure of APOBEC3A Bound to Single-Stranded DNA Reveals Structural Basis for Cytidine Deamination and Specificity. *Nat. Commun.* **2017**, *8* (1), 1–8. https://doi.org/10.1038/ncomms15024.

Chapter 5: General Discussion and Future Work

5.1 Summary

The importance of studying host-virus interactions lies in the relationship between viruses and their host cells. Viruses rely on host cells to provide energy, building blocks, and reproductive and translational machinery. Gaining a better understanding of how host cell factors contribute to the viral life cycle could give rise to the discovery of antiviral drug targets. In light of this goal, Chapter 2 presents a miRNA that modulates lipid metabolic pathways and produces an antiviral effect, Chapter 3 presents an antiviral nucleoside analog probe that covalently binds viral polymerases and can be adapted to the desired application using click chemistry, and lastly Chapter 4 presents the characterization of a novel hydrazone probe to determine its suitability as a probe to study host-virus interactions. The following discussion highlights the key findings of each chapter.

5.1.1 miR-124 Regulates Fatty Acid Oxidation and Inhibits HCV

MicroRNA-124 is the third most abundant miRNA in the nervous system but its role in liver metabolism is confounding considering its low expression level.[1] Chapter 2 sheds light on this phenomenon by using molecular biology techniques to determine how its expression is controlled and identify downstream pathways that lie under its modulatory effects. The expression of miR-124 was increased during serum depletion and decreased during HCV infection. Together this points to a role for miR-124 in regulating lipid metabolism. Transcriptomic methods showed that miR-124 downregulates genes involved in triglyceride hydrolysis and acyl-CoA-carnitine shuttling into the mitochondria, with an overall downregulation of fatty acid oxidation and increase in triglyceride accumulation. The repression of fatty acid hydrolysis was linked to a

downregulation of AADAC and CES1 serine hydrolases, both of which have been investigated previously for their role in promoting HCV replication.[2,3] Lastly, the overexpression of miR-124 reduced HCV infectivity, demonstrating its role as an antiviral modulator in liver immunometabolism. The repression of AADAC and CES1 expression was thereby paralleled by a decrease in HCV infectivity. The involvement of these serine hydrolases highlights the importance of this family of enzymes in liver immunometabolism and host-virus interactions.

5.1.2 Azauracil Probes Covalently Modify and Inhibit HIV RT

Modern treatment regimens for virus infections use nucleoside analogs to inhibit viral polymerases and prevent viruses from replicating their genetic code. The primary issues with these treatment regimens is spontaneous pyrophosphorolysis and mutations in viral populations giving rise to resistant chimeras.[4,5] HIV is no exception with most treatment regimens employing two or more HIV RT inhibitors with differing binding locations and mechanisms of action.[6,7] By using a multi-pronged approach there is less opportunity for a chimeric virus to become resistant to treatment and adds another avenue of inhibiting the RT if one of the NRTIs is more susceptible to pyrophosphorolysis. The nucleoside analog used in this project attempted to tackle this problem by introducing a covalent modification in the active site of the HIV RT. The azauracil probe was demonstrated to interact with HCV polymerase and HIV RT, showing a potential broadly antiviral mechanism. Mass spectrometry experiments concluded that the azauracil probe formed a covalent modification near the active site of HIV RT, potentially competing for incorporation into a replicating strand of viral RNA. The proximity to the nucleotide incorporation site suggested that the azauracil probe could potentially inhibit HIV RT activity by chain terminating the viral RNA. Unfortunately the azauracil probe was unable to inhibit RT activity but given its covalent

interaction with HIV RT and the location of the adduct, a bifunctional approach was adopted to link Zidovudine, a known HIV RT inhibitor, to the azauracil probe using click chemistry. Historically, Zidovudine treatment was linked to undesirable side effects due to its promiscuity with polymerases.[6] The bifunctional inhibitor showed 20-fold greater inhibition of HIV RT than Zidovudine on its own. The increase in inhibition is suspected to be due to the azauracil probe adduct functioning as a targeting mechanism for Zidovudine. Lastly, the bifunctional inhibitor was used in a primary cell culture model of HIV infection and showed a similar ability as Zidovudine to inhibit the infection. Taken together, these points demonstrate the application of click chemistry in targeting viral polymerases with a probe and then functionalizing the probe with an inhibitor. Given the specificity issues of Zidovudine this is a great improvement in making the antiviral therapy more specific to HIV RT and could help alleviate side effects that have been associated with Zidovudine treatment.

5.1.3 Hydrazone Probes Have a Labelling Profile Distinct from Fluorophosphonate

The FP probe was briefly introduced earlier in this thesis and is a well-established tool for examining serine hydrolase activity. The importance of serine hydrolases in liver immunometabolism was cited in Chapter 2 and demonstrated with the downregulation of AADAC and CES1 during miR-124 overexpression.[8] The affinity of FP for serine hydrolases is shared and even improved in carbamate-based probes.[9,10] Previously the targets of carbamate probes were demonstrated to be tunable with dozens of examples by simply modifying their leaving groups.[10,11] The hydrazone probe that was examined in Chapter 4 was born from an attempt to do this while also using carbamates probes as precursors to nitrogen-substituted isocyanates that are seen in many pharmaceuticals.[12,13] The reactivity of the hydrazone probe with the mammalian proteome

was examined and the labelling profile was found to be distinct from FP. The differing profile suggests that the hydrazone group changed the affinity of the adjacent carbamate group for serine hydrolases. Mass spectrometry was used to determine proteins that formed adducts with the hydrazone probe and APOBEC3A was highlighted from the list of interacting proteins due to its role in fighting HIV infection. Despite not being specific to serine hydrolases the hydrazone probe could offer an interesting tool for tracking APOBEC3A. Gel electrophoresis confirmed the interaction with the cytidine deaminase and mass spectrometry identified the adducts. A kinetic assay was used to examine if the hydrazone probe could inhibit APOBEC3A activity and a biotin group was added to the probe via click chemistry to offer additional steric factors that might be able to inhibit deaminase activity. The hydrazone probe did not inhibit the deaminase activity and thereafter its interaction with APOBEC3A was suspected to be affinity-based and not activity-based.

5.2 Future Work

5.2.1 MicroRNAs as Regulators of Liver Infection

Given that recent publications by our lab demonstrate roles for other miRNA-regulated serine hydrolases in HCV infection, there is cause to examine this phenomenon in the context of miR-124 overexpression as well.[8,14] Preliminary data points toward the dysregulation of serine hydrolases in support of a downregulation of lipid metabolism, corroborating the observed downregulation of AADAC and CES1. The involvement of any of these serine hydrolases could lead to a potential drug candidate to treat HCV infection and gene knockdowns of each should be examined to determine if they are antiviral or proviral and their role in liver immunometabolism in general.

There is a possibility that miR-124 is involved in the regulation of liver metabolism in a panviral response mechanism. This phenomenon should be studied in the context of other flaviviruses or even in other positive-sense single-stranded RNA viruses like DENV, ZIKV, or HIV-1. Given the recent pandemic and the systemic distribution of SARS-CoV-2, the role of miRNA-124 should be examined there as well.

5.2.2 The Azauracil Probe as a Building Block for Antivirals

The focus of this chapter was on HIV RT but there is also evidence presented that the azauracil probe can be used against HCV. It was demonstrated via in-gel fluorescence that the azauracil probe binds to the HCV polymerase. A future avenue of research could be to examine the interaction of the azauracil probe with the HCV polymerase and determine if it binds near the enzyme active site. If this is the case then the azauracil probe could be used once again in a bifunctional approach by reacting it with a nucleoside inhibitor of HCV polymerase such as Sofosbuvir or a derivative that is designed to possess an azide functional group.

It would be of interest to also test other viral polymerases against the azauracil probe to see if the targeting of the probe is conserved across viral polymerases or at least to RNA-dependent RNA polymerases and try to repeat this work using different covalent modifiers for each virus.

5.2.3 Modifying the Hydrazone Chemotype

Despite not binding the active site of A3A or inhibiting its activity there is a possibility that the hydrazone probe can be modified to be more selective for this enzyme. This kind of work has already been used in making carbamate probes specific to particular serine hydrolases simply by modifying the leaving group. In future, molecular docking experiments could be combined with

structure-activity relationship studies for the rational design of an alternative hydrazone probe that is more selective for A3A or even to work backward toward making the hydrazone probe more selective for serine hydrolases like a carbamate probe.

5.3 Concluding Remarks

The work presented in this thesis demonstrates three interesting perspectives for the discovery and characterization of host-virus interactions and the design of antiviral therapeutics. The application of activity-based protein profiling to this research question is demonstrated in Chapter 3 and 4 of this thesis and is left open-ended for future work in Chapter 2. ABPP is a powerful research tool as it focuses on enzymatically active proteins that are the effectors of the cell. By classifying these effectors as proviral or antiviral and linking interaction networks back to miRNAs or other druggable targets we can drive future antiviral research toward novel therapeutic options.

5.4 References

(1) Ludwig, N.; Leidinger, P.; Becker, K.; Backes, C.; Fehlmann, T.; Pallasch, C.; Rheinheimer, S.; Meder, B.; Meese, E.; Keller, A. Distribution of MiRNA Expression across Human Tissues. *Nucleic Acids Res.* **2016**, *44* (8), 3865–3877. https://doi.org/10.1093/nar/gkw116.

(2) Nourbakhsh, M.; Douglas, D. N.; Pu, C. H.; Lewis, J. T.; Kawahara, T.; Lisboa, L. F.; Wei, E.; Asthana, S.; Quiroga, A. D.; Law, L. M. J.; et al. Arylacetamide Deacetylase: A Novel Host Factor with Important Roles in the Lipolysis of Cellular Triacylglycerol Stores, VLDL Assembly and HCV Production. *J. Hepatol.* **2013**, *59* (2), 336–343. https://doi.org/10.1016/j.jhep.2013.03.022.

(3) Blais, D. R.; Lyn, R. K.; Joyce, M. A.; Rouleau, Y.; Steenbergen, R.; Barsby, N.; Zhu, L. F.; Pegoraro, A. F.; Stolow, A.; Tyrrell, D. L.; et al. Activity-Based Protein Profiling Identifies a Host Enzyme, Carboxylesterase 1, Which Is Differentially Active during Hepatitis C Virus Replication. *J. Biol. Chem.* **2010**, *285* (33), 25602. https://doi.org/10.1074/JBC.M110.135483.

(4) D'Aquila, R. T.; Johnson, V. A.; Welles, S. L.; Japour, A. J.; Kuritzkes, D. R.; DeGruttola, V.; Reichelderfer, P. S.; Coombs, R. W.; Crumpacker, C. S.; Kahn, J. O.; et al. Zidovudine Resistance and HIV-1 Disease Progression during Antiretroviral Therapy. *Ann. Intern. Med.* **1995**, *122* (6), 401–408. https://doi.org/10.7326/0003-4819-122-6-199503150-00001.

(5) Deval, J.; Powdrill, M. H.; D'Abramo, C. M.; Cellai, L.; Götte, M. Pyrophosphorolytic Excision of Nonobligate Chain Terminators by Hepatitis C Virus NS5B Polymerase. *Antimicrob. Agents Chemother.* **2007**, *51* (8), 2920–2928. https://doi.org/10.1128/AAC.00186-07.

(6) Gardner, K.; Hall, P. A.; Chinnery, P. F.; Payne, B. A. I. HIV Treatment and Associated Mitochondrial Pathology: Review of 25 Years of in Vitro, Animal, and Human Studies. *Toxicol. Pathol.* **2014**, *42*, 811–822. https://doi.org/10.1177/0192623313503519.

(7) Kumar, P. N.; Patel, P. Lamivudine for the Treatment of HIV. *Expert Opin. Drug Metab. Toxicol.* **2009**, *6* (1), 105–114. https://doi.org/10.1517/17425250903490418.

(8) Filip, R.; Desrochers, G. F.; Lefebvre, D. M.; Reed, A.; Cravatt, B. F.; Pezacki, J. P. Profiling : Linking Enzyme Activity to MicroRNA-185 Function. *Cell Chem. Biol.* **2022**,

28 (2), 202–212. https://doi.org/10.1016/j.chembiol.2020.12.009.Profiling.

(9) Li, W.; Blankman, J. L.; Cravatt, B. F. A Functional Proteomic Strategy to Discover Inhibitors for Uncharacterized Hydrolases. *J. Am. Chem. Soc.* **2007**, *129* (31), 9594–9595. https://doi.org/10.1021/ja073650c.

(10) Bachovchin, D. A.; Ji, T.; Li, W.; Simon, G. M.; Blankman, J. L.; Adibekian, A.; Hoover, H.; Niessen, S.; Cravatt, B. F. Superfamily-Wide Portrait of Serine Hydrolase Inhibition Achieved by Library-versus-Library Screening. *Proc. Natl. Acad. Sci. U. S. A.* **2010**, *107* (49), 20941–20946. https://doi.org/10.1073/pnas.1011663107.

(11) Armand Cognetta III, A. B.; Niphakis, M. J.; Lee, H.-C.; Martini, M. L.; Hulce, J. J. Selective N-Hydroxyhydantoin Carbamate Inhibitors of Mammalian Serine Hydrolases. *Chem. Biol.* **2015**, *22*, 928–937. https://doi.org/10.1016/j.chembiol.2015.05.018.

(12) Vincent-Rocan, J.-F.; Ivanovich, R. A.; Clavette, C.; Leckett, K.; Bejjani, J.; Beauchemin, A. M. Cascade Reactions of Nitrogen-Substituted Isocyanates: A New Tool in Heterocyclic Chemistry. *Chem. Sci.* **2016**, *7* (1), 315–328. https://doi.org/10.1039/C5SC03197D.

(13) Garland, K.; Gan, W.; Depatie-Sicard, C.; Beauchemin, A. M. A Practical Approach to Semicarbazone and Hydrazone Derivatives via Imino-Isocyanates. *Org. Lett.* **2013**, *15* (16), 4074–4077. https://doi.org/10.1021/ol4016089.

(14) Desrochers, G. F.; Filip, R.; Bastianelli, M.; Stern, T.; Pezacki, J. P. MicroRNA-27b Regulates Hepatic Lipase Enzyme LIPC and Reduces Triglyceride Degradation during Hepatitis C Virus Infection. *J. Biol. Chem.* **2022**, *298* (6), 101983.

https://doi.org/10.1016/j.jbc.2022.101983.

Chapter 6: Supplemental Material for Chapter 2

6.1 Supplemental Tables for Chapter 2

Table 6-1. Summary of top up- and down-regulated genes from microarray analysis of miR-124 mimic transfected Huh7.5 cells. Related to Figure 2.

Gene Symbol	Description	Fold Change
	Top up-regulated genes	
SLC2A2	solute carrier family 2 (facilitated glucose transporter), member 2	16.97
BEX1	brain expressed X-linked 1	12.08
RANBP3L	RAN binding protein 3-like	11.48
LOC101927482	uncharacterized LOC101927482	11.07
CYP3A5	cytochrome P450, family 3, subfamily A, polypeptide 5	8.65
LOC105375361	uncharacterized LOC105375361	6.84
B3GALT1	UDP-Gal:betaGlcNAc beta 1,3-galactosyltransferase 1	6.68
KCNJ3	potassium channel, inwardly rectifying subfamily J, member 3	6.34
KIF5C	kinesin family member 5C	6.22
DIO1	deiodinase, iodothyronine, type I	6.21
	Top down-regulated genes	
IQGAP1	IQ motif containing GTPase activating protein 1	-5.75
CP	ceruloplasmin (ferroxidase)	-5.76
LGALS3	lectin, galactoside-binding, soluble, 3	-5.92
AIM1	absent in melanoma 1	-6.01
TNFSF4	tumor necrosis factor (ligand) superfamily, member 4	-6.02
HEPACAM2	HEPACAM family member 2	-6.50
CD38	CD38 molecule	-6.99
AADAC	arylacetamide deacetylase	-8.40
VAMP3	vesicle associated membrane protein 3	-9.11
HP	haptoglobin	-15.69

Table 6-2. Gene ontology analysis classifying genes repressed by >1.5 fold in miR-124 mimic transfected Huh7.5 cells by biological process. Related to Figure 2-2.

Name	Source	*P*-value†
Fatty acid metabolism	SMPDB	1.63E-2
Fatty acid degradation	BioSystems: KEGG	1.65E-2

*Only biological processes with P < 0.05 are listed.

†Adjusted with Bonferroni correction.

Table 6-3. List of oligonucleotides used in this study. Related to Figures 2 & 4**.**

Oligonucleotide	Sequence
qPCR primers	
18S rRNA – FWD	GAGCTCCTGGGACTTCACCAT
18S rRNA – REV	ATCTGGGTCATCAAGGAGCTGT
AADAC – FWD	CTGCTCCGAGGTGTGTTTGTA
AADAC – REV	GGCAGCAAATTCAGACAAGTCA
ACADSB – FWD	GATGGCAAATGTAGACCCTACC
ACADSB – REV	AAGGCCCGGAGTATCACGA
ACADVL – FWD	TAGGAGAGGCAGGCAAACAGCT
ACADVL – REV	CACAGTGGCAAACTGCTCCAGA
CPT1A – FWD	TCCAGTTGGCTTATCGTGGTG
CPT1A – REV	TCCAGAGTCCGATTGATTTTTGC
ECI2 – FWD	TTCAACCGGCCCAAAAAGAAA
ECI2 – REV	ATTCCCTCAGTAAAACGGCATT
HADHA – FWD	AAATTGACAGCGTATGCCATGA
HADHA – REV	GCTTTCGCACTTTTTCTTCCACT
JFH1 HCV– FWD	GTCTGCGGAACCGGTGAGTA
JFH1 HCV – REV	GCCCAAATGGCCGGGATA
PECR – FWD	CGGAAAAGCCATCGTGAAGGAG
PECR – REV	ATGACTCGTGCCTGCTTTGTGG
PPARA – FWD	CTATCATTTGCTGTGGAGATCG
PPARA – REV	AAGATATCGTCCGGGTGGTT
PPARGC1A – FWD	GCTTTCTGGGTGGACTCAAGT
PPARGC1A – REV	GAGGGCAATCCGTCTTCATCC
SLC25A20 - FWD	CCGAGAACTGACAGACGGAG
SLC25A20 - REV	CCAAAGAAGCACACGGCAAA
CES1 - FWD	AACTGTCGCCCTTCCACGAT
CES1 - REV	CATCCCCTGTGCTGAAGAATCC
ALDH9A1 - FWD	GCAACCGGCCGAGTGATAG
ALDH9A1 - REV	ACCACATTGAAGAGCCCAGG

6.2 Supplemental Figures for Chapter 2

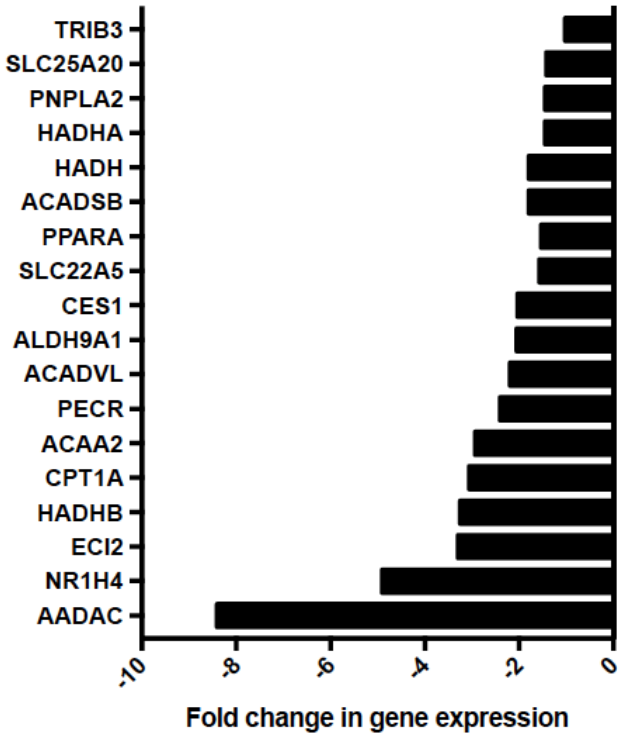

Figure 6-1. Microarray gene expression analysis in miR-124 transfected mimic Huh7.5 cells.

Related to Figure 2-2. Fold changes in gene expression of select lipid-metabolism-related genes in Huh7.5 cells transfected with 100 nM of miR-124 mimic are shown. Fold changes were calculated relative to gene expression in 100 nM control mimic-transfected Huh7.5 cells.

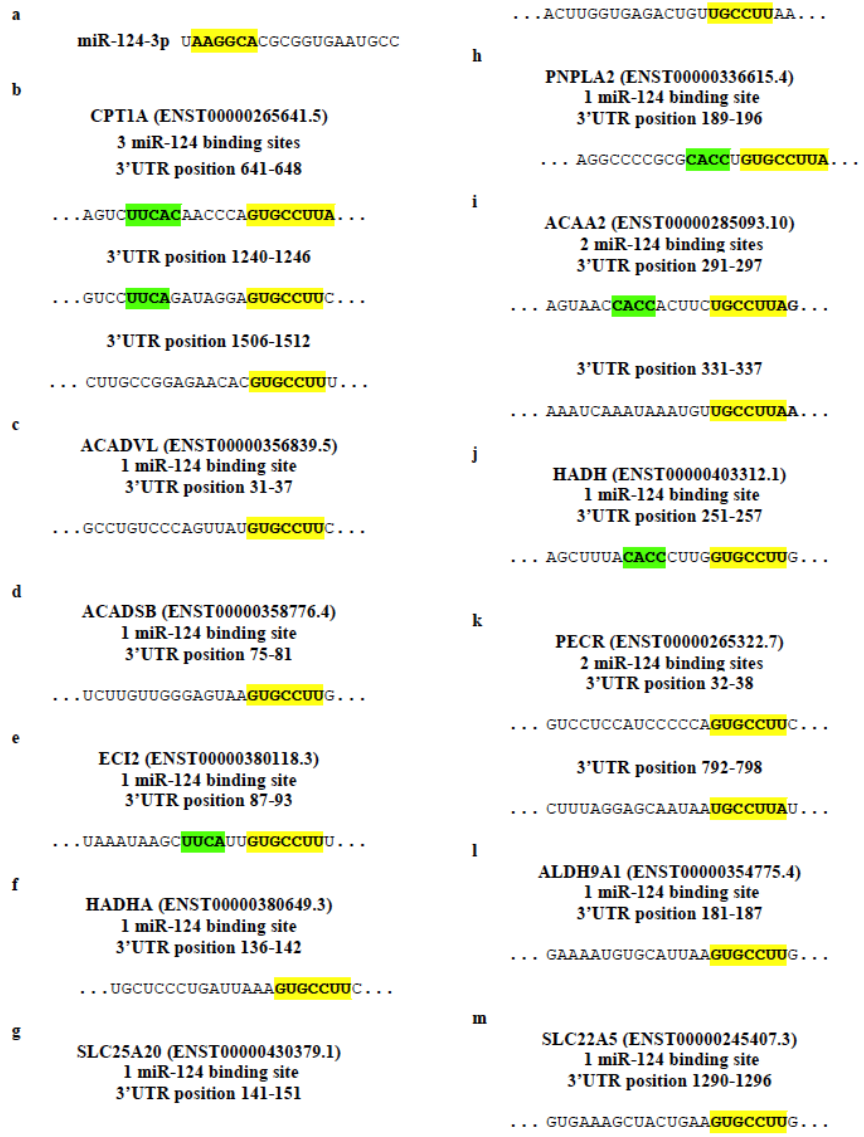

Figure 6-2. miRNA recognition elements in direct targets of miR-124.

Related to Figures 2-2 and 2-4. (a) Sequence of mature miR-124 with seed sequence highlighted in yellow. Sequence of miR-124 binding sites in the 3'UTRs of (b) CPT1A, (c) ACADVL, (d) ACADSB, (e) ECI2 (f) HADHA, (g) SLC25A20, (h) PNPLA2, (i) ACAA2, (j) HADH, (k) PECR, (l) ALDH9A1 and (m) SLC22A5. Sequences were taken from TargetScan. Seed sequences are highlighted in yellow, and nucleotides predicted to be involved in supplementary interactions with the 3' end of miR-124 are highlighted in green.

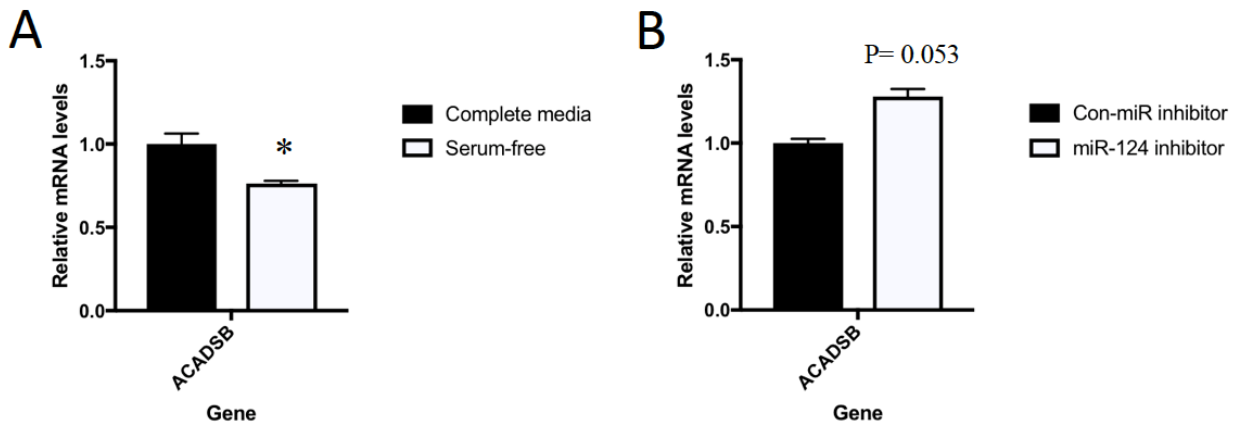

Figure 6-3. Expression of ACADSB during serum depletion and miR-124 inhibition.

Related to Figure 2-2. (A) Huh7.5 cells were cultured in complete or serum-free media for 48 h. qRT-PCR was performed to measure relative ACADSB expression (n = 4). (B) Huh7.5 cells were transfected with control or miR-124 inhibitor for 6 hours and were then cultured in complete or serum-free media for 48 hours. qRT-PCR was performed to measure relative ACADSB expression (n = 2). Data are represented as the mean ± SEM (*P < 0.05).

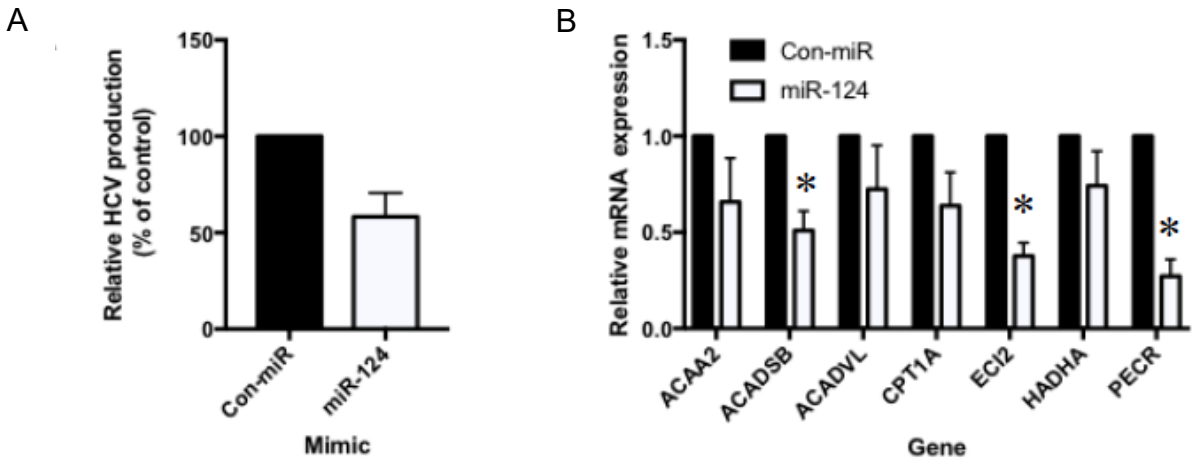

Figure 6-4. miR-124 regulates HCV infection.

Related to Figures 2-2 & 2-4. (A) Relative HCV production and (B) miR-124 target expression in control (Con-miR) and miR-124 mimic transfected Huh7.5 cells infected with HCV. Viral production was assessed by a focus-forming assay while target expression was measured via qRT-PCR analysis. Data are represented as the mean ± SEM.

NM_000183.2
TAGATCCAGAAGAAGTGACCTGAAGTTTCTGTGCAACACTCACACTAGGCAATGCC
ATTTCAATGCATTACTAAATGACATTTGTAGTTCCTAGCTCCTCTTAGGAAAACAGTT
CTTGTGGCCTTCTATTAAATAGTTTGCACTTAAGCCTTGCCAGTGTTCTGAGCTTTT
CAATAATCAGTTTACTGCTCTTTCAGGGATTTCTAAGCCACCAGAATCTCACATGAG
ATGTGTGGGTGGTTGTTTTTGGTCTCTGTTGTCACTAAAGACTAAATGAGGGTTTG
CAGTTGGGAAAGAGGTCAACTGAGATTTGGAAATCATCTTTGTAATATTTGCAAATT
ATACTTGTTCTTATCTGTGTCCTAAAGATGTGTTCTCTATAAAATACAAACCAACGTG
CCTAATTAATTATGGAAAAATAATTCAGAATCTAAACACCACTGAAAACTTATAAAAA
ATGTTTAGATACATAAATATGGTGGTCAGCGTTAATAAAGTGGAGAAATATTGGAAAAA
AAAA

NM_001281512.1
TAGATCCAGAAGAAGTGACCTGAAGTTTCTGTGCAACACTCACACTAGGCAATGCC
ATTTCAATGCATTACTAAATGACATTTGTAGTTCCTAGCTCCTCTTAGGAAAACAGTT
CTTGTGGCCTTCTATTAAATAGTTTGCACTTAAGCCTTGCCAGTGTTCTGAGCTTTT
CAATAATCAGTTTACTGCTCTTTCAGGGATTTCTAAGCCACCAGAATCTCACATGAG
ATGTGTGGGTGGTTGTTTTTGGTCTCTGTTGTCACTAAAGACTAAATGAGGGTTTG
CAGTTGGGAAAGAGGTCAACTGAGATTTGGAAATCATCTTTGTAATATTTGCAAATT
ATACTTGTTCTTATCTGTGTCCTAAAGATGTGTTCTCTATAAAATACAAACCAACGTG
CCTAATTAATTATGGAAAAATAATTCAGAATCTAAACACCACTGAAAACTTATAAAAA
ATGTTTAGATACATAAATATGGTGGTCAGCGTTAATAAAGTGGAGAAATATTGGAAAAA
AAAA

NM_001281513.1
TAGATCCAGAAGAAGTGACCTGAAGTTTCTGTGCAACACTCACACTAGGCAATGCC
ATTTCAATGCATTACTAAATGACATTTGTAGTTCCTAGCTCCTCTTAGGAAAACAGTT
CTTGTGGCCTTCTATTAAATAGTTTGCACTTAAGCCTTGCCAGTGTTCTGAGCTTTT
CAATAATCAGTTTACTGCTCTTTCAGGGATTTCTAAGCCACCAGAATCTCACATGAG
ATGTGTGGGTGGTTGTTTTTGGTCTCTGTTGTCACTAAAGACTAAATGAGGGTTTG
CAGTTGGGAAAGAGGTCAACTGAGATTTGGAAATCATCTTTGTAATATTTGCAAATT
ATACTTGTTCTTATCTGTGTCCTAAAGATGTGTTCTCTATAAAATACAAACCAACGTG
CCTAATTAATTATGGAAAAATAATTCAGAATCTAAACACCACTGAAAACTTATAAAAA
ATGTTTAGATACATAAATATGGTGGTCAGCGTTAATAAAGTGGAGAAATATTGGAAAAA
AAAA

Figure 6-5. miR-124 G-bulge binding site in HADHB 3'UTR.

Related to Figure 2-2. miR-124 G-bulge recognition sites are highlighted in red and bold for all three HADHB transcripts isoforms (NCBI reference sequences shown).

ATGGGAAGAAAATCGCTGTACCTTCTGATTGTGGGGATCCTCATAGCATATTATATT
TATACGCCTCTCCCAGATAACGTTGAGGAGCCATGGAGAATGATGTGGATAAACG
CACATCTGAAAACTATACAAAATTTGGCTACATTTGTGGAGCTCCTGGGACTTCAC
CATTTTATGGATTCCTTTAAGGTTGTCGGGAGCTTTGATGAAGTCCCACCAACCTCA
GATGAAAATGTCACTGTGACTGAGACAAAATTCAACAACATTCTTGTTCGGGTATAT
GTGCCAAAGAGAAAGTCTGAAGCACTAAGAAGGGGGTTGTTTTACATCCATGGTG
GAGGCTGGTGCGTGGGAAGTGCTGCTCTAAGTGGTTATGACTTGCTGTCAAGATG
GACAGCAGACAGACTTGATGCTGTCGTCGTATCAACCAACTACAGATTAGCACCTA
AGTATCATTTCCCAATTCAATTTGAAGATGTATATAATGCCTTAAGGTGGTTCTTAC
GTAAAAAAGTTCTTGCAAAATATGGTGTGAACCCTGAGAGAATCGGTATTTCTGGA
GATAGTGCAGGAGGGAATTTAGCTGCAGCAGTGACTCAACAGCTCCTTGATGACC
CAGATGTCAAGATCAAACTCAAGATCCAGTCTTTAATTTATCCTGCCCTTCAGCCTC
TTGATGTAGATTTACCGTCATATCAAGAAAATTCAAATTTTCTATTTCTATCCAAATC
ACTCATGGTCAGATTCTGGAGTGAATATTTTACCACTGATAGATCACTTGAAAAAGC
CATGCTTTCCAGACAACATGTACCTGTGGAATCAAGTCATCTCTTCAAATTTGTTAA
TTGGAGTTCCCTGCTCCCTGAGAGGTTTATAAAAGGACATGTTTATAACAATCCAAA
TTATGGCAGTTCTGAGCTGGCTAAAAAATATCCAGGGTTCCTAGATGTGAGGGCAG
CCCCTTTGTTGGCTGATGACAACAAATTACGTGGCTTACCCCTGACCTATGTCATC
ACCTGTCAATATGATCTCTTAAGAGATGATGGACTCATGTATGTCACCCGACTTCG
CAACACTGGGGTTCAGGTGACTCATAACCATGTTGAGGATGGATTCCATGGAGCAT
TTTCATTTCTGGGACTTAAAATTAGTCACAGACTTATAAATCAGTATATTGAGTGGCT
AAAGGAAAATCTATAG

Figure 6-6. miR-124 binding site in AADAC ORF.

Related to Figure 2-4. Sequence for AADAC ORF is shown (NCBI: NM_001086.2). The miR-124 binding site is shown in red letters, while the three rare codons are underlined and highlighted in yellow.

Chapter 7: Supplemental Material for Chapter 3

7.1 Supplemental Materials, Methods and Figures for Chapter 3

*7.1.1 The [3+2] Copper-Catalyzed Azide-Alkyne Cycloaddition (CuAAC/Click) Reaction of AzTTP/AzT with Probe **3**.*

The click reaction was prepared in 1X PBS using 10 mM Ascorbate, 10 mM $CuSO_4$, 1mM TBTA, 11 mM probe **3**, and 10 mM AzTTP or AzT. The components were reacted for 1 hour and excess copper was removed using Nickel NTA resin. The resin was washed with PBS, stripped three times with Ni^{2+} stripping buffer (20 mM $NaHPO_4$ pH 7.4, 500 mM NaCl, 50 mM EDTA) and dried before adding the click reaction and collecting the reaction by centrifuging at 700 x g for 2 minutes. AzTTP (Cedarlane) and AzT (Sigma Aldrich) were purchased from commercial sources. Spectral data for probe **3** matched previously reported characterization data.[1] After quantitative coupling via [3+2] CuAAC, the product (approximately 0.8 mg of **4** and 1.2 mg of **5**) was characterized by ^{1}H-NMR, ^{13}C-NMR, ^{31}P-NMR, and HMBC for **4**, and ESI mass spectrometry, ^{1}H-NMR, ^{13}C-NMR, and HSQC for **5** (ESI spectra were measured from D_2O samples), supporting structural assignment. Spectral data for the products was also consistent with similar previously reported AzT "clicked" analogues.[2]

Azauracil-AzTTP (4)

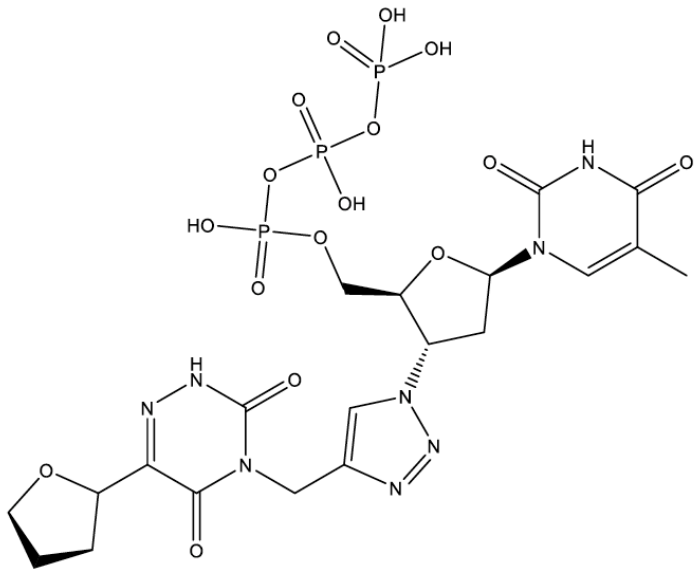

$C_{20}H_{27}N_8O_{16}P_3$

^{1}H-NMR (600 MHz, D_2O) δ 8.20 (s, 1H), 7.89 (s, 1H), 6.60 (t, *J* = 7.3 Hz, 1H), 5.64 (dt, *J* = 7.1, 3.2 Hz, 1H), 5.18 (s, 2H), 5.08 – 5.00 (m, 1H), 4.66 – 4.61 (m, 1H), 4.35 – 4.24 (m, 2H), 3.99 (q, *J* = 7.2 Hz, 1H), 3.92 – 3.87 (m, 1H), 2.83 – 2.75 (m, 2H), 2.33 – 2.26 (m, 1H), 2.09 – 2.03 (m, 1H), 2.03 – 1.97 (m, 2H), 1.95 (s, 3H). **^{13}C-NMR (**151 MHz, D_2O**)** δ 166.61, 156.35, 150.19, 141.59, 137.23, 111.98, 85.57, 75.55, 69.07, 65.83, 61.20, 59.65, 37.45, 34.75, 29.23, 24.86, 11.67. **HMBC ^{1}H-NMR (**600 MHz, D_2O**)** δ 8.15, 8.14, 7.85, 7.84, 7.84, 6.55, 6.55, 5.13, 5.13, 5.13, 5.13, 3.95, 3.94, 3.94, 3.85, 3.85, 3.84, 2.75, 2.74, 2.50, 2.25, 2.25, 2.01, 2.01, 2.01, 2.00, 2.00, 1.96, 1.95, 1.95, 1.90, 1.90, 1.90, 1.79. **HMBC ^{13}C-NMR (**151 MHz, D_2O**)** δ 141.59, 141.64, 166.69, 11.68, 151.73, 137.15, 151.72, 141.61, 156.36, 125.10, 150.47, 75.44, 24.72, 29.28, 24.71, 75.53, 29.26, 85.23, 61.05, 61.22, 24.93, 145.02, 69.01, 145.02, 75.54, 11.67, 24.86, 69.04, 75.75, 29.25, 166.66, 137.26, 111.98, 11.68. **^{31}P NMR** (203 MHz, D_2O) δ -9.26(br, 1P), -11.73 (d, *J* = 20.1 Hz, 1P), -22.82 (t, *J* = 19.3 Hz, 1P).

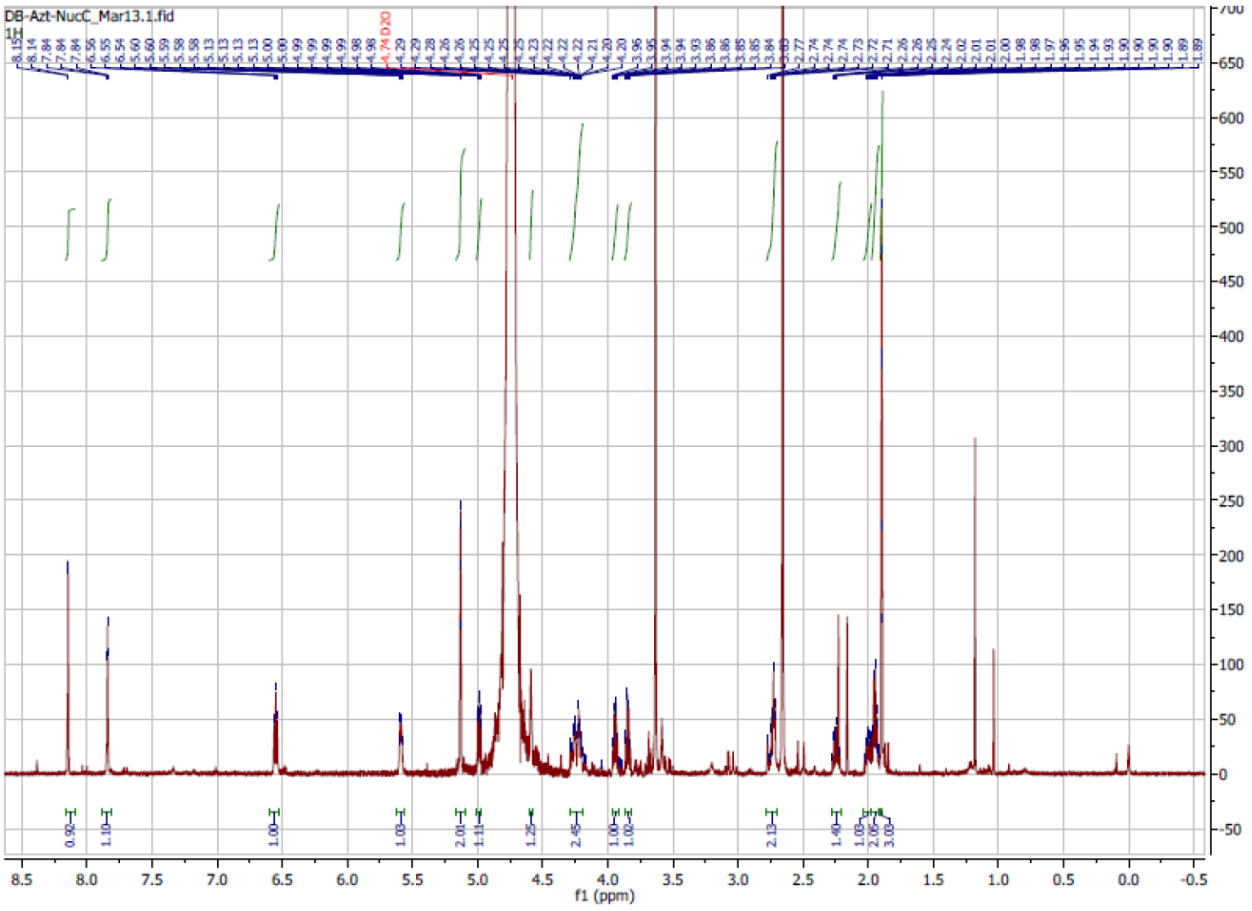

Figure 7-1. ^{1}H-NMR spectrum of Azauracil-AzTTP.

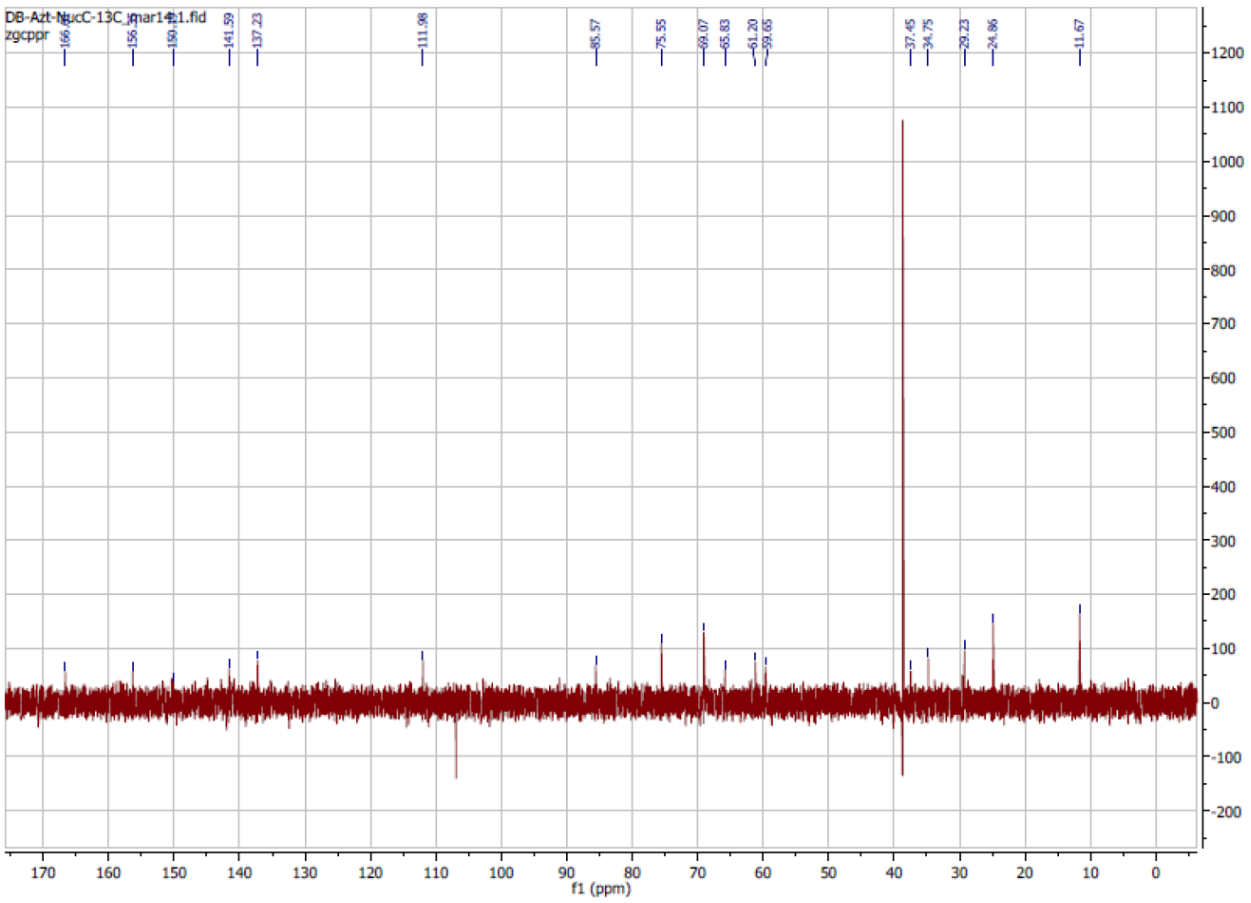

Figure 7-2. ^{13}C-NMR spectrum of Azauracil-AzTTP.

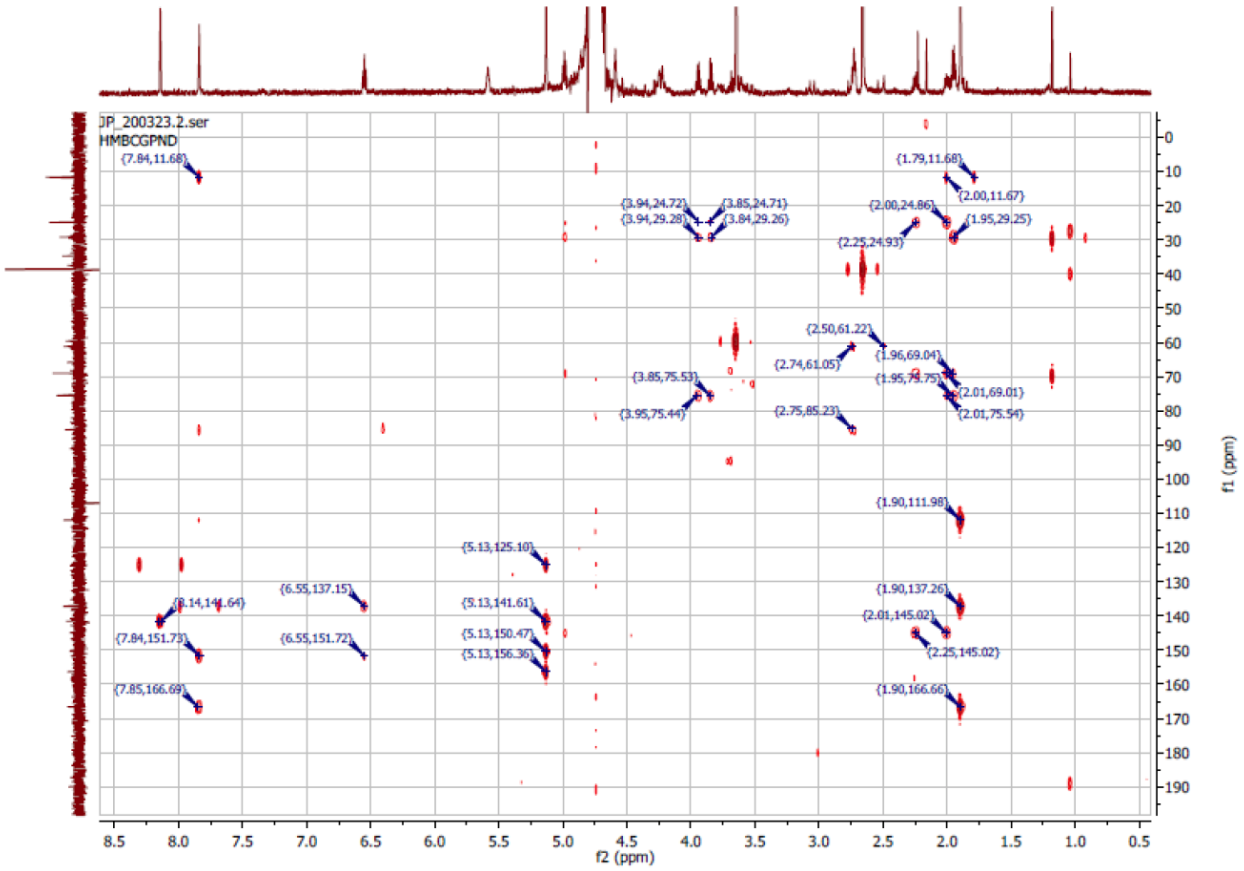

Figure 7-3. HMBC spectrum of Azauracil-AzTTP

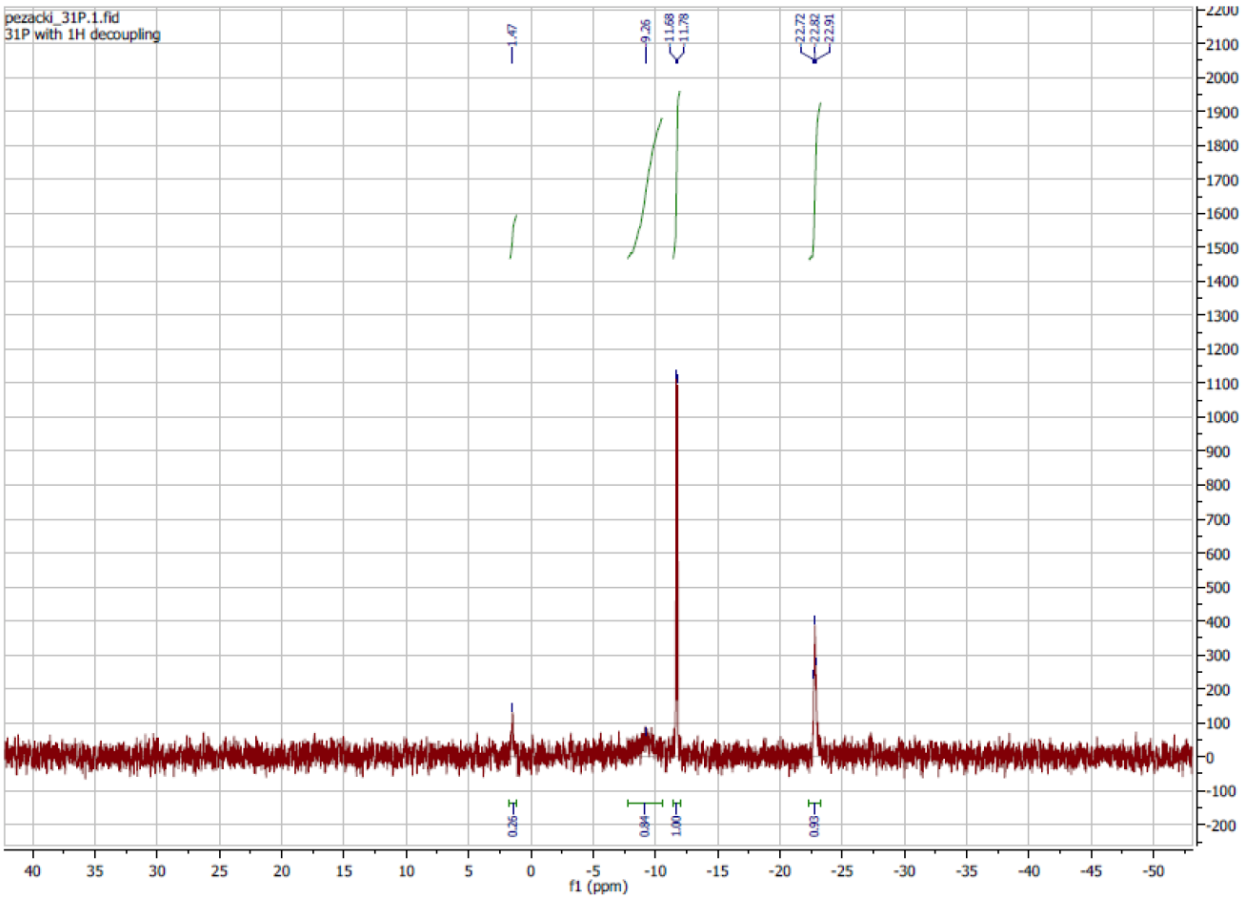

Figure 7-4. ^{31}P (^{1}H decoupled) spectrum of Azauracil-AzTTP

Azauracil-AzT (5)

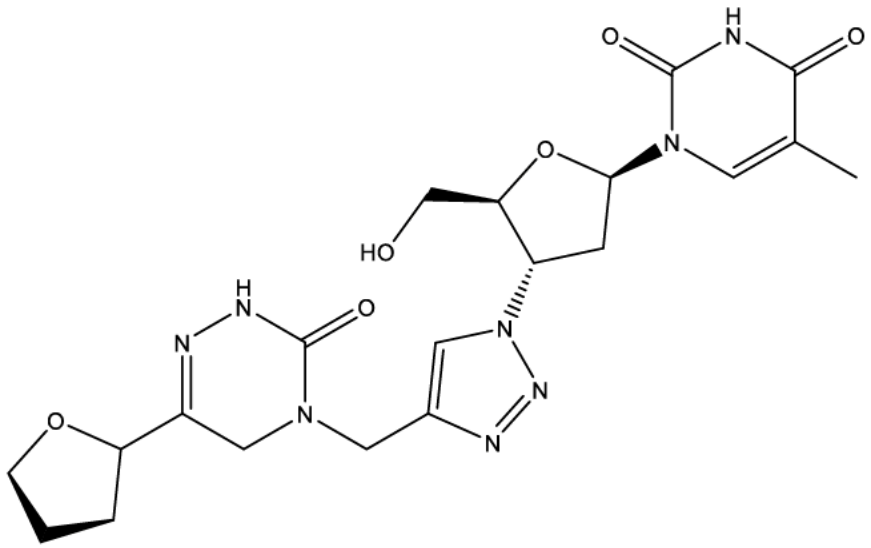

HRMS (ESI+) [M+Na]: calcd. for $C_{20}H_{23}D_3N_8O_6Na^+$: 514.1848, found: 514.2145

^{1}H-NMR (600 MHz, D_2O) δ 8.10 (s, 1H), 7.68 (s, 1H), 6.39 (t, *J* = 6.5 Hz, 1H), 5.36 (dt, *J* = 8.9, 6.1 Hz, 1H), 5.13 (s, 2H), 4.97-5.00 (m, 1H), 4.40 (dt, *J* = 6.7, 3.8 Hz, 1H), 3.94 (q, *J* = 7.0 Hz, 1H), 3.83-3.87 (m, 2H), 3.74 (dd, *J* = 12.7, 4.4 Hz, 1H), 2.87-2.93 (m, 1H), 2.82 – 2.73 (m, 1H), 2.29 – 2.20 (m, 1H), 2.04 – 1.90 (m, 3H), 1.86 (s, 3H). **^{13}C-NMR** (151 MHz, D_2O) δ 166.57, 156.36, 151.60, 150.39, 144.92, 137.78, 124.39, 111.49, 85.51, 84.18, 75.55, 69.08, 60.47, 59.55, 38.70, 36.84, 34.73, 29.16, 24.88, 11.53. **^{13}C/HSQC NMR** (151 MHz, D_2O) δ 124.51, 137.77, 85.54, 59.56, 34.72, 75.56, 84.21, 69.05, 69.08, 60.47, 60.47, 36.85, 36.83, 29.09, 29.08, 24.87, 11.47 **^{1}H/HSQC NMR** (600 MHz, D_2O) δ 8.09, 7.68, 6.39, 5.36, 5.13, 4.98, 4.40, 3.94, 3.85, 3.84, 3.74, 2.90, 2.78, 2.25, 2.01, 1.95, 1.86.

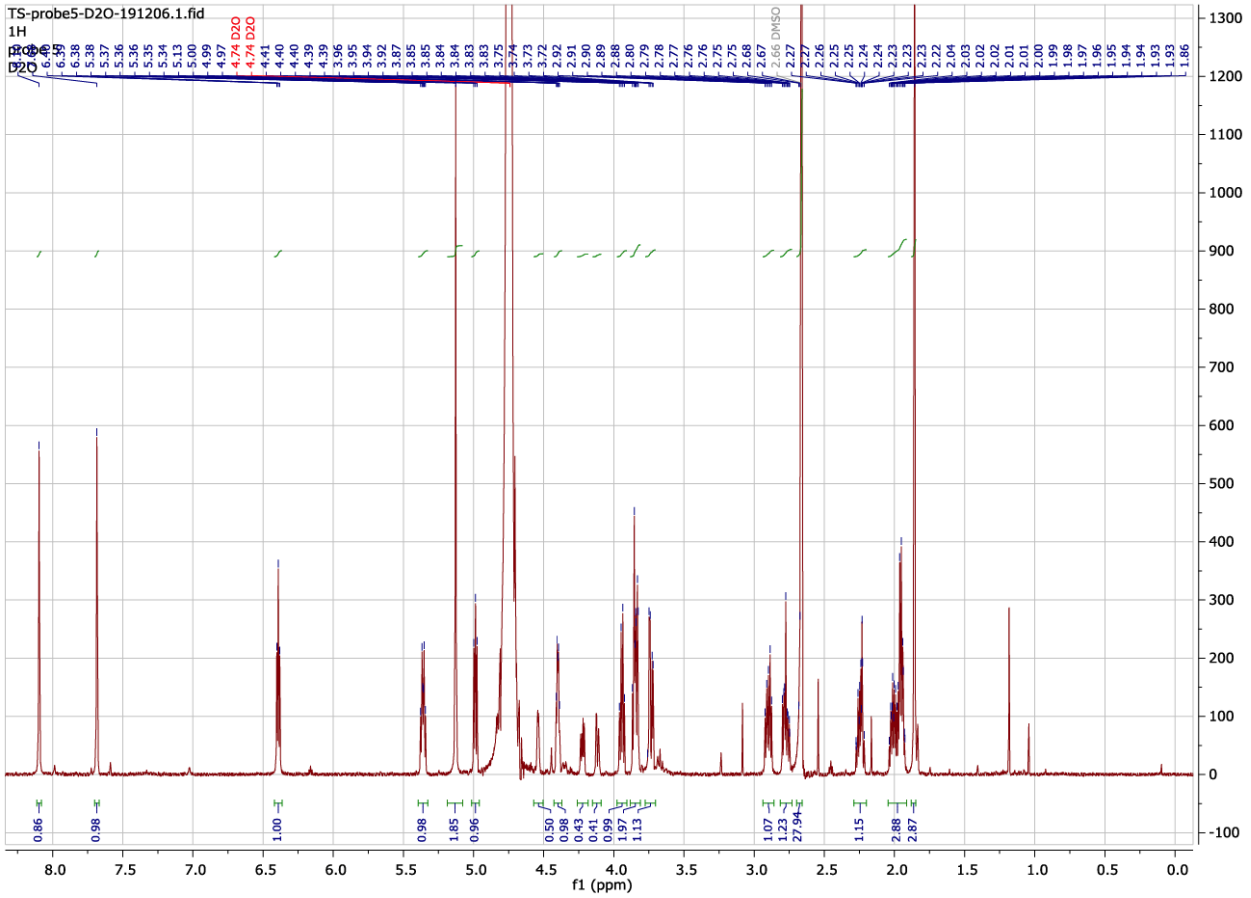

Figure 7-5. ^{1}H-NMR spectrum of Azauracil-AzT.

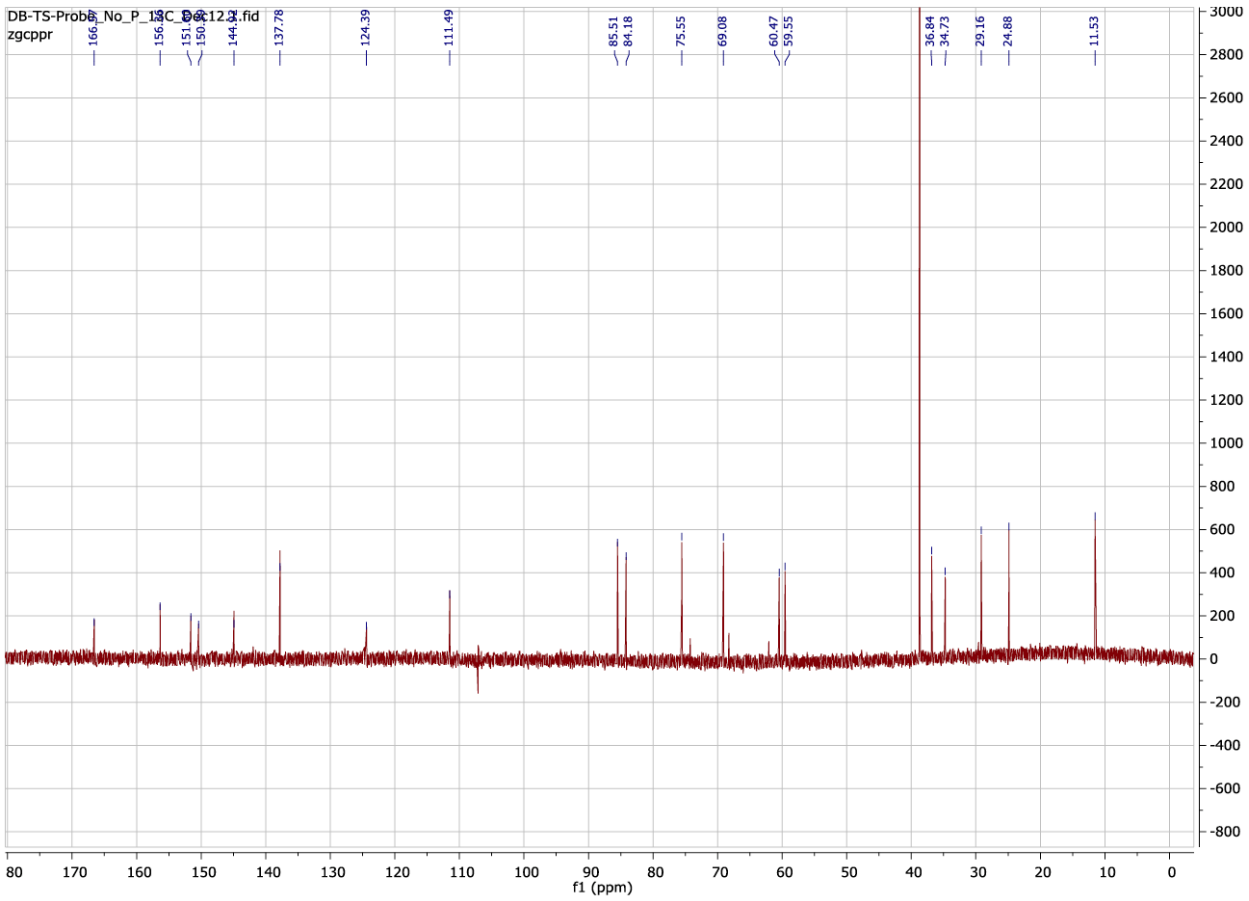

Figure 7-6. ^{13}C-NMR spectrum of Azauracil-AzT.

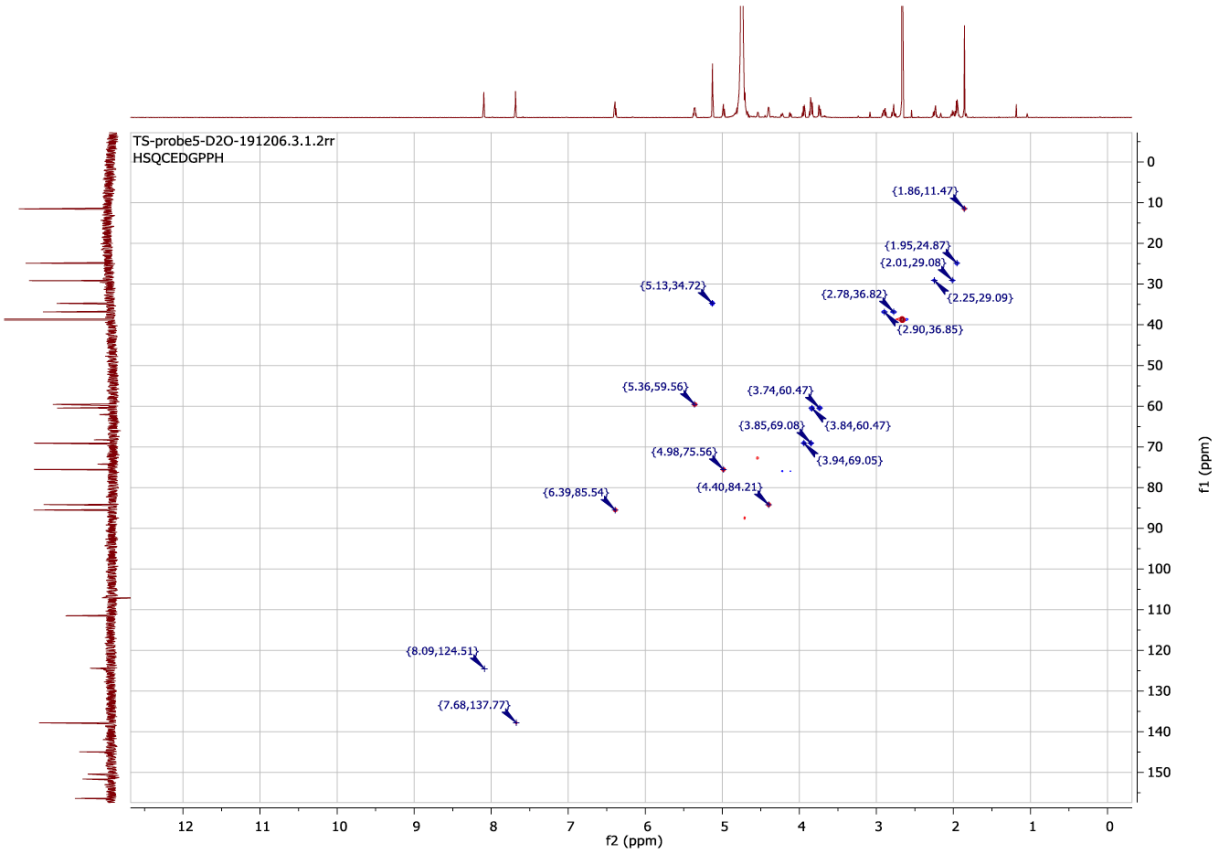

Figure 7-7. HSQC NMR spectrum of Azauracil-AzT

7.2 Supplemental Tables for Chapter 3

Table 7-1. Percentage coverage of HIV RT with chemically modified peptides by LC-MS/MS

	p66			p51		
	Labelled	Peptide ID ctrl	Labelling ctrl	Labelled	Peptide ID ctrl	Labelling ctrl
Probe **1**	86.0	84.8	86.2	98.4	96.6	99.3
Probe **2**	87.1	87.1	85.2	92.4	91.7	91.7
Probe **3**	88.3	86.7	87.1	98.7	95.7	92.6

Table 7-2. LC-MS/MS hits of p66 subunit peptides labelled with azauracil probes

Probe	Annotated Sequence	Modifications	Missed Cleavages	Charge	m/z [Da]	MH+ [Da]	DeltaM [ppm]	RT [min]	XCorr
	[R].GsELPIsPIETVPVK.[L]	S3	0	3	623.3219	1867.9511	6.769469224	39.71513	1.3253503
1	[K].yARMRGAHtNDVK.[Q]	Y354, T362	2	3	607.61139	1820.8196	0.115003425	43.6116	1.0448167
	[R].WGLTtPDKK.[H]	T216	1	2	605.80383	1210.6004	-6.015098489	35.29723	1.0266793
2	[K].HQKEPPFLWmGyELHPDKWTVQPIVLPEK.[D]	Y232	2	6	621.48138	3723.8519	-3.30851372	44.89825	1.5395731
	[-].mRGsELPIsPIETVPVKLKPGmDGPK.[V]	S3	2	5	650.93835	3250.6627	7.034926156	50.85798	1.0219656
	[-].mRGSELPIsPIEtVPVKLKPGmDGPK.[V]	S3, T7	2	5	650.93835	3250.6627	7.034926156	50.85798	1.0607207
3	[R].GTKALtEVIPLTEEAELELAENR.[E]	T290	1	3	916.46368	2747.3765	-8.458603087	56.65395	1.8054019

Table 7-3. LC-MS/MS hits of p51 subunit peptides labelled with azauracil probes.

Probe	Annotated Sequence	Modifications	Missed Cleavages	Charge	m/z [Da]	MH+ [Da]	DeltaM [ppm]	RT [min]	XCorr
2	[K].SVTVLDVGDAyFSVPLDEDFRK.[Y]	Y115	1	4	660.07355	2637.2724	1.161668674	52.10741	1.015239
	[K].IGPENPyNtPVFAIKKK.[D]	Y56, T58	2	4	590.30676	2358.2052	0.513781354	42.7129	1.1230226
3	[K].IGPENPyNtPVFAIKKK.[D]	Y56, T58	2	4	590.30713	2358.2067	1.134950576	41.95076	1.0856485

7.3 Supplemental References for Chapter 3

(1) Vincent-Rocan, J.-F.; Ivanovich, R. A.; Clavette, C.; Leckett, K.; Bejjani, J. and Beauchemin, A. M. Cascade reactions of nitrogen-substituted isocyanates: a new tool in heterocyclic chemistry *Chem. Sci.* **2016**, 7, 315–328. https://doi.org/10.1039/C5SC03197D.

(2) Zhou, L.; Amer, A.; Korn, M.; Burda, R.; Balzarini, J.; De Clercq, E.; Kern, E. R. and Torrence, P. F. Synthesis and antiviral activities of 1,2,3-triazole functionalized thymidines: 1,3-Dipolar cycloaddition for efficient regioselective diversity generation. *Antivir. Chem. Chemother.* **2005**, 16(6), 375–383. https://doi.org/10.1177/095632020501600604.

Chapter 8: Supplemental Material for Chapter 4

8.1 Supplemental Materials, Methods and Figures for Chapter 4

8.1.1 General

IR spectra were collected on all samples in the solid state on a Varian 640 FT-IR spectrometer in the 525-4000 cm^{-1} range.

8.1.2 Procedure for the Reaction Shown in Equation 8-1

The reaction was performed according to the procedure described in the literature,[i] on the reaction scale described above, and isolated by silica gel column chromatography to afford a white solid, m.p. 160-161°C. **^{1}H NMR** (400 MHz, DMSO-d_6) δ 10.75 (s, 1H), 8.15 (d, J = 7.9 Hz, 1H), 4.29 (td, J = 8.4, 4.7 Hz, 1H), 3.28 (dd, J = 13.5, 4.8 Hz, 1H), 2.89 (dd, J = 13.6, 8.7 Hz, 1H), 2.77 (t, J = 2.6 Hz, 1H), 2.27 (dd, J = 8.1, 7.0 Hz, 2H), 2.20 (td, J = 7.1, 2.7 Hz, 2H), 1.83 (s, 3H), 1.83 (s, 3H), 1.65 (m, 2H). **^{13}C NMR** (75 MHz, DMSO-d_6) δ 172.6, 170.5, 169.6, 153.8, 84.7, 71.9, 52.7, 37.3, 30.1, 24.9, 22.8, 17.7, 17.1. **IR (FT-IR):** 3277, 3176, 3056, 2919, 2850, 1703, 1652, 1539, 1419, 1271, 1227, 1177, 1112, 1041, 986, 817, 719, 647, 599, 563, 535 cm^{-1}. **HRMS (ESI):** Exact mass calculated for $C_{13}H_{19}N_3O_4SNa$ $[M+Na]^+$ 336.0994, found 336.0992. Similarly, a reaction was performed in D_2O at a concentration of 0.01 M. While the probe was not fully soluble at the beginning of the reaction, most of the probe dissolved as the reaction proceeded. After 24 hours, the reaction was analyzed by ^{1}H NMR spectroscopy, after adding a known amount of N,N-dimethylformamide to serve as internal standard. This revealed that 86% of the starting material was converted to the product in Eq. 8-1.

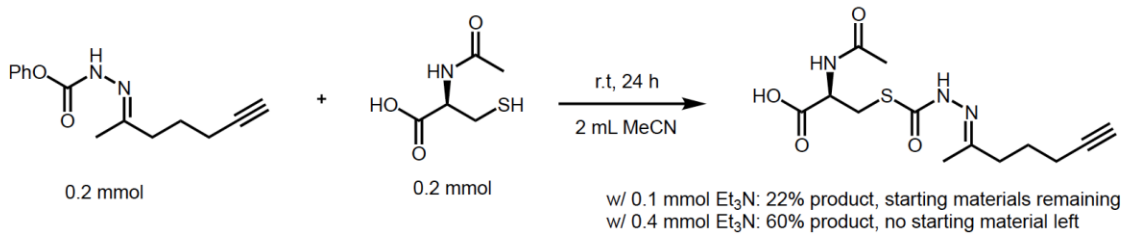

w/ 0.1 mmol Et_3N: 22% product, starting materials remaining
w/ 0.4 mmol Et_3N: 60% product, no starting material left

Eq. 8-1

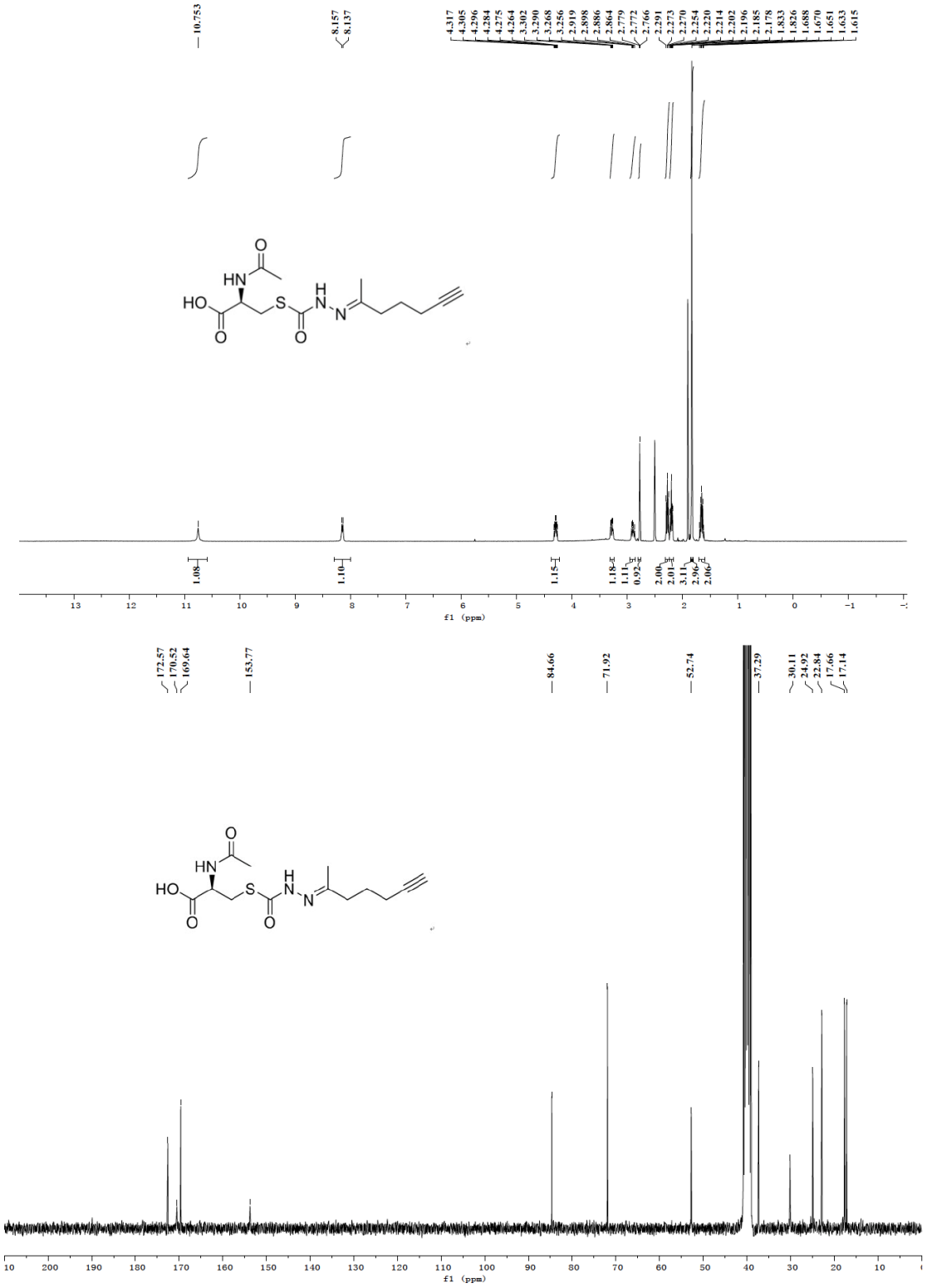

Figure 8-1. ^{1}H and ^{13}C NMR spectra of the N-AcCysteine–probe addition product (Eq. 8-1)

8.1.3 Procedure for the Reaction Shown in Equation 8-2

The reaction was performed according to the procedure described in the literature,[i] but using a 10-fold excess of isobutylamine but on half the reaction scale described above, and isolated by silica gel column chromatography to afford a yellow oil (18% yield): **^{1}H NMR** (300 MHz, $CDCl_3$) δ 7.52 (s, 1H), 6.20 (s, 1H), 3.14 – 3.06 (m, 2H), 2.41 – 2.28 (m, 2H), 2.22 (td, J = 7.0, 2.6 Hz, 2H), 1.95 (t, J = 2.6 Hz, 1H), 1.85 – 1.79 (m, 1H), 1.78 (s, 3H), 1.75 (dd, J = 6.9, 3.6 Hz, 2H), 0.92 (s, 3H), 0.90 (s, 3H). **^{13}C NMR** (75 MHz, $CDCl_3$) δ 156.5, 148.1, 83.8, 68.8, 47.0, 37.4, 29.0, 24.9, 20.0, 17.9, 15.3. **IR (FT-IR)**: 3417, 3310, 3208, 2956, 2870, 1671, 1532, 1467, 1386, 1369, 1341, 1291, 1240, 1163, 1107, 1057, 863, 821, 761, 625 cm^{-1}. **HRMS (ESI)**: Exact mass calculated for $C_{12}H_{21}N_3ONa$ $[M+Na]^+$ 246.1592, found 246.1582. For comparison, the same reaction was performed with the probe and conditions shown in equation 8-1, leading to a 58% yield.

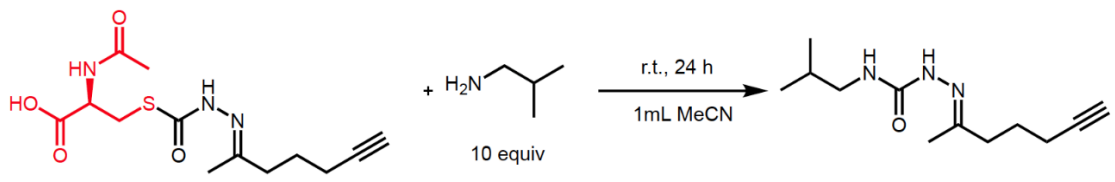

Eq. 8-2

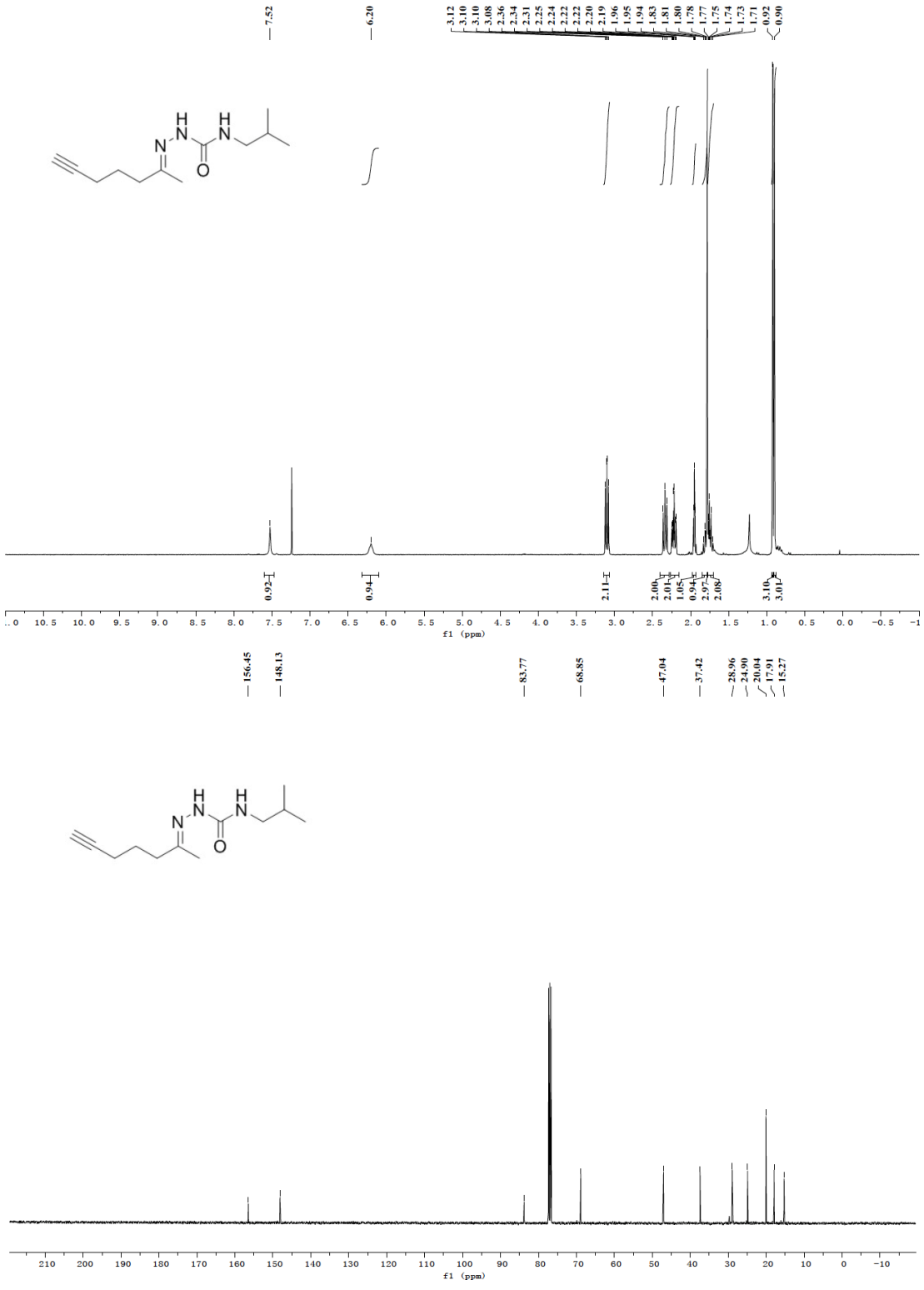

Figure 8-2. ^{1}H and ^{13}C NMR spectra of the substitution product of the reaction with isobutylamine (Eq. 8-2).

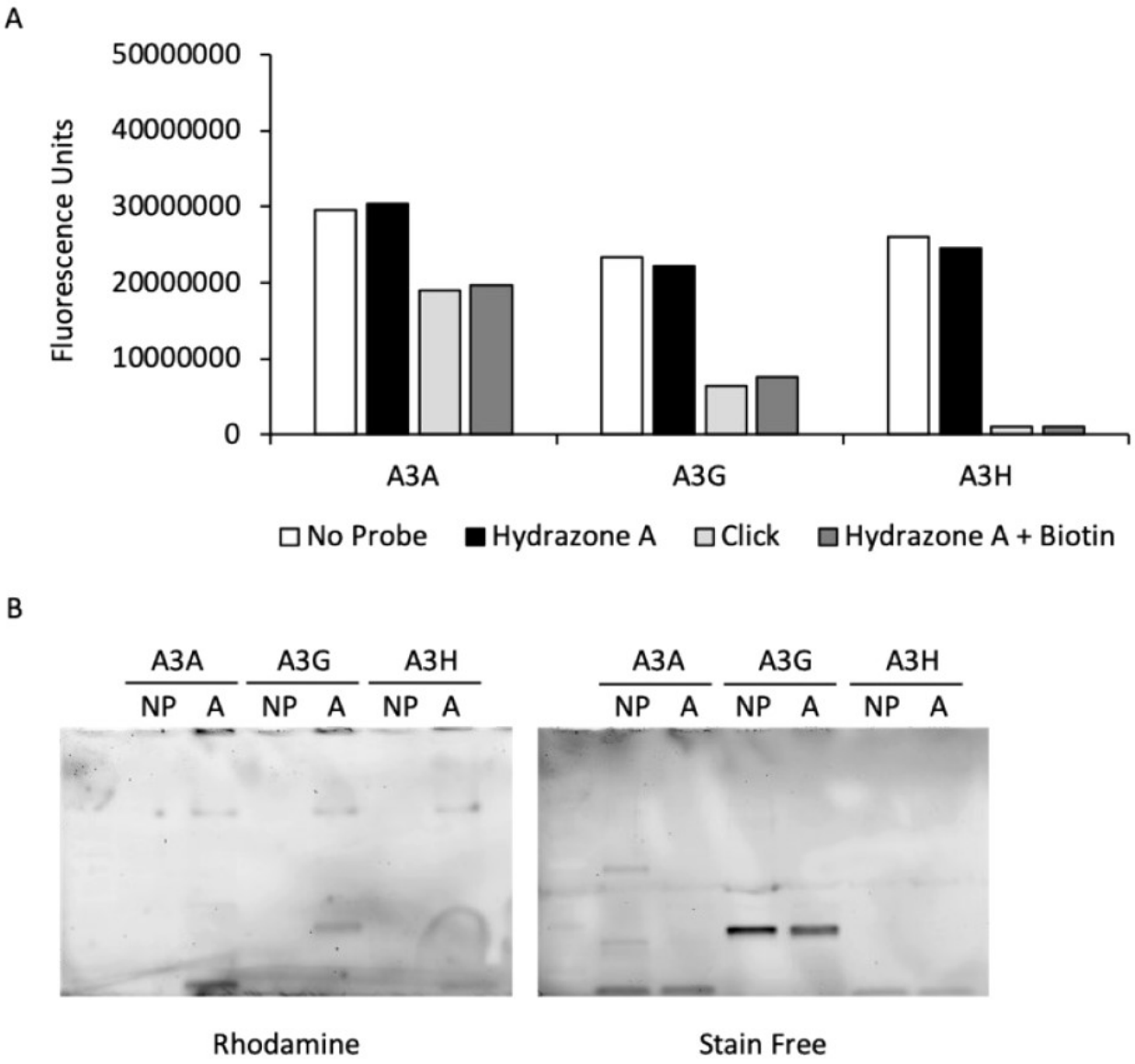

Figure 8-3. Activity of APOBEC proteins incubated with probe A.

Purified APOBEC proteins were incubated with probe A for 1 hour before being reacted with biotin azide, rhodamine azide or control. The proteins were then used for A) deamination assay or B) In-gel fluorescence showing rhodamine fluorescence from probe-labelled purified proteins, used as a control to confirm click reaction. On the right is corresponding stain free gel showing presence of proteins. APOBEC3A, 3G, and 3H are abbreviated A3A, A3G, and A3H. NP is no probe control.

8.2 Supplemental Tables for Chapter 4

Table 8-1. MS identification of putative targets of hydrazone probes A, B, and C by pull-down of Huh7 lysates and on-bead digest

Accession #	Protein ID	Mascot Score	MW (Da)	pI	Sequence Coverage (%)	# of Peptides
Hydrazone A						
IPI00021439	ACTB Actin, cytoplasmic 1	209	41710	5.29	20.8	6
IPI00166768	TUBA1C Uncharacterized protein	176	36719	8.76	10.7	2
IPI00065051	CCDC13 Coiled-coil domain-containing protein 13	48	80834	8.83	1.3	1
IPI00013876	APOBEC3A Isoform 1 of Probable DNA dC->dU-editing enzyme APOBEC-3A	42	22997	6.34	4.5	1
IPI00218429	PREX1 Isoform 2 of Phosphatidylinositol 3,4,5-trisphosphate-dependent Rac exchanger 1 protein	39	106026	5.32	2.1	1
Hydrazone B						
IPI00021439	ACTB Actin, cytoplasmic 1	548	41710	5.29	29.1	9
IPI00008603	ACTA2 Actin, aortic smooth muscle	438	41982	5.23	27.1	8
IPI00166768	TUBA1C Uncharacterized protein	385	36719	8.76	22.1	5
IPI00414676	HSP90AB1 Heat shock protein HSP 90-beta	344	83212	4.97	20.4	11
IPI00382470	HSP90AA1 Isoform 2 of Heat shock protein HSP 90-alpha	333	98099	5.07	9	6
IPI00007752	TUBB2C Tubulin beta-2C chain	194	49799	4.79	9.9	2
IPI00645452	TUBB Uncharacterized protein	162	47736	4.7	13.1	3
IPI00784154	HSPD1 60 kDa heat shock protein, mitochondrial	162	61016	5.7	4.4	1
IPI00219757	GSTP1 Glutathione S-transferase P	130	23341	5.43	9	1
IPI00005719	RAB1A Isoform 1 of Ras-related protein Rab-1A	121	22663	5.93	18.5	3
IPI00396485	EEF1A1 Elongation factor 1-alpha 1	115	50109	9.1	15.8	5
IPI00030131	TMPO Isoform Beta of Lamina-associated polypeptide 2, isoforms beta/gamma	113	50639	9.39	6.2	2
IPI00027223	IDH1 Isocitrate dehydrogenase [NADP] cytoplasmic	105	46630	6.53	6.3	2
IPI00978298	RPS3 Uncharacterized protein	97	25355	9.73	12.6	2
IPI00009235	SSR3 Translocon-associated protein subunit gamma	93	21067	9.61	7.6	1
IPI00218914	ALDH1A1 Retinal dehydrogenase 1	83	54827	6.3	2.6	1
IPI00031697	TMEM109 Transmembrane protein 109	71	26194	10.48	4.9	1
IPI00022202	SLC25A3 Isoform A of Phosphate carrier protein, mitochondrial	66	40069	9.45	3.3	1
IPI00186290	EEF2 Elongation factor 2	64	95277	6.41	4.7	1
IPI00023001	FAM162A Protein FAM162A	58	17331	9.81	7.1	1
IPI00329596	TMX2 Uncharacterized protein	58	42444	8.86	2.7	1
IPI00011893	- mRNA clone with similarity to L-glycerol-3-phosphate:NAD oxidoreductase and albumin gene sequences	54	12560	6.41	14.7	1
IPI00216587	RPS8;SNORD55 40S ribosomal protein S8	52	24190	10.32	5.3	1
IPI00013296	RPS18;RPS18P9 40S ribosomal protein S18	52	17708	10.99	7.2	1
IPI00000875	EEF1G cDNA FLJ56389, highly similar to Elongation factor 1-gamma	51	56114	7.6	4.7	1
IPI00292056	PIK3C2B Phosphatidylinositol-4-phosphate 3-kinase C2 domain-containing subunit beta	49	184651	6.95	0.5	1

Accession #	Protein ID	Mascot Score	MW (Da)	pI	Sequence Coverage (%)	# of Peptides
Hydrazone C						
IPI00021439	ACTB Actin, cytoplasmic 1	243	41710	5.29	24	6
IPI00166768	TUBA1C Uncharacterized protein	176	36719	8.76	10.7	2
IPI00218914	ALDH1A1 Retinal dehydrogenase 1	139	54827	6.3	8.6	3
IPI00014424	EEF1A2 Elongation factor 1-alpha 2	84	50438	9.11	4.3	1
IPI00878429	PRR14L Protein	42	23555	9.59	10.6	1
IPI00041320	MDM2 p53-binding protein	42	27289	5.22	3.3	1
IPI00386085	MAFK Putative uncharacterized protein DKFZp547K209 (Fragment)	40	20112	9.02	7.8	1
IPI00218429	PREX1 Isoform 2 of Phosphatidylinositol 3,4,5-trisphosphate-dependent Rac exchanger 1 protein	38	106026	5.32	2.1	1
IPI00440493	ATP5A1 ATP synthase subunit alpha, mitochondrial	47	59714	9.16	2.4	1
IPI00012493	SNORD54;RPS20 40S ribosomal protein S20	46	13364	9.95	12.6	1
IPI00160775	SIDT1 Isoform 2 of SID1 transmembrane family member 1	46	94295	6.6	1	1
IPI00872541	SCN10A Sodium channel protein type 10 subunit alpha	45	220484	5.67	0.4	1
IPI00215884	SRSF1 Isoform ASF-1 of Serine/arginine-rich splicing factor 1	45	27728	10.37	4.8	1
IPI00383879	AADAC Arylacetamide deacetylase	45	45705	8.75	3	1
IPI00976298	ASCC1 Protein	44	20583	6.27	8	1
IPI00735270	KIAA1109 185 kDa protein	43	185104	6.52	0.5	1
IPI00011399	IL24 Interleukin-24	41	23809	8.94	6.3	1
IPI00218429	PREX1 Isoform 2 of Phosphatidylinositol 3,4,5-trisphosphate-dependent Rac exchanger 1 protein	40	106026	5.32	2.1	1

Table 8-2. MS identification of interacting residues of APOBEC3A with probe A

	Trial 1		Trial 2		Trial 3	
Residue	Confidence	Xcorr	Confidence	Xcorr	Confidence	Xcorr
S4	High	1.392324	Medium	1.22949	High	0.720779
S7	High	0.698057	Medium	1.22949	Medium	1.0996
S20	High	1.654854	nd	nd	nd	nd
C34	High	2.57	Medium	0.597153	Medium	0.796544
C34	High	1.39	High	2.336112	High	1.012486
C34	High	1.01	High	1.098587	High	2.366712
S45	High	1.258144	Medium	0.587737	Medium	0.856634
S45	Medium	0.876965	High	0.894275	Medium	0.796544
S81	nd	nd	High	1.183304	High	1.638683
S97	nd	nd	High	1.183304	High	1.461768
S99	nd	nd	High	0.822397	High	1.461768
S103	nd	nd	High	0.822397	High	1.638683
S151	nd	nd	High	1.134772	nd	nd
C161	nd	nd	High	1.355711	nd	nd
C171	nd	nd	High	1.355711	nd	nd
S183	nd	nd	High	1.355711	nd	nd
S187	nd	nd	Medium	0.738073	nd	nd

Table 8-3. MS identification of interacting residues of APOBEC3A with probe A

	Confidence	Annotated Sequence	Modification	Charge	m/z [Da]	MH+ [Da]	DeltaM [ppm]	Deltam/z [Da]	XCorr	Area
Trial 1	High	[K].TYLcYEVER.[L]	C34 (+150)	2	663.3096	1325.612	1.831705	0.001214	2.574408	640610.2
Trial 2	High	[K].TYLcYEVER.[L]	C34 (+150)	2	663.3063	1325.605	-3.14095	-0.00208	2.336112	719621
Trial 3	High	[K].TYLcYEVER.[L]	C34 (+150)	2	663.3102	1325.613	2.844653	0.001885	2.366712	478769.8

8.3 Supplemental References for Chapter 4

(1) Garland, K.; Gan, W.; Depatie-Sicard, C.; Beauchemin, A. M. A Practical Approach to Semicarbazone and Hydrazone Derivatives via Imino-Isocyanates. *Org. Lett.* **2013**, 15 (16), 4074–4077. https://doi.org/10.1021/ol4016.